ALIGNMENT OF MICRO-CRYSTALS OF MN_{12}-ACETATE AND DIRECT OBSERVATION OF SINGLE MOLECULES THEREOF

A Dissertation

by

DONGMIN SEO

Submitted to the Office of Graduate Studies of
Texas A&M University
in partial fulfillment of the requirements for the degree of

DOCTOR OF PHILOSOPHY

December 2007

Major Subject: Physics

ALIGNMENT OF MICRO-CRYSTALS OF MN_{12}-ACETATE AND DIRECT OBSERVATION OF SINGLE MOLECULES THEREOF

A Dissertation

by

DONGMIN SEO

Submitted to the Office of Graduate Studies of
Texas A&M University
in partial fulfillment of the requirements for the degree of

DOCTOR OF PHILOSOPHY

Approved by:

Chair of Committee,	Winfried Teizer
Committee Members,	Joseph H. Ross Jr.
	Artem Abanov
	Kim R. Dunbar
Head of Department,	Edward Fry

December 2007

Major Subject: Physics

ABSTRACT

Alignment of Micro-crystals of Mn_{12}-acetate and Direct Observation of Single Molecules Thereof. (December 2007)

Dongmin Seo, B.S., Dankook University in Korea;

M.S., Seoul National University in Korea; M.S., Texas A&M University

Chair of Advisory Committee: Dr. Winfried Teizer

This dissertation focuses on three separate studies. First, magnetization of the Mn_{12}-acetate was studied by low temperature hysteresis loops and DC magnetization data on magnetically aligned Mn_{12}-acetate micro-crystals. Secondly, Mn_{12}-acetate thin films were fabricated and characterized by AFM and STM. Finally, magnetization of the film material was also studied.

Enhanced alignment of Mn_{12}-acetate micro-crystals as compared to prior studies was verified by observation of several sharp steps in low temperature hysteresis loops. It was found that ~ 0.5 T is sufficient to orient the micro-crystals in an organic solvent to a degree comparable to a single crystal. The degree of the alignment was controlled by varying the magnetic field at room temperature and during the cooling process. Subsequently, low temperature hysteresis loops and DC magnetizations were measured for each prepared orientation state of a sample. The high temperature magnetic anisotropy responsible for the alignment could not be measured, possibly due to its small magnitude.

Mn_{12}-acetate was deposited onto Si/SiO_2 by a solution evaporation method. Atomic force microscopy studies revealed that 2 nm thick films of molecular level smoothness were formed. Mn_{12}-acetate was also deposited onto a Highly Ordered Pyrolytic Graphite (HOPG) surface for scanning tunneling microscopy (STM) studies. A self-assembled triangular lattice was observed in the Mn_{12}-acetate thin films by STM at room temperature under ambient conditions. These STM images show typical center to center intermolecular separations of about 6.3 nm and height corrugation of less than 0.5 nm.

Magnetization measurements were not successful in Mn_{12}-acetate thin films due to the small amount of material in the film and the large background signal from the substrate. Therefore, a sample for the magnetization measurements, called "film material", was made by evaporating a dilute solution of Mn_{12}-acetate powder in acetonitrile. Significant changes in magnetic properties of the film material were observed from magnetization measurements. The blocking temperature of the film material was found to increase to $T_B > 10$ K at low magnetic fields.

To my grandparents

ACKNOWLEDGEMENTS

I joined Dr. Teizer's group in the fall semester of 2002 when I was admitted to the Physics Department at Texas A&M University. From that time, it was not easy to pursue both research work and course work. An international environment using a foreign language, English, made it even more difficult. The last five and half year is an important turning point to me not only in life but also in my scientific career: I have married and received a little daughter. And, as a Ph.D. candidate during this time, I was lucky to meet so many exceptional people who helped me to become more than a scientist and to make this dissertation possible.

My Ph.D. advisor, Winfried Teizer, allowed me to pursue my own research interests while giving clear direction in the big picture. He also taught me how to write scientific papers and to give effective conference talks about experimental results. I greatly appreciate him for invaluable instructions and continuing guidance for my Ph.D. work. Thanks also go to Meenakshi Viswanathan, our postdoctoral researcher, for her help with my initial settlement in our laboratory and on experiments. Without her help in the beginning of my work, it may not have been possible to finish my research work within time. I am grateful to my group members: Joel Means, Kyongwan Kim, Huachun Xu, Arlene Ford, Raj Srivastava, Luohan Peng, John Noel, and Tracey Wellington for their assistance in the experiments and laboratory life. Thanks to John for the English correction of this dissertation.

It was my pleasure to know a number of professors here at Texas A&M University. Thanks to Dr. Joseph H. Ross Jr., Dr. Artem Abanov, and Dr. Kim R. Dumbar as committee members. Their time and effort was important to finish my Ph.D. work not only by reviewing my dissertation, but also by their guidance and support for this work. I would also like to thank Dr. Donald G. Naugle and Dr. Valery L. Pokrovsky for their helpful discussions and suggestions for this work. I like to thank current MCF staff, Dr. Orla Wilson and Dr. Gang Liang, and previous staff, Dr. William Lackowski and Yulia Vasilyeva, for their help in using experimental facilities such as AFM, STM, and XPS. I would also like to thank Dr. Hanhua Zhao for Mn_{12}-aceate samples and Dr. Andrew Prosvirin for his help in using the SQUID. This dissertation is as much theirs as it is mine. I cannot forget Sandi Smith, departmental staff. Her kind help for my official work was more than that.

Finally, I am deeply indebted to my parents and parents-in-law in Korea for their constant love and support. I also thank my wife, Jieun Kim and my little daughter, Jeewoo for their love and patience.

This research was supported by the Robert A. Welch Foundation (A-1585) and the National Science Foundation (DMR-0103455 and NSF-9974899).

TABLE OF CONTENTS

Page

ABSTRACT iii

DEDICATION v

ACKNOWLEDGEMENTS vi

TABLE OF CONTENTS viii

LIST OF FIGURES x

CHAPTER

I INTRODUCTION 1

1.1 Outline 1
1.2 Review of Single-Molecule Magnets 1
1.3 Background on Mn_{12}-acetate 8

II EXPERIMENTAL 15

2.1 Suspension Alignment in a Capsule 15
2.2 Thin Film and 'Film Material' Preparation 20
2.2.1 Thin Film Deposition on Si/SiO_2 20
2.2.2 Thin Film Deposition on HOPG 21
2.2.3 Film Material Preparation 21
2.3 Magnetization Measurements 22
2.3.1 SQUID Magnetometer 22
2.3.2 Magnetization Measurements 25
2.4 Microscopy Measurements 26
2.4.1 Basics of AFM and STM 26
2.4.2 AFM Measurements 30
2.4.3 STM Measurements 31
2.5 Other Measurements 33

III ALIGNMENT OF MN_{12}-ACETATE 34

3.1 Introduction and Motivation 34
3.2 Experimental 35

CHAPTER Page

3.3 Results and Discussions 36
3.3.1 Preliminary Data and Discussions 36
3.3.2 Hysteresis Data 44
3.3.3 DC Magnetization Data 52
3.4 Summary 63

IV THIN FILM OF MN_{12}-ACETATE 65

4.1 Motivation 65
4.2 Experimental 68
4.3 Results and Discussions 69
4.3.1 Mn_{12}-acetate Thin Films on Si/SiO_2 69
4.3.2 Mn_{12}-acetate Thin Films on HOPG 80
4.4 Summary 87

V MAGNETIZATION OF THE FILM MATERIAL 88

5.1 Background 88
5.2 Experimental 89
5.3 Results and Discussions 90
5.3.1 Magnetic Properties of the Film Material 90
5.3.2 Mass Spectroscopy Data 97
5.4 Summary 99

VI CONCLUSIONS 100

REFERENCES 103

APPENDIX A 109

APPENDIX B 112

APPENDIX C 119

APPENDIX D 120

APPENDIX E 122

VITA 126

LIST OF FIGURES

FIGURE Page

1.1. Magnetic energy of the SMMs as a function of the magnetic moment from the magnetic easy axis 4

1.2. Magnetization relaxation of Mn_{12}-acetate powder at 2.5 K and 3.5 K with applied magnetic field (– 0.5 T) 5

1.3. Field Cooled (FC) and Zero Field Cooled (ZFC) magnetization of Mn_{12}-acetate powder at H = 0.7 T 7

1.4. Structure of the Mn_{12}-acetate molecule 9

1.5. Out-of-phase AC-susceptibility (χ'') signals of Mn_{12}-acetate powder at different frequencies (1 Hz, 50 Hz, 500 Hz, and 1000 Hz) as a function of temperature 11

1.6. Magnetization versus magnetic field hysteresis loops of Mn_{12}-acetate single crystal at 1.77 K, 2.1 K, and 2.64 K 13

1.7. The drawing depicts how double-well potential (longitudinal terms) changes as the magnetic field (Zeeman term) is swept from H = 0 T to H = 0.44 T 14

2.1. Hysteresis loop of Mn_{12}-acetate solution (10mg/10 mL in isopropanol) after letting the solution settle 20 minutes 17

2.2. Hysteresis loops of similarly concentrated Mn_{12}-acetate solution in both the bucket and the capsule 19

2.3. A home made plastic capsule with a cap and a commercial sealed plastic bucket 19

2.4. Schematic drawing for (a) the SQUID and (c) second derivative pick-up coil 24

2.5. Schematic drawing of AFM operation 28

2.6. Schematic drawing for STM operation 29

FIGURE Page

2.7. Topographical top-view of a Si/SiO_2 substrate with 1×1 μm^2 scan size 30

2.8. Constant-height STM images of the HOPG surface 32

3.1. Background signal from the solution container with solvent..... 38

3.2. Time evolution of the magnetization of the Mn_{12}-acetate suspension with the background signal at 0.5 T and 300 K 40

3.3. Hysteresis loops at 1.8 K for the Mn_{12}-acetate suspension just after preparation (takes ~ 1 hour before cooling the sample), and after storing 1 and 2 weeks at room temperature. 41

3.4. M vs. H hysteresis loops of the suspension at 1.8 K 43

3.5. Simplified schematic drawing of the suspension that shows only single molecules and micro-crystals of Mn_{12}-acetate 45

3.6. Hysteresis loops from Mn_{12}-acetate suspension in the plastic container at 1.8, 2.1, 2.4, and 2.64 K, respectively 47

3.7. Series of hysteresis loops at 1.8 K for different orientations of the suspension by applying different orientation fields (H_{orient} = 0, 0.005, 0.05, 0.1, and 0.5 T), respectively at room temperature. 49

3.8. Hysteresis loops at 1.8 K for different degrees of alignment of the Mn_{12}-acetate suspension obtained by applying an orientation field H_{orient} = 0.5 T at different orientation temperatures (T_{orient} = 100, 150, 200, and 250 K) 51

3.9. Series of DC magnetizations as a function of temperature (2 ~ 20 K) with a magnetic field of 0.5 T for differently oriented suspension obtained by applying different orientation fields (H_{orient} = 0, 0.005, 0.05, 0.1, 0.2, 0.5 and 1 T), respectively at room temperature 53

3.10. DC magnetization curves at H = 0.5 T for both aligned (H_{orient} = 1 T) and randomly-oriented (H_{orient} = 0 T) states of the sample over the temperature range 2 ~ 300 K 56

3.11. The normalized magnetization (M/M') as a function of the orientation magnetic field (H_{orient}) 58

FIGURE Page

3.12. Fig. 3.12. Schematic drawings depict the "energy competition model" .. 60

3.13. The graph shows both experimental and calculated data 62

4.1. STM images of Mn_{12} family deposited on Au surface for (a) – (f) 67

4.2. AFM images of a Mn_{12}-acetate thin film formed by the solution evaporation method 70

4.3. AFM images of the Mn_{12}-acetate thin film with 2×2 μm^2 and 0.5×0.5 μm^2 scan sizes for (a) and (b), respectively 72

4.4. AFM images of four Mn_{12}-acetate films formed using different solution concentrations 73

4.5. RMS-roughness dependence on the solution concentration 74

4.6. AFM images for different DAD cycles 75

4.7. AFM image of artificially patterned Mn_{12}-acetate thin film 77

4.8. XPS Spectra of the Mn 2p core level for the crystalline Mn_{12}-acetate pellet and the Mn_{12}-acetate thin films 78

4.9. Si 2p narrow scan spectra of the Mn_{12}-acetate thin films which were used for AFM investigations 79

4.10. Constant-current STM images of the Mn_{12}-acetate thin film deposited on HOPG 81

4.11. (a) AFM images with 3×3 μm^2 scan size, and (b) 0.2×0.2 μm^2 scan size on the Mn_{12}-acetate thin film 83

4.12. STM images of (a) the solvent exposed HOPG, and (b) the Mn_{12}-acetate thin film on HOPG with same conditions 84

4.13. Core level XPS spectra of the Mn 2p peaks for a crystalline Mn_{12}-acetate (pellet) and the Mn_{12}-acetate thin film on HOPG surface 86

5.1. Temperature dependence of real (χ') and imaginary (χ'') parts of AC-susceptibility at different frequencies 91

FIGURE Page

5.2. Zero-field-cooled and field-cooled magnetization vs temperature curves at H_{app}= 500 Oe 92

5.3. Magnetization relaxation of Mn_{12}-acetate film material at 5.5 K with an applied field of - 0.5 T 94

5.4. Magnetization versus magnetic field hysteresis loop of Mn_{12}-acetate film material at 1.8 K 96

5.5. ESI-MS spectrum (positive mode) of a solution of Mn_{12}-acetate in acetonitrile ~ 30 minutes after making the solution 98

A.1. Schematic diagram illustrating the absence of spin tunneling at H = 1 T up to 300 K..... 110

A.2. A diagram for volume comparison of the Mn_{12}-acetate micro-crystal and the single molecule with typical sizes given 111

A.3. DC magnetization at H = 0.5 T as a function of temperature for differently aligned states of the suspension 114

A.4. M vs. H hysteresis loop data of the aligned suspension at 1.8 K 116

A.5. Magnetization difference between two extreme states 118

A.6. (a) M vs. H graph on the straw piece at 1.8 K, (b) hysteresis loop of the Mn_{12}-acetate film deposited on the straw piece at 1.8 K, (c) pure Mn_{12}-acetate film data found by subtracting (a) from (b) 123

A.7. (a) M vs. H graph on the straw piece at 1.8 K, (b) magnetization of the Mn_{12}-acetate film by 2 DAD-cycles with the straw piece at 1.8 K, (c) pure Mn_{12}-acetate film data by subtracting (a) from (b), (d) magnetization of the other straw piece at 1.8 K, (e) hysteresis loop of the relatively thick Mn_{12}-acetate film by 20 DAD-cycles with the straw piece, (f) magnetization of the pure Mn_{12}-acetate thick film by subtracting (d) from (e) 125

CHAPTER I

INTRODUCTION

1.1 Outline

The main topic of this dissertation is the fundamental magnetic study and application of Mn_{12}-acetate Single-Molecule Magnets (SMMs) with a focus on magnetic alignment and thin film fabrication and characterization. Magnetic alignment of Mn_{12}-acetate micro-crystals has been demonstrated and studied in an organic solvent. Mn_{12}-acetate thin films have also been deposited on surfaces and characterized by various experimental techniques.

This dissertation is organized as follows: the general properties of SMMs and a background on Mn_{12}-acetate SMM will be discussed in Chapter I. Experimental details for this dissertation will be described in Chapter II. Chapter III will deal with the magnetic alignment of Mn_{12}-acetate micro-crystals, and Chapter IV will discuss Mn_{12}-acetate thin film deposition and characterization. Chapter V will discuss the magnetization of the film material. Finally, Chapter VI will summarize the main conclusions of this dissertation.

1.2 Review of Single-Molecule Magnets

Classical concepts of magnetism were developed from ancient times when the lodestone was found to attract other lodestones or pieces of iron. Quantum aspects of magnetism started with the discovery of the spin in the 1920s.

This dissertation follows the style of Journal of Magnetism and Magnetic Materials.

The gap between the microscopic world of quantum-mechanical atomic magnets and the macroscopic world of classical magnets was more recently filled by studying mesoscopic magnetism. Towards the end of the twentieth century the first example of molecular based magnets were discovered. A particularly appealing area in molecular magnetism is that the molecular magnets show slow relaxation of the magnetization at low temperature and are behaving as independent magnetic molecules consequently they are known also as Single-Molecule Magnets (SMMs). This system attracted much interest for the coexistence of quantum and classical phenomena and for its mesoscopic magnetism [1, 2]. SMMs also provide a nice system to check nanomagnetism theory. Magnetic samples that are too small for the formation of a magnetic domain wall behave like a single magnetic domain. Magnetization changes are then expected to occur solely by uniform rotation of the magnetization rather than domain wall motion as in bulk magnets. The theory of magnetization changes in such single domain particles was developed by Neel in 1947 [3, 4]. He pointed out that, if single-domain particles became small enough, magnetic energy barriers would become so small that the thermal fluctuation energy could overcome the anisotropy barrier and spontaneously reverse the magnetization of a particle from one easy direction to the other, even in the absence of an applied field. A rigorous experimental test of the model was possible after well characterized single particles such as SMMs were studied. SMMs are made by the bottom-up approach using chemistry to grow well defined nanoscale magnetic particles. A uniform distribution of molecular size and shape makes it possible to compare experiments with nanomagnetism theory [5]. Therefore, SMMs, in which a magnetic

domain can be reduced to the size of a single molecule, are ideal systems to study nanoscale magnetism [6]. Mn_{12}-acetate [7], Fe_8 [8], the $[Mn_4]_2$ dimer [9], and V_{15} [10] are typical SMMs. The single-molecule regime is interesting because magnetism arises from unpaired electronic spins and is thus quantum mechanical in nature [11]. Therefore, SMMs have provided physicists with a useful sample for the study of quantum mechanics such as in the form of Quantum Tunneling of the Magnetization (QTM) [12, 13].

QTM can be understood in terms of an anisotropy energy barrier concept [14], as is discussed in the next section. A high spin ground state and a strong uniaxial magnetic anisotropy of the SMMs lead to the anisotropy energy barrier, which is why SMMs are so useful. The anisotropy energy barrier makes the magnetization align along specific directions rather than randomly fluctuate over time. The energy barrier (U) is defined as: $U = S^2|D|$, where S is the dimensionless total spin state and D is the zero-field splitting parameter. The higher the barrier, the longer a material remains magnetized. The energy of the system as a function of the orientation of the magnetic moment from the magnetic easy axis is shown in Fig. 1.1. The bottom of the left well corresponds to magnetization down, the bottom of the right well to magnetization up, and the top to the magnetization at 90° from the magnetic easy axis. Spin up and spin down states are doubly degenerate and give a zero net magnetization of the system in the absence of magnetic field.

The effect of the energy barrier in SMMs is experimentally observed in the magnetization relaxation [15] and stepwise magnetic-hysteresis loops below a certain temperature, the so-called blocking temperature (T_B). The magnetization reversal or

relaxation becomes slow compared to the time scale of a particular investigation technique below T_B. For example, a Mn_{12}-acetate molecule magnetized at 2 K will keep 40 % of its magnetization after 2 months and by lowering the temperature to 1.5 K this time extends to 40 years. The slow relaxation of the magnetization below T_B results in a magnetic hysteresis loop, which is now commonly considered the fingerprint of QTM and will be discussed in the next section. Fig. 1.2 shows the magnetization relaxation of Mn_{12}-acetate powder measured at 2.5 K and 3.5 K (below and above T_B, respectively) with applied field - 0.5 T. The sample was saturated by applying 5 T before the measurement. Below the blocking temperature of Mn_{12}-acetate, an exponential decay law [$\Delta M = \Delta M_f (1 - \exp(-t / \tau))$] can be applied to give a relaxation time (τ), typically of ~ 10^3 seconds at 2.5 K, for example.

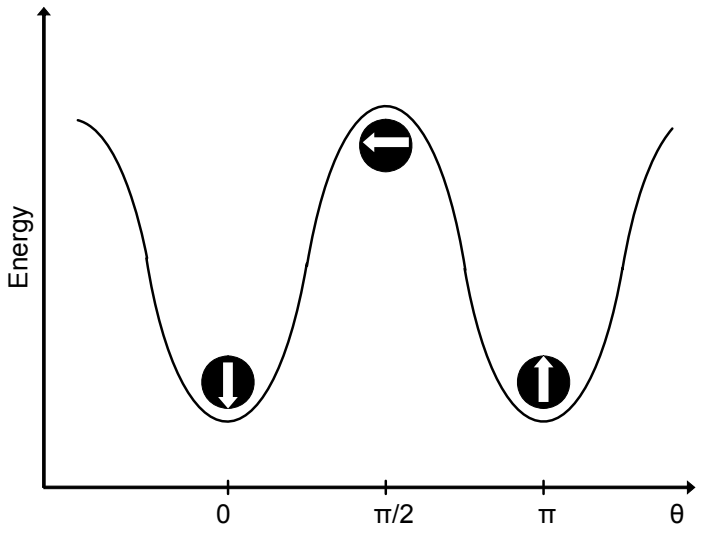

Fig. 1.1. Magnetic energy of the SMMs as a function of the angle of the magnetic moment from the magnetic easy axis.

Here, ΔM is the difference between the starting value of the magnetization and the measured value at time t, and ΔM_f is the difference between the initial and final M at infinite time. In general, the relaxation process depends on the temperature and the applied magnetic field. The aligned sample, like single crystals, should be used in the relaxation measurement to observe energy level effects. However, randomly-oriented powder could also be used to estimate the relaxation time of the compound from measurements below T_B. AC-susceptibility data can be used to evaluate the relaxation time of the compound above T_B, as will be discussed in the next section.

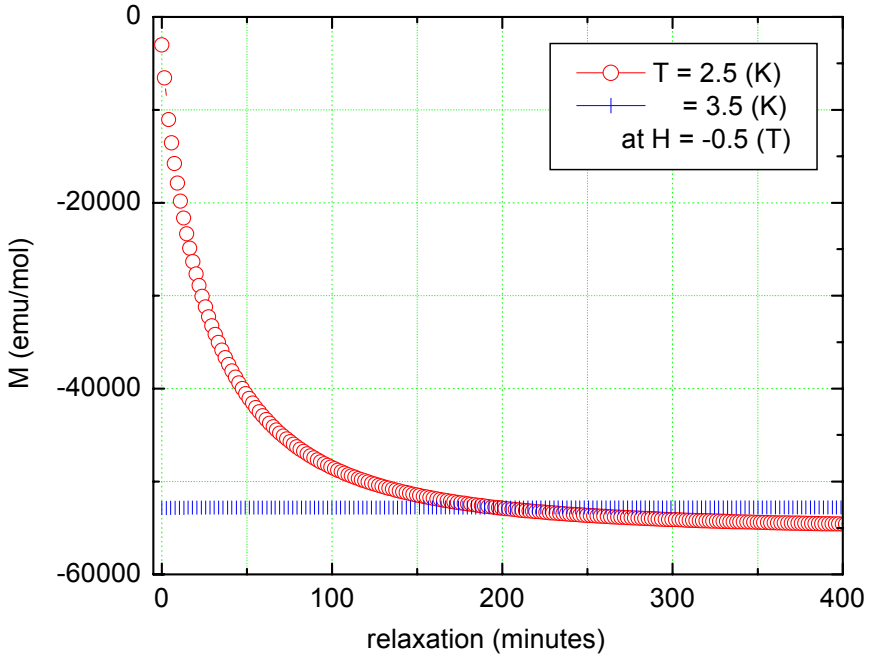

Fig. 1.2. Magnetization relaxation of Mn_{12}-acetate powder at 2.5 K and 3.5 K with applied magnetic field (– 0.5 T). Relaxation is very fast at T = 3.5 K (> T_B) compared to the typical measurement time window. [Data from D. Seo]

At this point, we want to define T_B. The slow magnetization relaxation observed at low temperature is responsible for the difference between Field Cooled (FC) and Zero Field Cooled (ZFC) magnetizations. Fig. 1.3 shows both the FC and ZFC magnetizations of Mn_{12}-acetate powder as a function of temperature. Both curves diverge below ~ 3 K, where the maximum of the ZFC is observed. Experimentally, the peak in the ZFC magnetization curve, which depends on the applied field, corresponds to T_B [16, 17]. T_B is also defined for SMMs as [18]

$T_B = U/[k_B \cdot \ln(t_m/\tau_\circ)]$,

which is derived from the exponential law,

$\tau = \tau_\circ \exp(U/ k_B T)$,

where, $1/\tau_\circ$ = attempt frequency, t_m = typical measurement time and k_B = Boltzmann constant. This exponential law describes well the spin dynamics of superparamagnets like SMMs [19]. For example, U/k_B = 67 K for Mn_{12}-acetate and with t_m = 100 seconds and $\tau_\circ = 3 \times 10^{-7}$ seconds, $T_B \sim 3.4$ K, which is normally observed in the ZFC curve of Mn_{12}-acetate. The blocking temperature corresponds to the temperature where the relaxation time of the magnetization equals the characteristic time of the experiment because T_B depends on t_m as well as U/k_B. Above T_B, the magnetization direction of the SMMs will fluctuate randomly in absence of any external magnetic field. This effect is called "superparamagnetism" [17, 20]. Below T_B, however, molecules show bistability in which the magnetization becomes frozen in one of two potential wells. This bistability of the SMMs promise the realization of the smallest practical unit for magnetic memory at low temperature.

Although some important properties of SMMs are discussed with only magnetization data, various experiments including Nuclear Magnetic Resonance (NMR) [21], Electron Paramagnetic Resonance (EPR) [22], neutron scattering [23], optical [24], and thermal [25, 26] measurements are continuing for fundamental studies of SMMs.

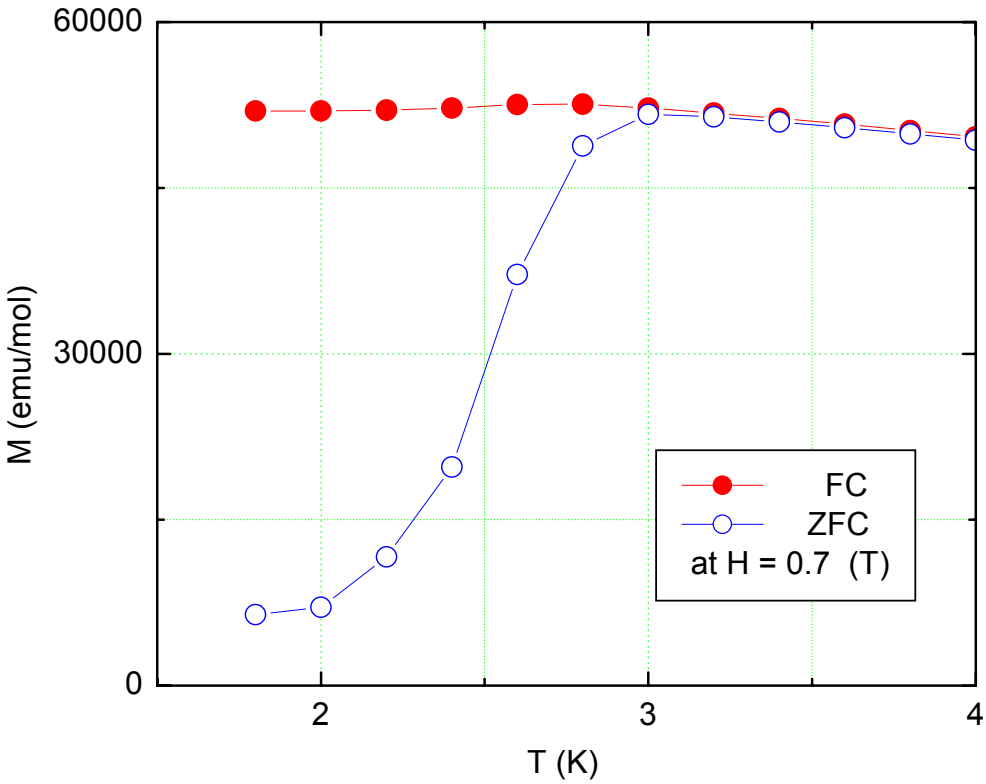

Fig. 1.3. Field Cooled (FC) and Zero Field Cooled (ZFC) magnetization of Mn_{12}-acetate powder at H = 0.7 T. Both curves diverge below ~ 3 K, where the ZFC magnetization shows a maximum of the curve. [Data from D. Seo]

SMMs have advantages over traditional magnets such as: solubility in organic solvents, small size, uniform size, and crystallization [6]. Two main studies in this dissertation (chapter III and chapter IV) were made possible by the presence of those properties in Mn_{12}-acetate SMM. The magnetic alignment of Mn_{12}-acetate micro-crystals in organic solvent was possible because of the crystallization of the compound. Thin film deposition to surfaces in the molecular dimension was possible because of the solubility of Mn_{12}-acetate SMM in organic solvents.

1.3 Background on Mn_{12}-acetate

$[Mn_{12}O_{12}(CH_3COO)_{16}(H_2O)_4]\cdot 2CH_3COOH\cdot 4H_2O$ (Mn_{12}-acetate) is the most studied SMM [7]. The physical and chemical properties of the Mn_{12}-acetate, described below, make this system well suited for studies of quantum phenomena at the nanoscopic scale at low temperature. Magnetism in transition-metal ions (like the Mn ions in a Mn_{12}-acetate molecule) arises from unpaired spins residing in the d-orbital. Four Mn^{IV} ($3d^3$, S = 3/2) ions in a central tetrahedron are ferromagnetically coupled to give S = 6 and the surrounding eight Mn^{III} ($3d^4$, S = 2) ions are also ferromagnetically coupled for a total of S = 16 in a Mn_{12}-acetate molecule, as seen in Fig. 1.4. These two subsystems are antiferromagnetically coupled by oxygen bridges to form the net spin of S = 10 at low temperature and thus each molecule has 2S + 1 = 21 magnetic energy levels [27]. These identical weakly interacting magnetic molecules crystallize into a tetragonal lattice (a = b = 1.73 nm and c = 1.24 nm).

Each molecule shows significant magnetic anisotropy as well as the large-spin ground state of S = 10. The anisotropy splits the energy levels corresponding to different M_s (M_s = - S, - S + 1, …, S - 1, S). The large-spin provides an energy barrier for the reorientation of the spins between "spin-up" and "spin-down" at low temperature. As the magnetic field is cycled, the conversion between +Ms and –Ms levels is very slow and typical relaxation phenomena, such as out-of-phase AC-susceptibility (χ'') signals [1], are observed. Important information about the energy barrier (U/k_B) and the attempt frequency ($\tau_\circ^{-1}$) can be derived from the χ'' signal. A weak oscillating field is applied to a sample to study relaxation dynamics in AC-susceptibility measurements. When the reorientation of the magnetization in the molecule is resonant with the operating frequency, the χ'' signal is observed. The temperature dependence of the relaxation time (τ) is determined from the maximum of each χ'' curve above T_B.

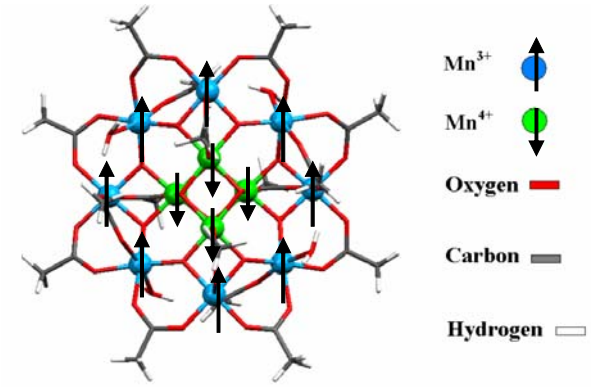

Acta crystallogr. **B 36** (1980) 2042

Fig. 1.4. Structure of the Mn_{12}-acetate molecule. The arrows indicate a possible configuration of the spins. Four Mn^{IV} ($3d^3$, S = 3/2) ions and eight Mn^{III} ($3d^4$, S = 2) ions are magnetically coupled to give S = 10. The molecule also has 16 acetate and 4 water ligands.

The relaxation time below T_B can be derived by relaxation measurements, as discussed in the previous section. Fig.1.5 (a) shows the χ'' signal of Mn_{12}-acetate powder at four different frequencies (1 Hz, 50 Hz, 500 Hz, and 1000 Hz), and (b) shows relaxation time as a function of inverse temperature extracted from the maxima in (a). The relaxation time of the compound is the inverse of the applied frequency at the temperature where the maximum of χ'' is observed. Values of $U/k_B \sim 64$ K and $\tau_\circ \sim 2.6 \times 10^{-7}$ s were obtained from χ'' data in the literature [28], and the dashed line in Fig. 1.5(b) was drawn from these data. Significantly, the near straight line behavior of the data point in (b) illustrates that the relaxation time of Mn_{12}-acetate follows an exponential law or the Arrhenius law, $\tau = \tau_\circ \exp(U/k_BT)$ [28, 29]. The equation for the blocking temperature, $T_B = U/[k_B \cdot \ln(t_m/\tau_\circ)]$, can be applied to Mn_{12}-acetate because the spin dynamics of the compound follows the Arrhenius law.

It is worth mentioning at this point that the magnetization relaxation, FC and ZFC magnetizations, and AC-susceptibility data as in Figs. 1.2, 1.3, and 1.5, respectively can be measured from randomly-oriented Mn_{12}-acetate powder, although relative magnetizations are decreasing from single crystals or an oriented sample. However, hysteresis loop data from randomly-oriented powder are not well suited for the study of the energy levels (spin states), as will be clear below.

Mn_{12}-acetate provides a model system for the study of Quantum Tunneling of the Magnetization (QTM) because of evenly spaced steps in the low temperature hysteresis loops. The hysteresis loops appear due to the slow magnetization relaxation below T_B. The width of the hysteresis loops (coercivity) increases with decreasing temperature.

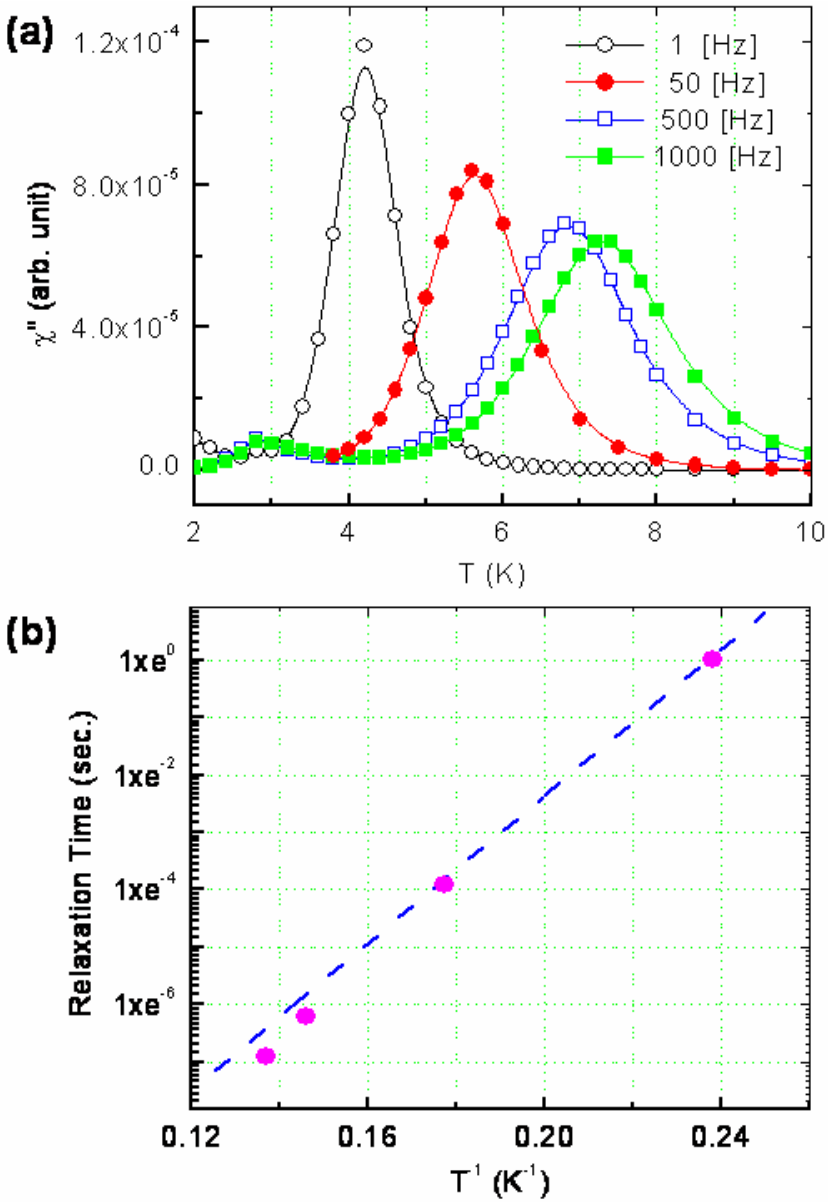

Fig. 1.5. (a) Out-of-phase AC-susceptibility (χ″) signals of Mn_{12}-acetate powder at different frequencies (1 Hz, 50 Hz, 500 Hz, and 1000 Hz) as a function of temperature. (b) Temperature dependence of the relaxation time extracted from the maxima in (a). The dashed line in (b) was drawn based on the results from the literature (U/k_B ~ 64 K and $\tau_\circ$ ~ 2.6 × 10^{-7} s). [Data from D. Seo]

The fact that the hysteresis loops originate from isolated molecules was verified by experiments on frozen, diluted solutions of Mn_{12}-acetate in organic solvents [13, 30, 31]. Magnetization measurements as a function of applied field have been done on single crystals or aligned micro-crystals of Mn_{12}-acetate to observe sharp steps in the hysteresis loops. Fig. 1.6 shows typical hysteresis loops of a Mn_{12}-acetate single crystal at three different temperatures [32]. This hysteresis loop data can be easily understood with the aid of the double-well potential model, as seen in Fig. 1.7. Each sharp step in the loops in Fig. 1.6 can be explained by field-tuned resonant tunneling [33] as shown in Fig. 1.7 (a) and (c), represented by horizontal arrows. The magnetization jump at H = 0.44 T shown in Fig.1.6, for example, corresponds to the energy of the - i^{th} (i = 10, 9,…,2) level matching the energy of the $(i\text{-}1)^{th}$ level across the barrier in the double-well potential scheme as can be checked in Fig. 1.7 (c), where only a few energy levels are shown for simplicity. On the other hand, resonant tunneling is not allowed while the field is sweeping from 0 T to 0.44 T, as shown in Fig. 1.7 (b). The temperature dependent hysteresis loops, Fig. 1.6, shows evidence for thermally assisted tunneling [16, 34], which is also illustrated with vertical arrows in Fig. 1.7. Now, we discuss the origin of the double-well potential diagram.

The double-well potential diagram, used above, is based on a spin Hamiltonian for Mn_{12}-acetate, which is given by [35-37]

$$\mathscr{H} = -DS_z^2 - BS_z^4 - g_z\mu_B H_z S_z + \mathscr{H}' .$$

The zero-field splitting parameter D has been determined by inelastic neutron spectroscopy to be D = 0.548 K and $B = 1.173 \times 10^{-3}$ K. And, g_z is estimated to be 1.94.

Therefore, the energy barrier for the magnetization reversal is ~ 67 K. The third term is the Zeeman energy for fields applied parallel to the easy axis. $\mathcal{H}'$ represents small terms that produce tunneling by breaking the axial symmetry. $\mathcal{H}''$ is due to transverse fields and higher-order magnetic anisotropies [36, 38, 39].

Not only of fundamental interest (e.g. QTM) of the Mn_{12}-acetate, it also has been considered for future applications such as quantum computing and information storage devices, which utilize these interesting magnetic properties [40, 41].

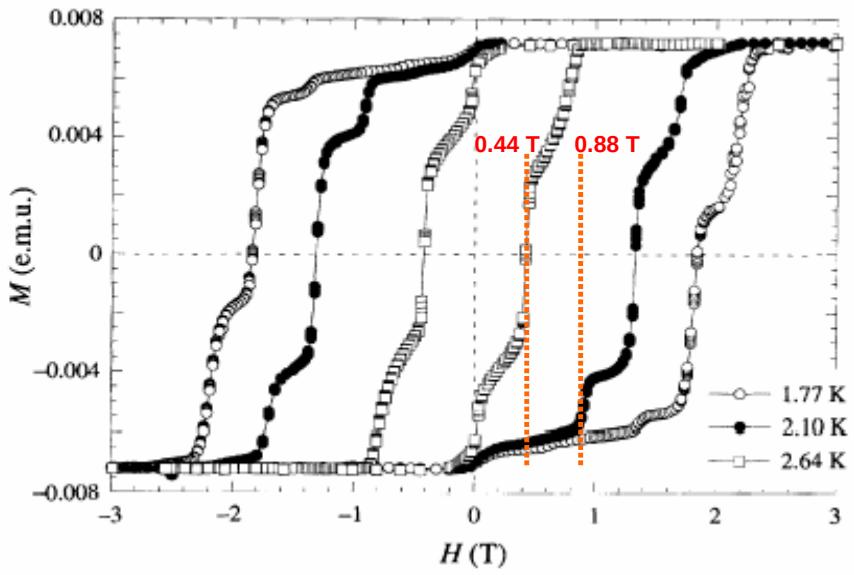

Nature **383**, (1996) 145

Fig. 1.6. Magnetization versus magnetic field hysteresis loops of Mn_{12}-acetate single crystal at 1.77 K, 2.1 K, and 2.64 K. The magnetic field was applied along the tetragonal axis of the crystal, which is the magnetic easy axis of Mn_{12}-acetate. Resonant magnetization tunneling is allowed at evenly spaced fields (0.44 T, 0.88 T, and so forth), where sharp steps are observed as indicated by dashed lines.

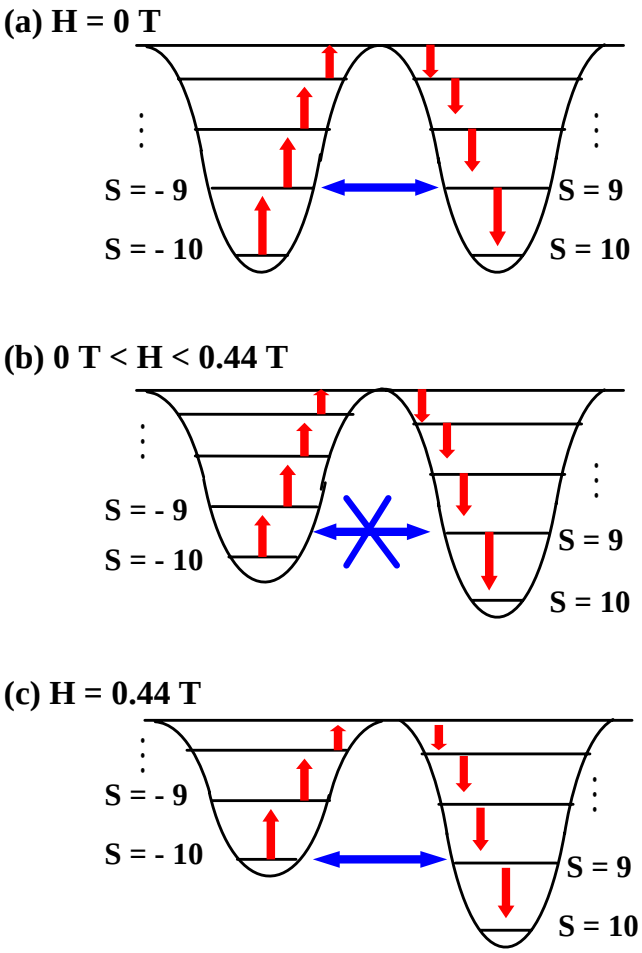

Fig. 1.7. The drawing depicts how double-well potential (longitudinal terms) changes as the magnetic field (Zeeman term) is swept from H = 0 T to H = 0.44 T. Resonant magnetization tunneling occurs when the energy levels on the opposite parts of the wells coincide as in (a) and (c), while it is not allowed in (b). Vertical arrows represent thermally-assisted tunneling over the barrier.

CHAPTER II

EXPERIMENTAL

Experimental details for the studies presented in this dissertation will be discussed in this chapter. Three separate main studies of 'Magnetic alignment of Mn_{12}-acetate micro-crystals', 'Thin film of Mn_{12}-acetate', and 'Magnetization of the film material' will be discussed together as the same facilities have been used for those studies.

Suspension samples and thin films were prepared in an environmental fume hood. A SQUID magnetometer was accessed in Dr. Dunbar's group. Atomic Force Microscopy (AFM), Scanning Tunneling Microscopy (STM), and X-ray photoelectron spectroscopy (XPS) were accessed in the Materials Characterization Facility. A Scanning Electron Microscope (SEM) and a thermal evaporator were used in the Nanolab. Mass spectroscopy data were acquired at the Laboratory for Biological Mass Spectrometry in the Chemistry department.

Some detailed measurement parameters in the SQUID and the STM measurements are included for the benefit of a reader who wants to do similar measurements. It is recommended to refer to the respective manuals to learn about detailed usage of those parameters.

2.1 Suspension Alignment in a Capsule

The preparation of suspension samples (an oversaturated Mn_{12}-acetate solution), solution sample containers (a capsule and a mini "bucket") for the magnetic

measurements, and a magnetic alignment process of the suspension will be described in this section.

- Suspension Preparation

Starting material of Mn_{12}-acetate powder was prepared by Dr. Hanhua Zhao in Dr. Dunbar's group, our collaborator in the Chemistry department at Texas A&M University. Typically, 15 to 20 mg of Mn_{12}-acetate powder was dissolved in 10 ml of isopropanol ($CH_3CHOHCH_3$) to produce the suspension sample. A few repetitions of manual agitation and sonication were used to homogenize the distribution of the suspension in the solvent.

It should be noted that if the concentration of Mn_{12}-acetate solution is less than 15 mg/10 mL, the sample does not give a clean signal. Also, if the solution is not used within ~ 10 minutes, settling may occur. Low signal-to-noise is a result of either low concentration or settling of the suspension. If there is a negative diamagnetic background signal of comparable intensity to the positive Mn_{12}-acetate signal, the data acquisition process faces a centering problem in the SQUID magnetometer

Fig. 2.1(a) shows a poor hysteresis loop at 10 mg/10 mL which was used 20 minutes after homogenization. Data is noisy from the centering problem when $|H| \geq 2$ T, which is checked by raw data in the SQUID. Fig. 2.1(b) and (c) show magnetization as a function of a relative position of the sample to the pick-up coil from 0 cm to 4 cm at H = 0.01 T and 2.9 T, respectively. While the maximum of the graph is at ~ 2 cm at relatively low field, as seen in Fig. 2.1(b), it is shifted at relatively high field, as seen in Fig. 2.1(c).

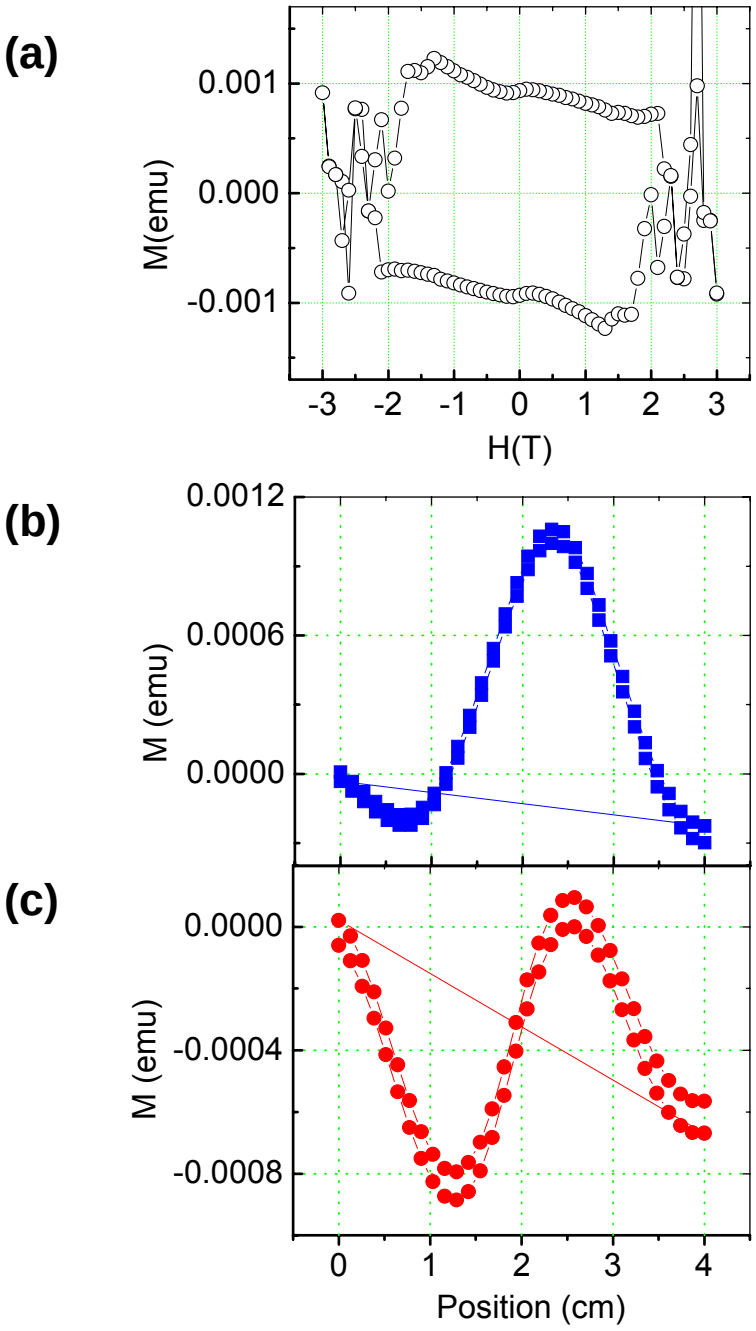

Fig. 2.1 (a). Hysteresis loop of Mn_{12}-acetate solution (10mg/10 mL in isopropanol) after letting the solution settle 20 minutes. Raw magnetization data (b) at H = 0.01 T and (c) at H = 2.9 T. Scan parameters of the two averaged scans and 32 data points can be checked in (b) and (c).

As the field increases, the diamagnetic signal from the capsule increases continuously, but the magnetization of the Mn_{12}-acetate doesn't. Therefore, at relatively high fields, both positive and negative magnetizations are comparable to each other and so the centering faces a problem, as seen in Fig. 2.1 (c).

- Solution Sample Container

A homemade sealed plastic capsule was used as a suspension container for most magnetic measurements in this dissertation. A capsule was prepared from a hypodermic needle cover and a cap from a push pin. Typical weights are 67 mg for the capsule and 35 mg for the capsule cap.

Another solution sample container was available from Quantum Design called 'sealed plastic bucket'. It was checked that using the bucket gives better results than using the capsule mainly due to the bucket containing more suspension than the capsule.

Two hysteresis loops of Mn_{12}-acetate suspensions of similarly concentrated and aligned solutions using both the plastic capsule and the bucket are shown in Fig. 2.2. While the sharper steps come from using the bucket than using the plastic capsule, the bucket has a problem of potential leakage during measurements. Strong glue (LOCTITE SUPER GLUE) was used to prevent leakage when the homemade plastic capsule was used. Therefore, results throughout this dissertation were obtained by using the capsule. Fig. 2.3 shows images for the two types of solution sample containers, which are compared with a quarter to show scale.

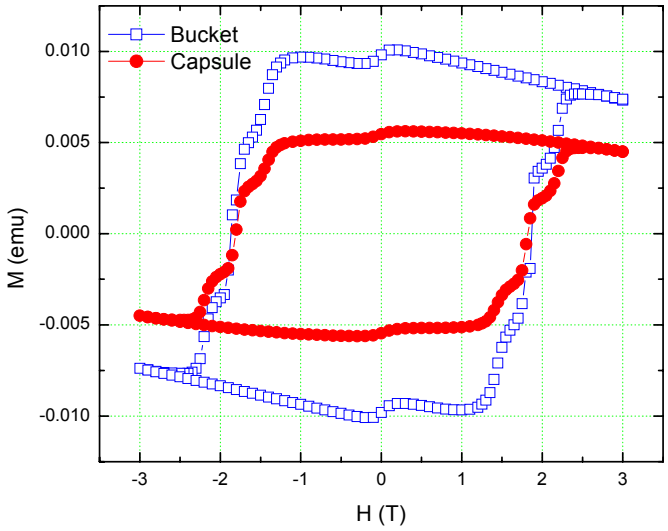

Fig. 2.2. Hysteresis loops of similarly concentrated Mn_{12}-acetate solution in both the bucket and the capsule. The solution in the bucket shows sharper steps than the capsule. Negative slopes in both loops come from the diamagnetic background signal from each of the solution containers.

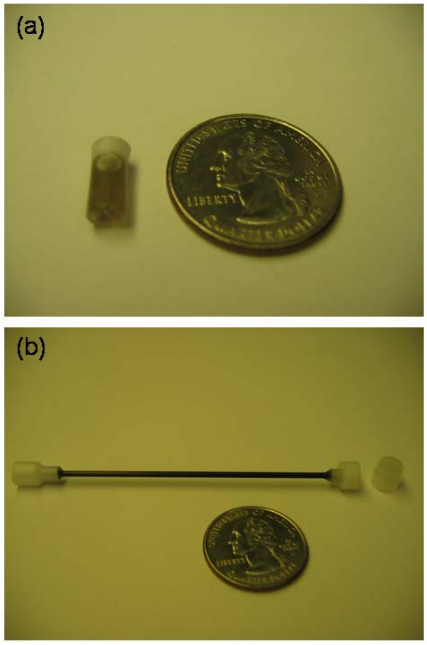

Fig. 2.3. (a) A home made plastic capsule with a cap and (b) a commercial sealed plastic bucket. A quarter is shown for scale comparison of both solution containers.

- Suspension Alignment

For the magnetic alignment, the capsule with the suspension was inserted into the sample space of the SQUID with the appropriate magnetic field, typically 0.5 T applied. Just after loading the sample, the system was cooled down to well below a freezing point of the solvent (185 K). Various magnetic fields (0 T ~ 5 T) were applied at room temperature to study the range of the magnetic alignment as a function of external magnetic fields (as will be discussed in 3.3.2). Also, a magnetic field of 0.5 T was applied at various temperatures to determine the temperature range where the magnetic alignment occurs.

2.2 Thin Film and 'Film Material' Preparation

Mn_{12}-acetate thin films have been deposited on Si/SiO_2 and Highly Ordered Pyrolytic Graphite (HOPG) by the solution evaporation method [42]. So called 'Film material' has been introduced for magnetic studies as magnetic measurements were not successful on Mn_{12}-acetate thin films.

2.2.1 Thin Film Deposition on Si/SiO_2

A fresh sample of Mn_{12}-acetate was prepared by Dr Dunbar's group in the Chemistry Department. For a typical preparation of films described below by the solution evaporation method, 2.2 ± 0.1 mg of Mn_{12}-acetate was dissolved in 10 ml of acetonitrile (CH_3CN) to produce a 1.1×10^{-4} M solution [Appendix C]. Simple manual agitation was used to dissolve the compound in acetonitrile. Prior to the solution evaporation method, the Si/SiO_2 substrate was rinsed with acetone and isopropanol. The clean wafer was

dipped in the prepared Mn_{12}-acetate solution and immediately removed. Accumulation of the solution on the side of the surface was removed by Kimwipes immediately after removing the substrates from the solution. The solution remaining on the substrate dried within a few seconds to produce a thin film of Mn_{12}-acetate. All procedures were carried out inside a fume hood under ambient conditions. If isopropanol was used instead of acetonitrile [appendix D], both manual agitation and sonication were used to dissolve molecules in the solvent as the isopropanol is milder than the acetonitrile. Dissolution of the compound was confirmed by an absence of visible micro-crystals, which start settling down within ~ 10 minutes after mixing.

2.2.2 Thin Film Deposition on HOPG

A thin film deposition procedure similar to that for Si/SiO_2 has been adopted for the HOPG. The only difference is the substrate preparation. The newly cleaved HOPG was attached on a metal disk using double-sided tape and dipped in the prepared solution.

While two types of commercial HOPG were tried for thin film formation, SPI-2 Grade (SPI Supplies) gave better results than ZYB Grade (MikroMasch). Isopropanol does not form high quality thin films on HOPG, so only acetonitrile was used for HOPG based films.

2.2.3 Film Material Preparation

Attempts at acquiring magnetization data using Mn_{12}-acetate thin films directly were not successful due to the small amount of material in the film and the large background signal from the substrate. Therefore, to accumulate sufficient material, a sample for the

magnetization measurements was made by a similar method to the solution evaporation method, but on a larger scale.

A solution of ~ 1×10^{-3} M (21 mg of Mn_{12}-acetate in 10 mg acetonitrile) concentration was prepared in a beaker. Only the top ~ 90 % portion of this solution was used to assure that no sediment was present. Subsequently, this solution was evaporated over the course of 1 hour in a glass Petri dish. The magnetization sample was obtained by scraping the powder from the dish using a razor blade.

2.3 Magnetization Measurements

All of the magnetization data in this dissertation were acquired on a Quantum Design MPMS-XL magnetometer. This Magnetic Property Measurement System (MPMS) is a Superconducting QUantum Interference Device (SQUID)-based magnetometer. Both the basic operation of the SQUID magnetometer and details on the magnetization measurements made with this SQUID will be described in this section.

2.3.1 SQUID Magnetometer

SQUID magnetometry is one of the most sensitive types of magnetometry. The MPMS from Quantum Design is a fully automated SQUID magnetometer. This device combines two physical phenomena: the quantization of the flux in a superconducting loop, and Josephson tunnelling. The SQUID operates over a wide range of temperatures and applied magnetic fields. The sample temperature can be varied from 1.8 K to 400 K and the field ranges from – 7 T to + 7 T. Magnetic moments of a sample are measured by a pickup coil, or gradiometer, in the sample space, which is inductively coupled to the

SQUID, as shown in Fig. 2.4. The SQUID is magnetically shielded from the sample space. Fig. 2.4 (a) shows a DC SQUID which is a superconducting loop formed by two Josephson junctions (marked × in the loop). The Josephson junction is made of two superconducting strips separated by a thin insulating material. As the separation decreases, the strength of the coupling between the two electron-pair waves increases. The tunneling of the electron-pairs across the gap carries with it a superconducting current, and is called Josephson tunneling. The DC SQUID detects very small magnetic fields with resolution up to ~ 10^{-15} T or greater. The high sensitivity of the SQUID is associated with measuring changes in magnetic flux. An external source applies a constant bias current (I) in the loop in order to induce pairs of electrons to tunnel through the junctions. A magnetic field applied to the ring changes the quantum-mechanical phase difference between the two junctions and, as a result, affects the critical current of the SQUID. In practice, the voltage, V, across the SQUID is measured. V oscillates with the changes in phase at the two junctions, which depends on the change of the magnetic flux (Φ). Fig. 2.4 (b) shows the voltage variation for steadily changing magnetic flux. The flux change can be evaluated by counting the voltage oscillations. One period of flux variation ($\Delta\Phi$) corresponds to an increase of one flux quantum:

$\Phi_0 = h/2e \approx 2.07 \times 10^{-15}$ T·m^2.

In practice, a pick-up coil is used to detect the magnetic moment of a sample as the SQUID is too sensitive to measure it. Therefore, a change in magnetic field at the pick-up coil is read out as an output voltage from the SQUID. The MPMS magnetometer pick-up coil takes the form of a second-order gradiometer, as seen in Fig. 2.4 (c), so that

only second and higher order gradients of fields can be measured. This coil set reduces background noise as this does not respond to uniform and first order gradients of fields. Fig. 2.4 (d) shows the SQUID response as a function of sample position, z, when a magnetic sample is moved through the coil set.

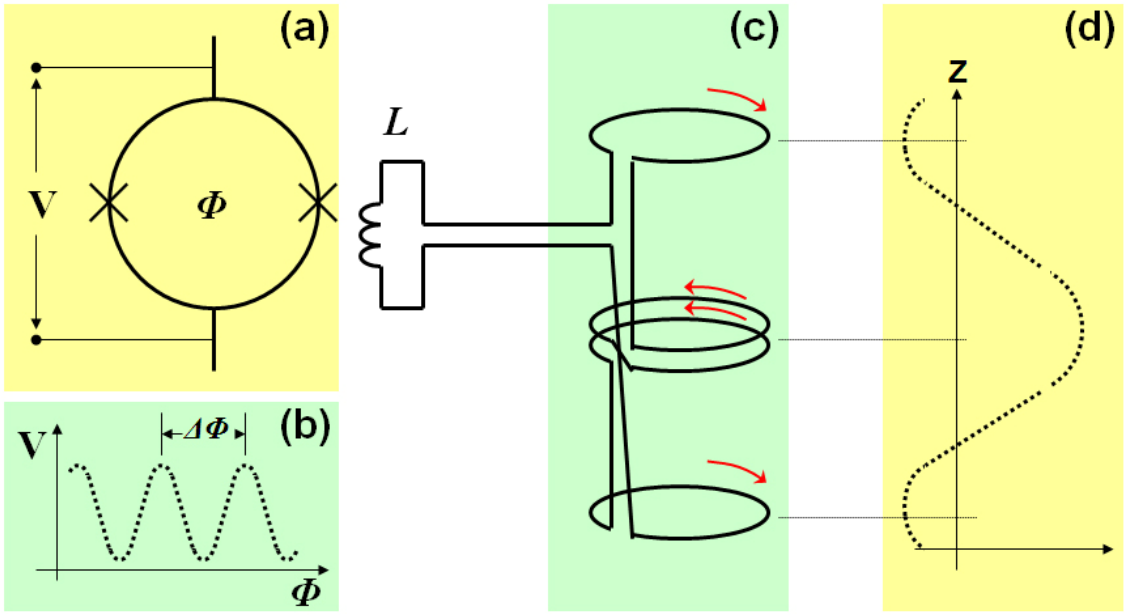

Fig. 2.4. Schematic drawing for (a) the SQUID and (c) second derivative pick-up coil. Both are inductively coupled. (b) Voltage variation in the SQUID for steadily changing field. One period of voltage variation (ΔΦ) corresponds to an increase of one flux quantum (Φ_0). (d) Output signal of the magnetometer as a function of magnetized sample position, z.

2.3.2 Magnetization Measurements

Both hysteresis and DC magnetization were measured on the suspension for the magnetic alignment study. In this case, the background signal of the capsule with pure solvent was acquired separately and subtracted from all the magnetization data to give the pure Mn_{12}-acetate signal.

Field Cooled (FC) and Zero Field Cooled (ZFC) magnetization, AC-susceptibility, and relaxation measurements were done on 'Film Material' in a vinyl bag. A plastic straw was used as a sample holder. Typical scan parameters such as scan length 4 cm, 2 scans for averaging, and 32 data points were used.

- Hysteresis: Hysteresis loops were taken between – 3 T and + 3 T at 1.8 K. 'Oscillate mode' for the field sweep rather than 'hysteresis mode' and 'no overshoot mode' was used to obtain accurate magnetic fields.
- DC magnetization: The sample was cooled down to 2 K at 0.5 T and the magnetic moment was measured from 2 K to 300 K during warm up, which is same as the FC magnetization below.
- ZFC and FC magnetization: DC magnetization as a function of temperature has two different measurements. In the ZFC measurement, the sample is cooled to a lowest temperature in zero field (1.8 K in our system). The magnetic field (10 Oe ~ 5000 Oe) is turned on at the base temperature and measurements are taken as the temperature is raised. For the FC magnetization, the system is cooled to 1.8 K with an applied field of (10 Oe ~ 5000 Oe) and magnetic moments were measured during warm up.

• AC-susceptibility: A sample was cooled to 1.8 K in zero field. A weak oscillating field (3 Oe or 5 Oe) with frequencies 1 Hz to 1000 Hz was applied and magnetic moments were measured during warm up.

• Relaxation: The sample was cooled to the desired temperature in zero field, and the magnetization of the sample was saturated by applying a field of 5 T. The field was then decreased to the desired measuring field (– 0.5 T in this dissertation) and magnetization was measured as a function of time.

2.4 Microscopy Measurements

An Atomic Force Microscope (AFM) was used to characterize Mn_{12}-acetate thin films deposited on a Si/SiO_2 surface. A Scanning Tunneling Microscope (STM) was used for HOPG based film characterizations. A Scanning Electron Microscope (JEOL JSM-6460) and an optical microscope, which is available in the AFM system, were used to characterize the Mn_{12}-acetate micro-crystals deposited on Si/SiO_2 from a suspension. Basic principles for both AFM and STM will be given as these were the main techniques used for surface characterizations of Mn_{12}-acetate thin films.

2.4.1 Basics of AFM and STM

An AFM probes the surface of a sample, which can be an insulator, conductor, or semiconductors, with a sharp tip with a radius of curvature on the order of nanometers [43]. The tip is located at the free end of a cantilever that is some hundreds of micrometers long and a few micrometers wide. When the tip is brought into proximity of a sample surface, the force between the tip and the sample surface causes the cantilever

to bend. The cantilever deflection is measured by a photo detector as seen in Fig.2.5 (a), and a computer generates the surface topography. The force most commonly associated with the AFM is an interatomic force. This force is also known as total [44] van der Waals force or Lennard-Jones potential, which includes an attractive force at long ranges and a repulsive force at short ranges. The dependence of this van der Waals force on the tip-to-sample distance is shown in Fig. 2.5 (b). In the contact regime, the tip-to-sample distance is a few angstroms, and the interatomic force between the tip and the sample is repulsive. Contact mode (static mode) is used for AFM in this force regime. An attractive van der Waals force between the tip and the sample is acting in the non-contact regime, where the distance is a few tens to hundreds of angstroms. In the dynamic modes, which include non-contact and intermittent-contact (tapping) modes, the cantilever is externally oscillated at its resonance frequency. The modified resonance as well as oscillation amplitude and phase due to the tip-sample interaction force are used to make an image of the sample surface. Very soft and fragile samples can be imaged with the tapping mode, which oscillates a stiff cantilever closer to the sample, and hence shows better resolution than in non-contact or contact modes.

STM is a non-optical microscope, like AFM, that scans a probe (tip) over a surface to detect a weak electric current flowing between the tip and the surface. The STM uses a sharpened tip with a bias voltage applied between the tip and the sample, as seen in Fig. 2.6 (a). When the tip is brought within about 1 nm of the sample, electrons tunnel through the potential barrier between the tip and the sample surface [45]. Both the tip and the sample must be conducting carriers in order for tunneling to be investigated. The

magnitude of a tunneling current is exponentially dependent on the distance between the tip and the surface. This exponential dependence gives STM sub-angstrom precision vertically and atomic resolution laterally. There are two types of modes for STM measurements, as shown in Fig. 2.6 (b). In constant height mode, while the tip is maintained to make the distance between the tip and the sample surface constant, the tunneling current is measured. This mode is useful for relatively smooth surfaces and the measurement can be made faster in this mode. In constant current mode, the tunneling current is held set constant by adjusting the height of the scanner or sample at each point, and the height is measured. This mode can measure rougher surface, but takes more measuring time than the constant height mode.

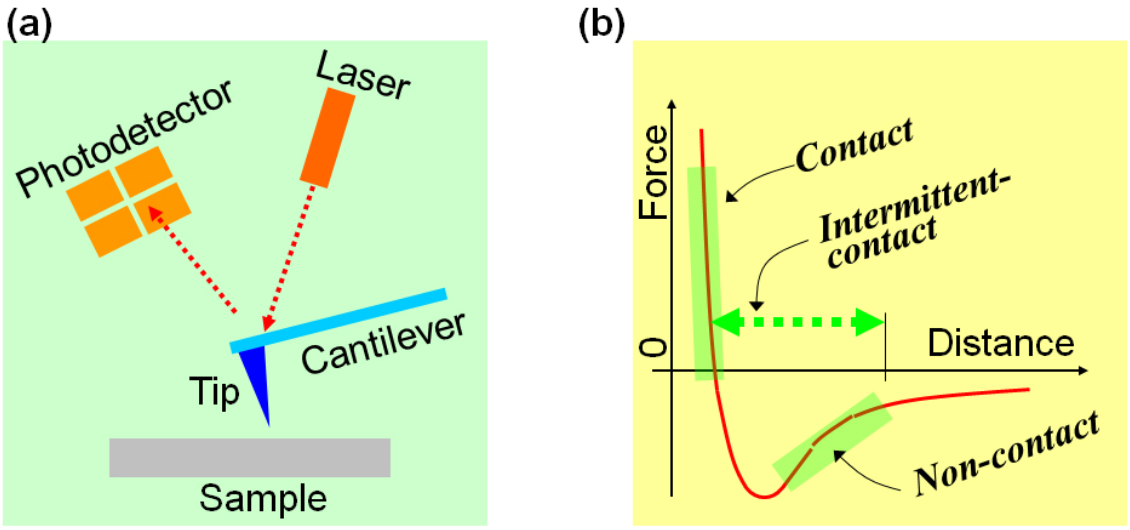

Fig. 2.5. (a) Schematic drawing of AFM operation. (b) Total van der Waals force as a function of the distance between a tip and a sample.

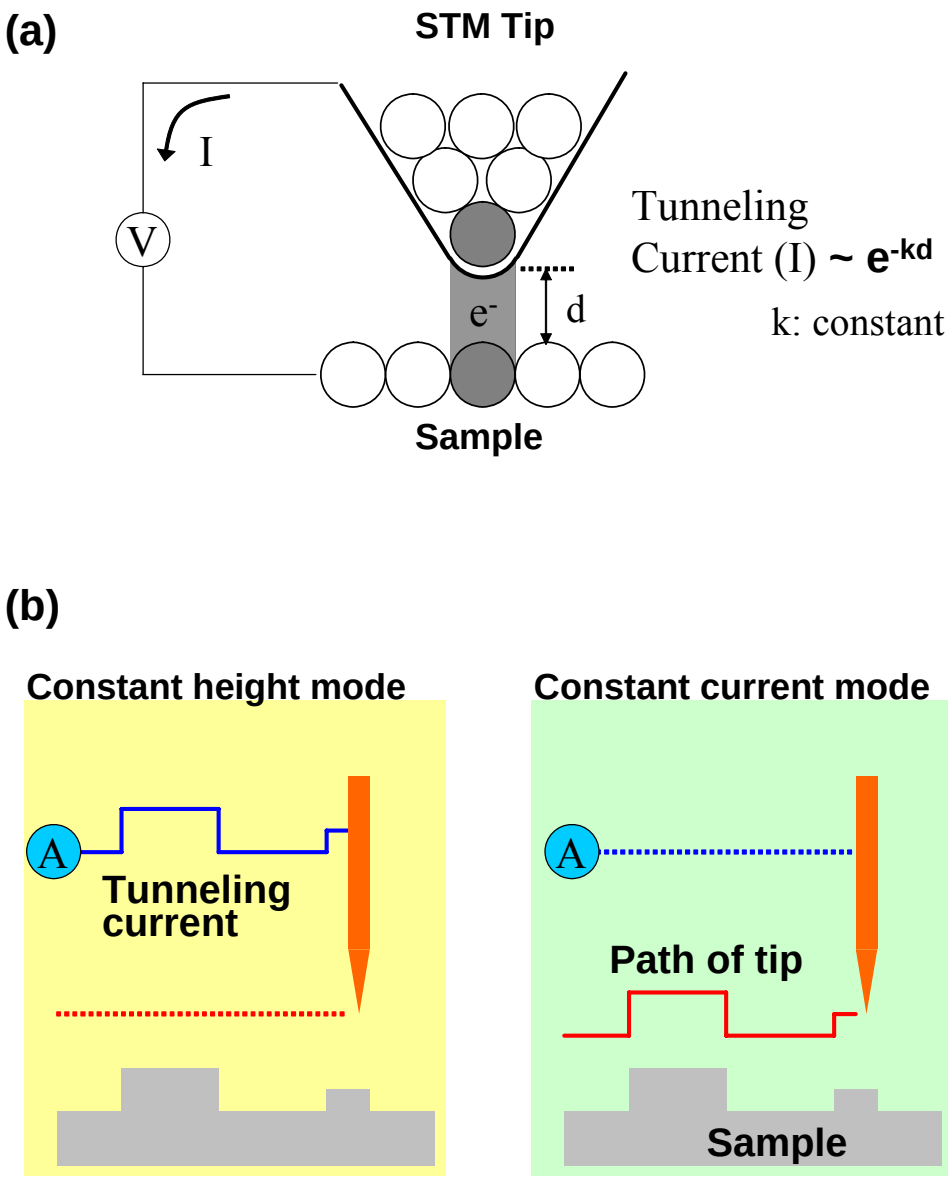

Fig. 2.6. (a) Schematic drawing for STM operation. (b) Comparison of the constant height and constant current modes for STM.

2.4.2 AFM Measurements

AFM images were acquired on a Digital Instruments Nanoscope IIIa. The AFM images were acquired in the tapping mode with a silicon cantilever and tip at room temperature and under ambient conditions. Typical parameters are scan size: 0.2 ~ 3 μm, scan rate: 1 Hz, integral gain: 0.04, proportional gain: 1.2, and amplitude setpoint: 1.6 V. An AFM image of Si/SiO_2 is shown in Fig. 2.7 as a reference with 1 × 1 μm^2 scan size and a vertical scale of 5 nm. A flat surface except for electronic noise on the order of less than 0.2 nm was observed.

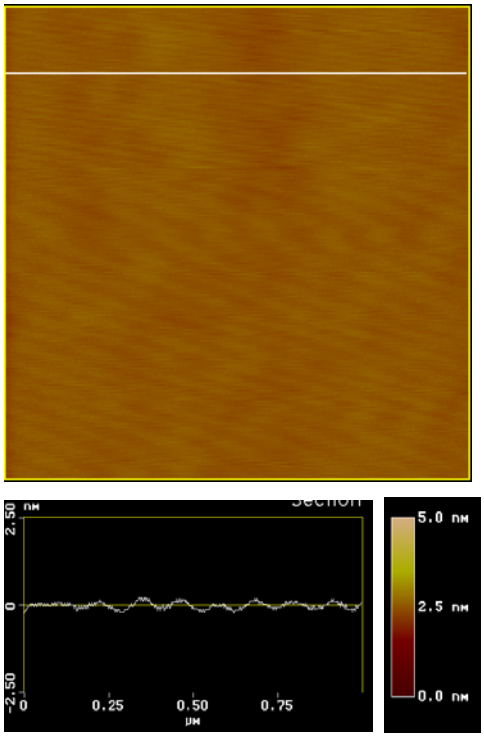

Fig. 2.7. Topographical top-view of a Si/SiO_2 substrate with 1 × 1 μm^2 scan size. The height profile, which is taken in the top-view indicated by the white line, is shown in the bottom. The height scale bar of 5 nm is shown in the bottom right.

2.4.3 STM Measurements

STM images were acquired using mechanically sharpened commercial Pt/Ir tips. While the same infrastructure system was used for both AFM and STM measurements, the 'A' scanner was used for STM measurements and the 'J' scanner for AFM measurements. Scan size was less than 400 nm in the STM measurements.

The constant-height mode that records tunneling current was used for pure HOPG images. Typical parameters for this case are scan size: 3 ~ 20 nm, scan rate: 61 Hz, current setpoint: 500 pA, integral gain: 0.01, proportional gain: 0.2, and bias: 50 mV. The constant-current mode that records height of the sample as the tip is scanning was adopted for Mn_{12}-acetate thin films. Typical parameters for this case are scan size: 50 ~ 90 nm, scan rate: 4 ~ 10 Hz, current setpoint: 10 pA, integral gain: 2, proportional gain: 3, and bias: 900 ~ 1200 mV. Relatively low scan rate and current setpoint, and high sample bias were required as Mn_{12}-acetate films have poor conductivity.

To ensure the tip was sharp enough, the parameters were optimized to observe the carbon atoms of the HOPG surface before or during any measurements. Typical STM images of HOPG are shown in Fig. 2.8 as 10×10 nm^2 and 2×2 nm^2 scans, respectively. The distortion of the hexagonal structure, especially in Fig. 2.8 (b), could be improved by further reduction of environmental vibration or noise. Low temperature and UHV conditions may also help to reduce electrical noise, thus showing the hexagonal structure more clearly.

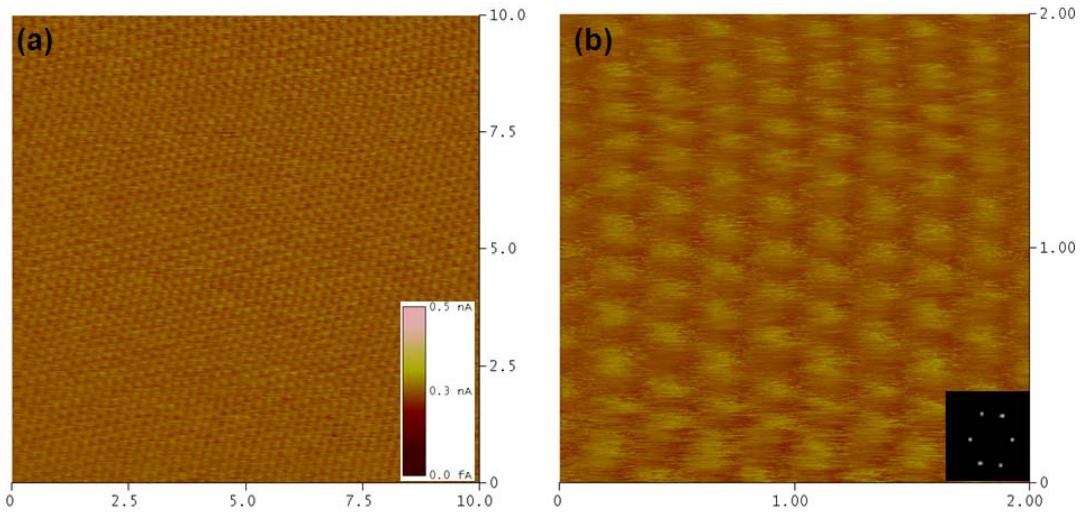

Fig. 2.8. Constant-height STM images of the HOPG surface. Scan areas are 10 × 10 nm^2 (a) and 2 × 2 nm^2 (b), respectively. The current scale of 0.5 nA for both images is shown on the right side in (a). The Fourier transformation (Spectrum 2D) of the image (b) is shown in the right bottom in (b) to confirm the hexagonal structure of the HOPG.

2.5 Other Measurements

X-ray photoelectron spectroscopy (XPS) measurements were carried out to analyze the electronic structure and chemical composition of the Mn_{12}-acetate thin films. XPS measurements were carried out on both thin films and as-produced Mn_{12}-acetate for comparison. Room temperature core level XPS measurements were performed using a Kratos AXIS ULTRA spectrometer equipped with a concentric hemispherical analyzer using the Al Kα radiation (hν=1486.6 eV) and a base pressure of ~ 2×10^{-8} Torr. The binding energies were calibrated with respect to the C 1s peak (284.8 eV) [46].

Electrospray ionization mass spectrometry (ESI-MS) data was used to understand the effect of acetonitrile on Mn_{12}-acetate molecules. ESI-MS data were obtained on a PE SCIEX QSTAR instrument in the chemistry department. In this case, a relatively low concentrated Mn_{12}-acetate solution in acetonitrile (~ 1.3×10^{-5} M) was used to make sure that the signal comes from the monodispersed Mn_{12}-acetate molecules in the solvent.

CHAPTER III

ALIGNMENT OF Mn_{12}-ACETATE

3.1 Introduction and Motivation

The dependence of magnetic properties on a preferred direction is called magnetic anisotropy, which is mainly affected by magnetocrystallinity (crystal structure), shape (grain shape), and stress (applied or residual stresses) [47-50]. The magnetic anisotropy has been used for magnetic alignment of Single Molecule Magnets (SMMs) [16, 51, 52] and other compounds [53-56].

Most of the measurements of Mn_{12}-acetate have been performed on as-produced powder [5, 28, 29] and large single crystals [32, 38, 57, 58]. Magnetic alignment of Mn_{12}-acetate may be important for three reasons: (1) it allows experiments of interest if a SMM is not available in a big enough single crystal, (2) the alignment process itself is interesting to study because Mn_{12}-acetate shows superparamagnetic behavior (i.e. no or negligible magnetic anisotropy) in the temperature range where alignment happens, and (3) controlling the alignment of dilute Mn_{12}-acetate micro-crystals is a prerequisite for the design and fabrication of aligned arrays or films of such crystals, specifically when combined with various addressing or patterning techniques for Mn_{12} clusters on surfaces [42, 59-62].

To our knowledge no further alignment results have been reported after the initial attempts to align Mn_{12}-acetate micro-crystals in epoxy [16, 51, 52], where alignment was limited by the viscosity of the epoxy matrix and the high temperature of curing.

Magnetic alignment of the Mn_{12}-acetate was motivated by seeing less sharp steps in the hysteresis loops data of aligned Mn_{12}-acetate micro-crystals [16] than single crystals [32]. Enhanced magnetic alignment of Mn_{12}-acetate in organic solvents was attempted in order to obtain sharper steps in the low temperature hysteresis loops [63, 64]. Studies of Mn_{12}-acetate in toluene are shown in Friedman's Ph. D. thesis [64]. These studies show better magnetic alignment as compared to experiments using Stycast 1266 epoxy, but research on the solution samples was discontinued due to a lack of reproducibility of results. As will be clear below (3.3.1), there was no reproducibility problem in our data using isopropanol as a solvent [63].

3.2 Experimental

For a typical preparation of the suspension, ~ 18 mg of Mn_{12}-acetate powder was dissolved in 10 ml of isopropanol ($CH_3CHOHCH_3$) to produce a 8.7×10^{-4} M suspension. Both manual agitation and sonication were used to homogenize the distribution of the suspension in the solvent. Magnetic alignment of the suspension was achieved by applying typically 0.5 T at room temperature, and the temperature was cooled down well below the freezing point of the solvent (185 K) with this constant magnetic field applied. Magnetic measurements were subsequently carried out on a Quantum Design MPMS-XL SQUID magnetometer. M vs. H hysteresis loop data were acquired in fields $|H| \leq 3$ T and below the blocking temperature (~ 3.5 K) [16]. DC magnetization data were acquired in H = 0.5 T over the temperature range 2 ~ 300 K. A home-made sealed plastic capsule was used as a suspension container in the magnetic

measurements. The background signal of the capsule with pure solvent was acquired separately and subtracted from all the magnetization data to give the pure Mn_{12}-acetate signal.

The suspension was also used for the solution evaporation method for film deposition, which will be discussed in the next chapter in detail. Mn_{12}-acetate was deposited onto a Si/SiO_2 surface to check the size distribution of the oversaturated Mn_{12}-acetate solution. After preparation, the surface morphology of the films was studied by Scanning Electron Microscopy (SEM) and Atomic Force Microscopy (AFM). The AFM images were acquired in the tapping mode with a silicon cantilever and tip under ambient conditions on a Digital Instruments Nanoscope IIIa.

3.3 Results and Discussions

3.3.1 Preliminary Data and Discussions

If the reader is interested only in the main results of the magnetic alignment, this subsection could be skipped. However, for understanding the background measurements and/or trying a similar alignment study of Mn_{12}-acetate suspension, this subsection will be useful.

- Background Signal

Both M vs. H at 1.8 K and DC magnetization at 0.5 T of the background signal from the solution container (capsule + lid) with pure solvent were measured as seen in Fig. 3.1. A negative slope in the M vs. H and negative value in the DC magnetization are observed as normally seen from diamagnetic material. The origin of the peak at 50 K in the DC magnetization, which is always seen from the solution container, is not clear but it is an artifact unrelated to Mn_{12}-acetate. This peak does not affect the pure Mn_{12}-acetate signal as was verified by comparing the pure suspension signal with an as-produced Mn_{12}-acetate signal and observing similar behavior from both graphs. Magnetization data of the pure Mn_{12}-acetate suspension were acquired by subtracting these background signals from appropriate original data. It should be noted that the solution container (capsule + lid) was sealed by strong glue (LOCTITE SUPER GLUE) to make sure the solution did not leak. As a result, the capsule can be used only once. Thus, the solution containers for the background signal measurements are not precisely identical to those for Mn_{12}-acetate suspension measurements. Therefore, a small difference between the background signals for each subtraction could be possible even though the solution containers were the same size and weight.

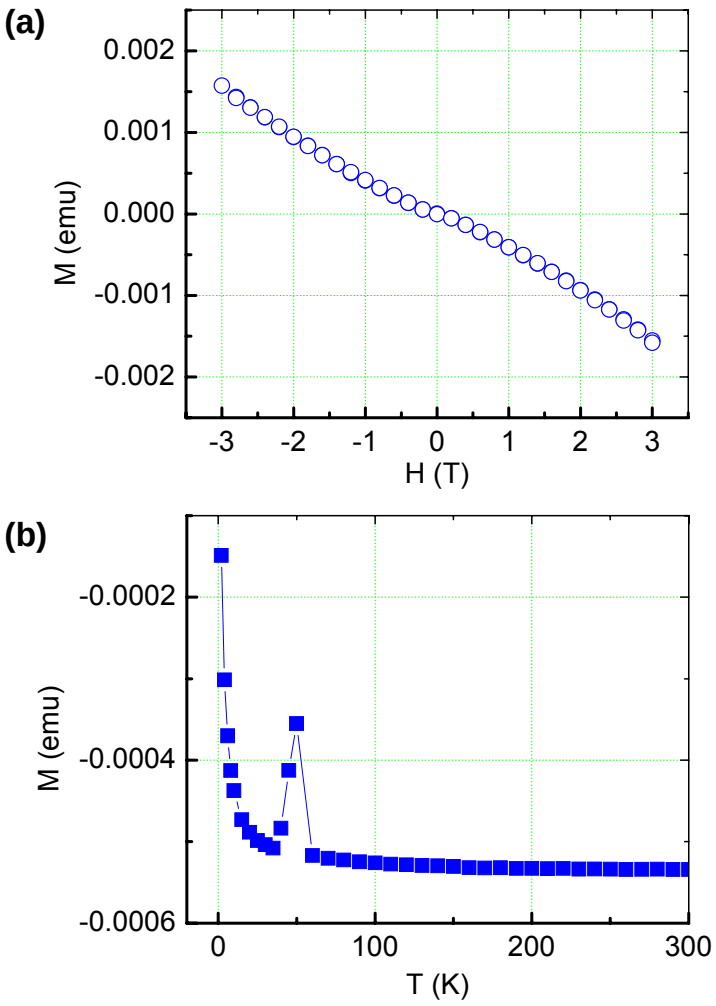

Fig. 3.1. Background signal from the solution container (capsule + lid) with solvent. (a) M vs. H of the background at 1.8 K as a function of magnetic field. (b) DC magnetization of the background at 0.5 T as a function of the temperature (2 K ~ 300 K). The anomalous peak in (b) is always observed from the background. Its origin is not clear.

- Time Evolution of the Magnetization

It was observed by bare eyes that the suspension starts settling down ~ 10 minutes after homogenizing the solution sample. This settlement of micro-crystals may also occur while cooling down the sample from room temperature in the SQUID magnetometer. Therefore, it is necessary to check whether the settlement of the suspension affects the magnetic data. A change in magnetization of the suspension was measured at room temperature as a function of time. Fig. 3.2 (a) shows M vs. time at 300 K, where a gradual decrease of the magnetization (lasting ~ 10 minutes) was observed. However, this magnetization change can be neglected by comparing with the hysteresis loop at 1.8 K and DC magnetization data at 0.5 T on similar suspensions as shown in Fig. 3.2 (b) and (c).

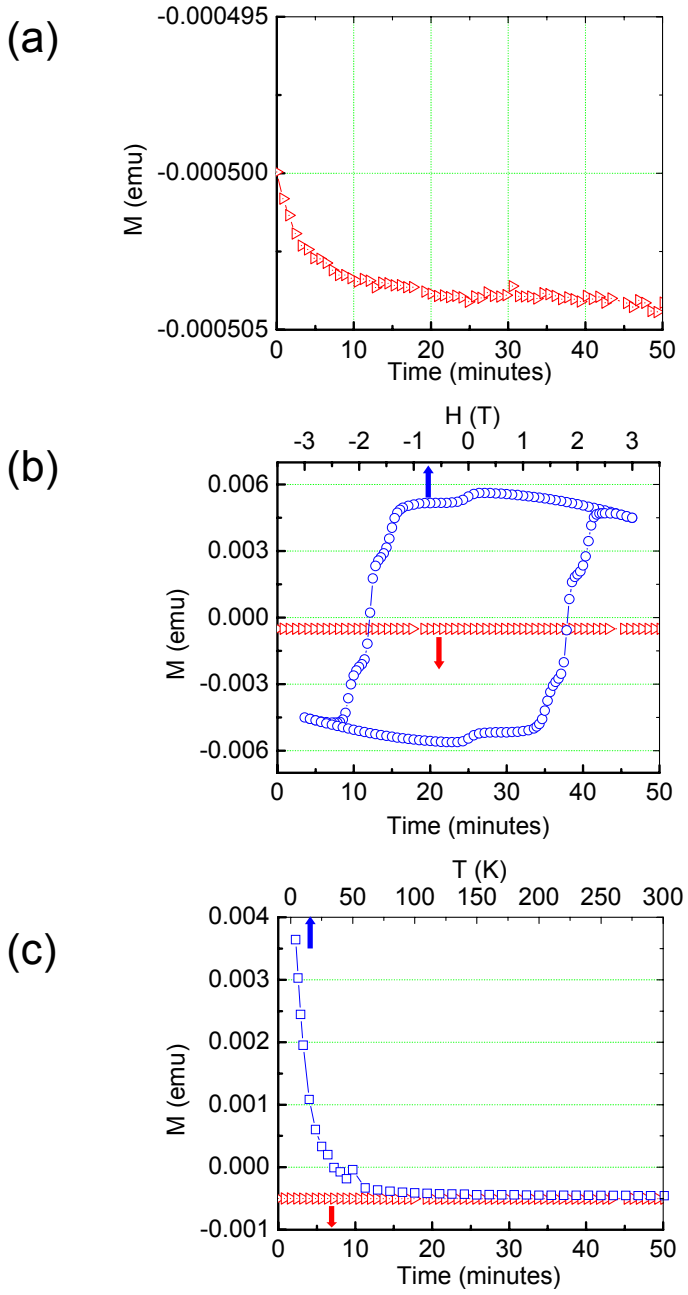

Fig. 3.2 (a) Time evolution of the magnetization of the Mn_{12}-acetate suspension with the background signal at 0.5 T and 300 K. (b) Comparison between the data in (a) and the hysteresis loop of a similar suspension at 1.8 K. (c) Comparison between the data in (a) and DC magnetization data of the similar suspension at 0.5 T. Both comparisons (b) and (c) show that the decrease of the magnetization in the first 10 minutes can be neglected.

- Stability and Reproducibility

The final topic to discuss is the time stability of the sample in the solvent and the reproducibility of the data. A reduction of the magnetization of ~ 17 % and ~ 42 % from the initial value was observed in the hysteresis loops data storing the suspension for 1 and 2 weeks, respectively, as shown in Fig. 3.3. Degradation of the observed magnetization after 1 or 2 weeks may be due to solvent effects on the molecules. However, the magnetization of the suspension did not significantly change within one series of measurements, which were usually completed in less than 3 days.

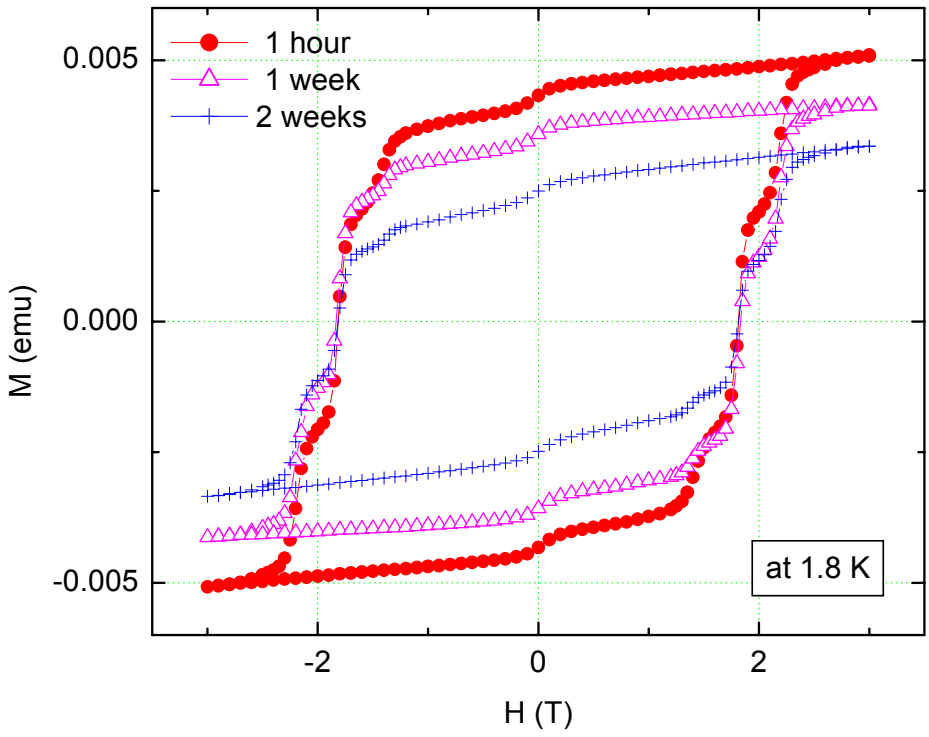

Fig. 3.3. Hysteresis loops at 1.8 K for the Mn_{12}-acetate suspension just after preparation (takes ~ 1 hour before cooling the sample), and after storing 1 and 2 weeks at room temperature.

Reproducibility of the data was verified by obtaining hysteresis loops after re-freezing the suspension from room temperature in the same orientation field. Fig. 3.4 shows hysteresis loops of three aligned states obtained by applying an orientation field (H_{orient}) of 0.5 T at room temperature after each measurement. The hysteresis loop of the randomly-oriented sample, H_{orient} = 0 T at room temperature, compared with the loop from the oriented sample contrasts the difference between two extreme states. Small differences in the oriented states may come from non-homogeneity of the solution container and the suspension distribution.

A small shift of the magnetization was observed when the sample was re-loaded during a series of measurements. A variation of the normalized magnetization ($\Delta M/H$) up to $\sim 1 \times 10^{-8}$ emu·Oe^{-1} was observed [Appendix B], which can be neglected in hysteresis loops studies. However, this small difference is important when investigating the high temperature magnetic anisotropy, as will be discussed in 3.3.3 and Appendix B.

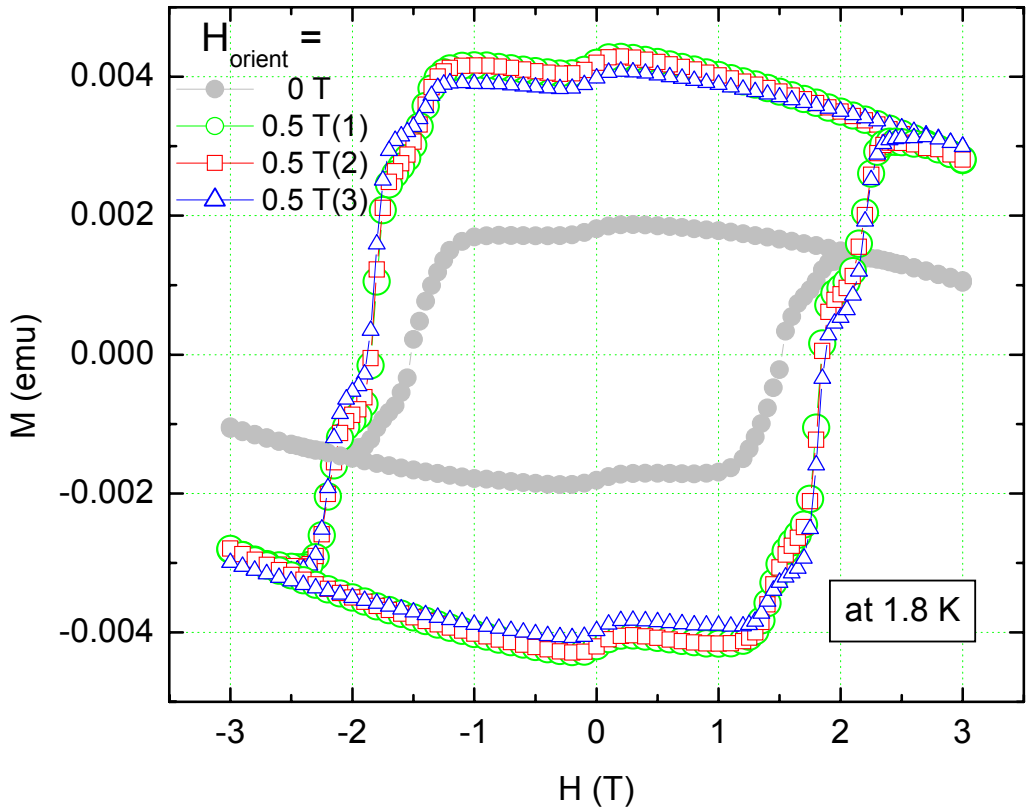

Fig. 3.4. M vs. H hysteresis loops of the suspension at 1.8 K. One is from a randomly-oriented state found by cooling the sample without orientation field (H_{orient} = 0 T). The other three are from well-oriented states found by applying H_{orient} = 0.5 T at room temperature after each measurement. A diamagnetic background signal was not subtracted for all the loops, as a result decrease of the magnetization at higher magnetic fields was observed.

3.3.2 Hysteresis Data

Fig. 3.5 allows characterization of the Mn_{12}-acetate compounds in the sample that was used for the magnetization measurements. Fig. 3.5 (a) shows a schematic diagram of the Mn_{12}-acetate oversaturated solution, in which only micro-crystals and single molecules are shown for simplicity. Fig. 3.5 (b) shows an optical image of a film that was deposited onto Si/SiO_2 by this suspension, where micro-crystals are evenly distributed on the surface. Fig. 3.5 (c) shows an SEM image of a Mn_{12}-acetate micro-crystal with typical size 3×15 μm^2 based on a scale bar of 2 μm. Fig. 3.5 (d) shows an AFM image of a smooth region of the Mn_{12}-acetate film with 1×1 μm^2 scan size. The AFM scans were carried out on the surface of Fig. 3.5 (b) where no micro-crystals are present, which will be discussed in detail in Chapter IV. The number of clusters, which contain > 1 molecule, is increasing as higher concentrated suspensions are used. In fact, the solution used for AFM studies was slightly less concentrated ($\sim 5 \times 10^{-4}$ M) than that used for magnetic measurements (8.7×10^{-4} M) in order to limit the amount of clusters and thus find regions without clusters where the presence of single molecules could be investigated. Fig. 3.5 (e) shows a height profile that was taken at the location indicated by the white line in (d). It indicates roughness on the molecular scale. Taken together, optical, SEM, and AFM images indicate that the oversaturated Mn_{12}-acetate solutions, which have been used for the magnetization studies, are composed of mainly two species; micro-crystals, as seen in the optical and SEM images, and single molecules in between micro-crystals, as seen in the AFM image. Simple energy considerations, by comparing both magnetic and thermal energy for single Mn_{12}-acetate

molecules, show that the magnetic alignment occurs in micro-crystals, not single molecules [appendix A].

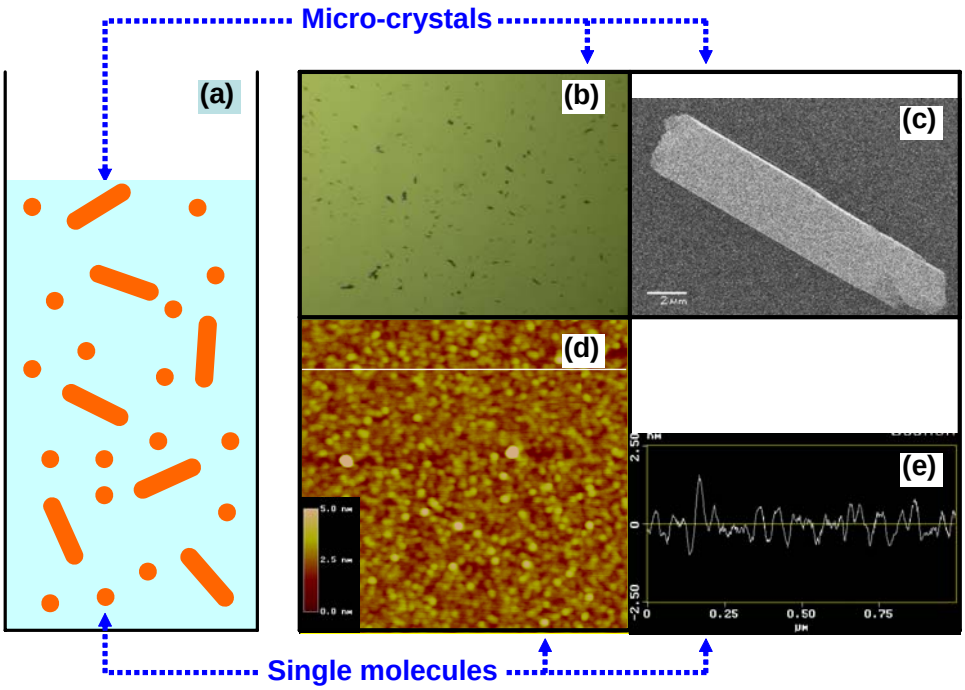

Fig. 3.5. (a) Simplified schematic drawing of the suspension that shows only single molecules and micro-crystals of Mn_{12}-acetate. (b) Optical microscopy image (~ 1 × 1 mm^2) of a film made from the suspension (c) Scanning electron microscopy image of the same sample, which shows a micro-crystal with a typical size of 3 × 15 μm^2. The scale bar shown indicates 2 μm. (d) Atomic force microscopy image (~ 1 × 1 μm^2) of an area in (b) where no micro-crystals are present. The height scale bar (max. = 5 nm) is shown in the corner. (e) A height profile, which is taken along the white line indicated in (d).

Next, the magnetization as a function of magnetic field was studied in the Mn_{12}-acetate suspension (Fig. 3.6). After sealing the suspension in a plastic capsule, a magnetic field of 0.5 T was applied at room temperature. With the constant field applied, the temperature was lowered to 5 K, which is well below the freezing point of the solvent (185 K). This process serves to align the crystal c-axis of the micro-crystals parallel to the external field. Hysteresis loops were then acquired at different temperatures (1.8 K, 2.1 K, 2.4 K, and 2.64 K) as shown in Fig. 3.6 (a). A diamagnetic background signal, resulting from both plastic capsule and solvent, was measured separately without Mn_{12}-acetate (shown in Fig. 3.6 (b)), and subtracted from the original data (a) to give the pure Mn_{12}-acetate signal as shown in Fig. 3.6 (c). Sharp steps in the hysteresis loops, which are typically only observed in large single crystals when spin levels are crossing [32], are observed in Fig. 3.6 (c), indicating significantly better alignment of the Mn_{12}-acetate crystallites than earlier studies [16, 51, 52].

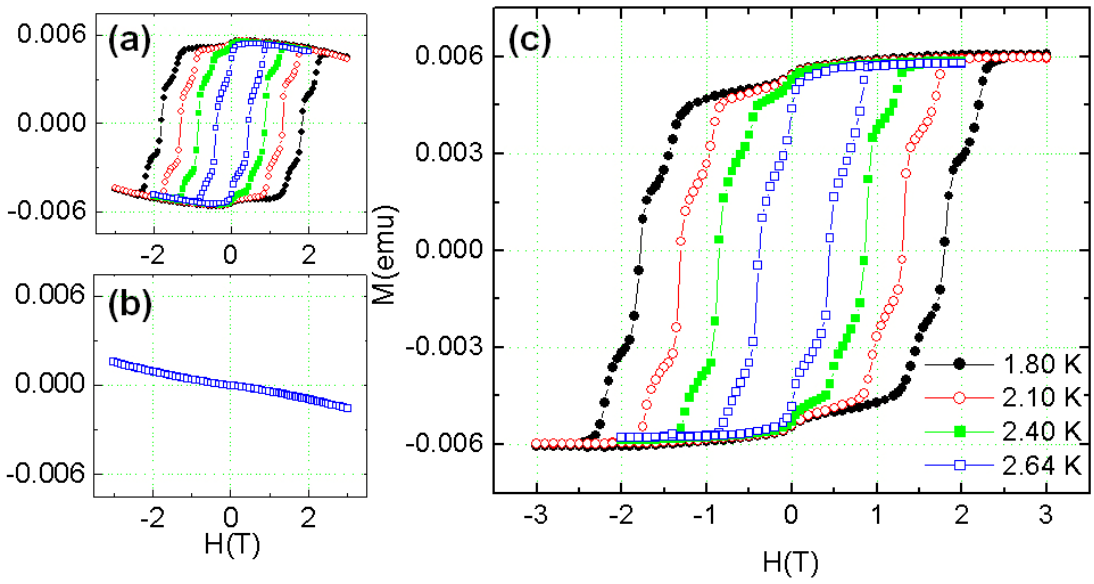

Fig. 3.6. (a) Hysteresis loops from Mn_{12}-acetate suspension in the plastic container at 1.8, 2.1, 2.4, and 2.64 K, respectively. (b) Diamagnetic background signal from the container with solvent at 1.8 K. (c) Hysteresis loops of the pure Mn_{12}-acetate obtained by subtracting the background signal (b) from the original data (a).

Fig. 3.7 (a) shows a series of hysteresis loops of the Mn_{12}-acetate suspension at T = 1.8 K after background subtraction. Sample alignment states ranging from well-aligned to randomly-oriented states of the sample were achieved by applying different orientation fields (H_{orient}), ranging from 0 to 0.5 T, for alignment at room temperature. After applying 0.005 T at room temperature, the hysteresis curve at 1.8 K shows a random Mn_{12}-acetate orientation since it is almost identical with the H_{orient} = 0 T case (cooled without field). Fig. 3.7 (b) shows the magnetization M in Fig. 3.7 (a) at H = 0 T normalized with the magnetization of the H_{orient} = 0.5 T data at H = 0 T as a function of different orientation fields (H_{orient} = 0, 0.05, 0.1, and 0.5 T), respectively for circles. Triangles are used to depict a different series of hysteresis loops for H_{orient} = 0.05, 0.2, 0.5, 1, and 5 T (not shown). As was mentioned in the Stability and Reproducibility section (3.3.1), the relative magnetization of the suspension was slightly reduced by long measurement times well in excess of 3 days presumably due to solvent degradation, which forced two separate series of measurements for the graph of Fig. 3.7 (b). The graph shows that ~ 0.5 T is sufficient to mostly align the Mn_{12}-acetate species, since the relative magnetization does not appreciably increase in higher orientation fields, which is also confirmed in the next subsection (3.3.3). The greater the orientation field (H_{orient}) during alignment, the sharper the steps became in the hysteresis loops. In addition, the saturation magnetization also increases in this range.

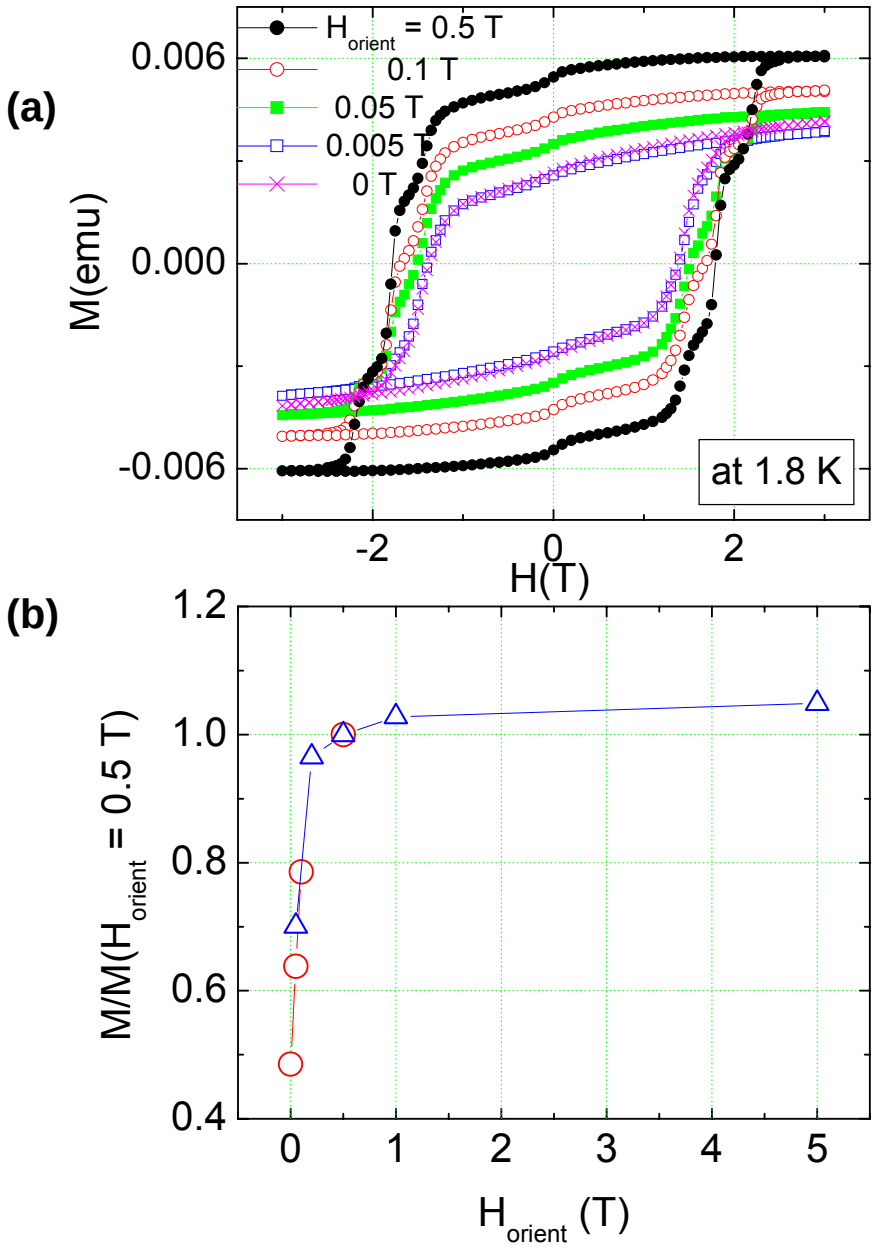

Fig. 3.7. (a) Series of hysteresis loops at 1.8 K for different orientations of the suspension by applying different orientation fields (H_{orient} = 0, 0.005, 0.05, 0.1, and 0.5 T), respectively at room temperature. Both 0 T and 0.005 T cases are overlapping. (b) The magnetizations M at H = 0 T were normalized with magnetization of H_{orient} = 0.5 T at H = 0 T (Circles). (Triangles at H_{orient} = 0.05, 0.2, 0.5, 1, and 5 T are from different series of hysteresis loops, not shown). The line is a guide for the eye.

Fig. 3.8 shows a series of hysteresis loops at T = 1.8 K of a sample that was aligned by applying an orientation field H_{orient} = 0.5 T at different orientation temperatures (T_{orient} = 100, 150, 200, and 250 K), respectively. It should be mentioned that the cooling occurs at a constant rate (10 K/min.) while applying the magnetic field, which takes ~ 2 min. to reach 0.5 T. This means that magnetic field ramp started at 260 K and reached H_{orient} = 0.5 T at ~ 240 K for the case of T_{orient} = 250 K, for example. When applying H_{orient} = 0.5 T at T_{orient} = 200 and 250 K, the loops are similar to the one that was prepared by applying H_{orient} = 0.5 T at 300 K (sharp steps). On the other hand, when applying H_{orient} = 0.5 T at 100 K and to a lesser extent at T_{orient} = 150 K, the loop is similar to the one that is randomly-oriented by cooling without field. These data reveal that the alignment of the suspension is occurring above 100 K, as would be expected since the melting point of isopropanol is T = 185 K. For the case of H_{orient} = 0.5 T at T_{orient} = 150 K, partial alignment may be due to partial freezing in the sample. These data indicate that the alignment indeed occurs in the liquid phase of the matrix solvent. After checking that the alignment is happening above 150 K by applying only 0.5 T at room temperature, the question arose as to the source of the observed alignment. In other word; what is the origin of a high temperature magnetic anisotropy? To answer this question, DC magnetizations were measured on both extreme states (randomly-oriented and well-oriented states) of one sample to see different magnetizations for different orientation states, especially, above 150 K.

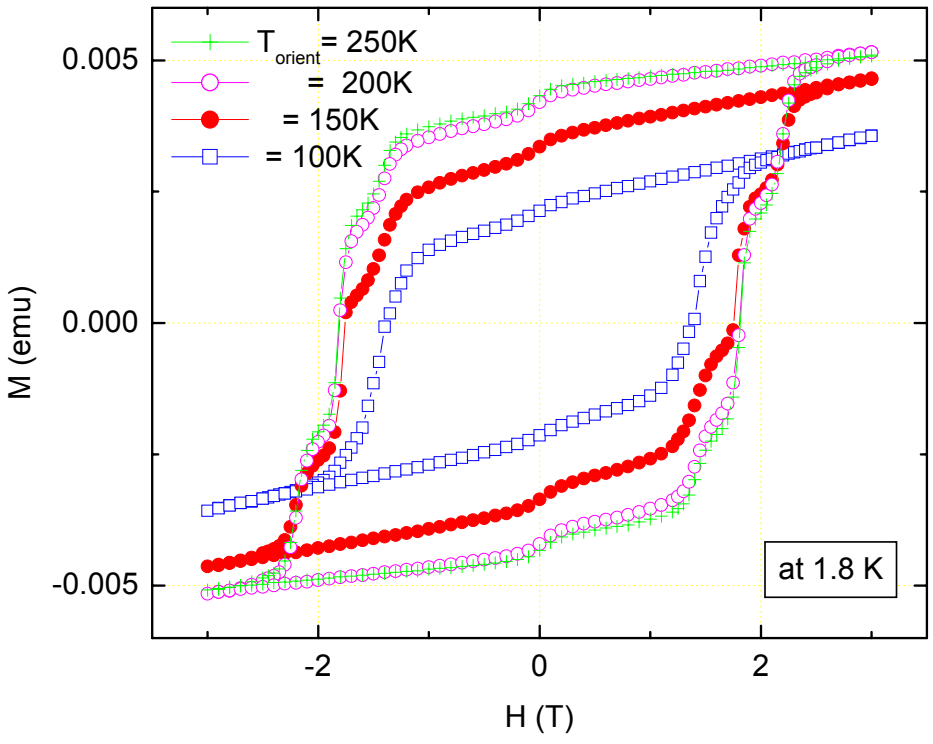

Fig. 3.8. Hysteresis loops at 1.8 K for different degrees of alignment of the Mn_{12}-acetate suspension obtained by applying an orientation field H_{orient} = 0.5 T at different orientation temperatures (T_{orient} = 100, 150, 200, and 250 K).

3.3.3 DC Magnetization Data

Fig. 3.9 shows a series of DC magnetization curves as a function of temperature (2 K ~ 20 K) at a magnetic field of 0.5 T for differently aligned states of one sample. Various orientations of Mn_{12}-acetate micro-crystals in one suspension sample were prepared by applying different orientation fields (H_{orient} = 0, 0.005, 0.05, 0.1, 0.2, 0.5, 1 T) at room temperature. The magnetization curve for H_{orient} = 0.005 T shows a random Mn_{12}-acetate orientation since it is almost identical with the H_{orient} = 0 T case (cooled without field). Also, the curve for H_{orient} = 0.5 T is almost identical with the curve for H_{orient} = 1 T showing that alignment of the suspension is saturated at around 0.5 T. Fig. 3.9 (b) shows the magnetizations (M) at T = 2 K in Fig. 3.9 (a) normalized with the magnetization of the H_{orient} = 1 T data at T = 2 K as a function of different orientation fields (H_{orient} = 0, 0.05, 0.1, 0.2, 0.5 and 1 T), respectively. The graph shows that near perfect alignment of the Mn_{12}-acetate species occurred when a magnetic field ~ 0.5 T was applied, since the relative magnetization does not appreciably increase at higher orientation fields, consistent with the previous hysteresis loops study. This alignment behavior is clearly seen up to T = 20 K in Fig. 3.9 (a).

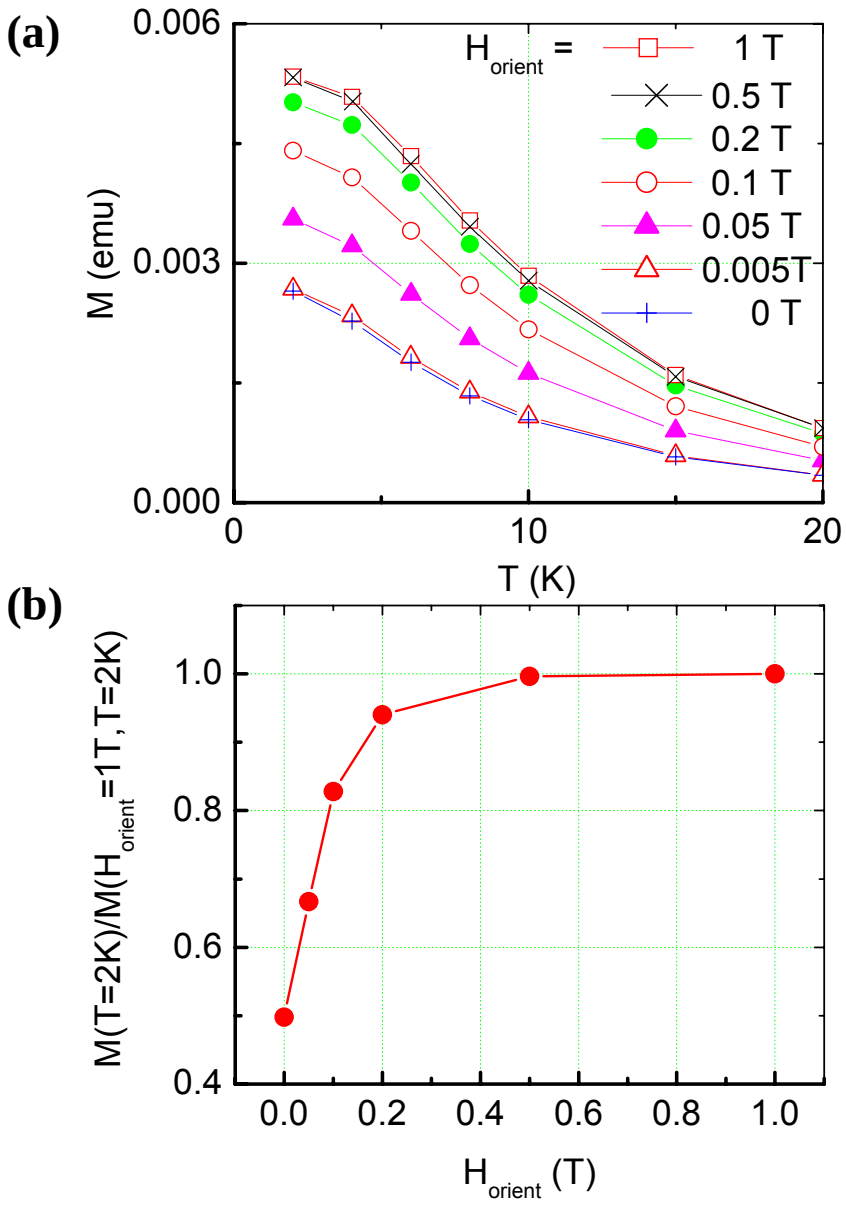

Fig. 3.9. (a) Series of DC magnetizations as a function of temperature (2 ~ 20 K) with a magnetic field of 0.5 T for differently oriented suspension obtained by applying different orientation fields (H_{orient} = 0, 0.005, 0.05, 0.1, 0.2, 0.5 and 1 T), respectively at room temperature. Both 0 T and 0.005 T cases, and 0.5 T and 1 T cases are almost identical, respectively. (b) The magnetization of each state normalized to the case of 1 T as a function of different orientation fields (H_{orient} = 0, 0.05, 0.1, 0.2, 0.5, and 1 T). The line is a guide for the eye.

Fig. 3.10 shows DC magnetizations as a function of temperature (2 K ~ 300 K) at 0.5 T for two extreme states of the suspension sample, which were prepared by applying orientation fields of 1 T and 0 T at room temperature, respectively. The inset shows the relative magnetization of the curve of H_{orient} = 0 T divided by the case of H_{orient} = 1 T. The relative magnetizations for three different samples are shown because the data is noisy, around 50 K, due to a background signal from the plastic capsule (discussed in 3.3.1). For T < 50 K, the well-aligned state of the sample shows a higher magnetization than the randomly-oriented state (i.e. the relative magnetization is less than unity). However, for T > 100 K, no significant difference in magnetization was observed between the different states (i.e. the relative magnetization is about unity). The observed magnetization difference below 50 K comes from the magnetocrystalline anisotropy, which favors the alignment of the magnetization along certain crystallographic directions. The magnetocrystalline anisotropy of the Mn_{12}-acetate was verified by low temperature magnetization measurements on different crystallographic directions of a Mn_{12}-acetate single crystal [65, 66]. When the field was applied parallel to the c-axis of the crystal, the magnetization saturates quickly to a value of 20 μ_B. The magnetization saturation however, required a field as high as 10 T when the field was perpendicular to the c-axis. This verified the magnetocrystalline anisotropy of the compound, and the observed magnetization difference between two extreme states below 50 K can be explained by this anisotropy. The decrease of the relative magnetization, seen in the inset of Fig. 3.10, showed a decrease of the magneticrystalline anisotropy as temperature increased. The absence of a significant difference in magnetization for T > 100 K, as

seen in Fig. 3.10, shows that the magnetic anisotropy responsible for the alignment may be quite small. Although the high temperature anisotropy could not be measured experimentally here, it may be important to explain the mechanism for the observed alignment. In general, the magnetic Hamiltonian can be written as

$\mathscr{H} = (1/2)M_i \cdot \chi_{ij}^{-1} \cdot M_j - H_i \cdot M_i$.

Where, χ_{ij} = magnetic susceptibility tensor (i,j = 1,2,3), H_i = magnetic field, and M_i = magnetization. So that the definition of the magnetic susceptibility, $\chi = M/H$, can be derived from the first derivative of $\mathscr{H}$ with respect to M. Single crystals are magnetically aligned to minimize $\mathscr{H}$.

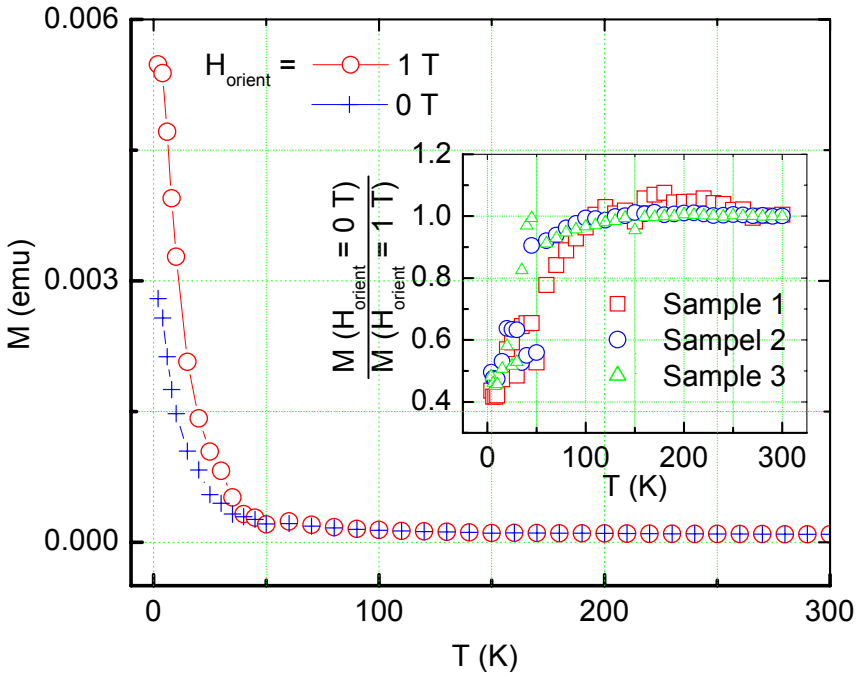

Fig. 3.10. DC magnetization curves at H = 0.5 T for both aligned (H_{orient} = 1 T) and randomly-oriented (H_{orient} = 0 T) states of the sample over the temperature range 2 ~ 300 K. The inset shows the relative magnetization of the two orientations for three different samples. The noise around 50 K comes from the background signal.

Magnetizations of the crystal for different crystallographic directions should be measured to determine χ for ideal experiments. The anisotropy of the susceptibility tensor may be attributed to the shape anisotropy and the magnetocrystalline anisotropy. The shape anisotropy can be thought from the fact that the typical size of micro-crystals deposited out of the suspension onto a surface is 3×15 μm^2. Shape anisotropy affects the magnetic properties in various microscopic particles [47, 48, 67, 68]. A magnetized body will produce magnetic charges or poles at the surface, resulting in a demagnetizing field. The demagnetizing field will be less if the magnetization is along the long axis than if it is along one of the short axes [50]. Both shape and magnetocrystalline anisotropies can be added up as crystals c-axis (major axis) is parallel to the magnetization easy axis of Mn_{12}-acetate molecules.

Recently, $\Delta M/H \sim 2 \times 10^{-10}$ emu·Oe^{-1} was observed for both extreme states of one sample in the enhanced experiment. Where, ΔM is the magnetization difference between the well-aligned and randomly-oriented states. The sample was kept in the SQUID sample space without homogenization in this series of measurements, which is different from previous measurements [Appendix B]. This small magnetization difference for both states is within the noise level, and is too small to change the relative magnetization seen in the inset of Fig. 3.10.

Fig. 3.11 shows both normalized magnetizations again from Figs. 3.7 and 3.9. M' is the well-saturated magnetization at the highest H_{orient} for each case as indicated in both figures. The two data match well, indicating reproducibility of the alignment behavior. The best fits of the overall alignment behavior for $H_{orient} \leq 0.5$ T have been achieved by

both the “two energy level model”, a simplified model of this system and the “energy competition model”. Before these calculations, it should be emphasized that the normalized magnetization indicates the degree of the alignment in the micro-crystals rather than magnitude of magnetization. All the magnetizations were measured at the same field (0 T after saturation in Fig. 3.7 and 0.5 T in Fig. 3.9) for different aligned states of a sample (controlled by applying various orientation fields, H_{orient}). In other words, this graph does not show the relationship between magnetization and field. Instead, this graph shows the relationship between the micro-crystal orientation with respect to the field direction and the orientation field for the alignment.

For the calculation in the “two energy level model”, suppose there are only two levels, μ (spin-aligned) and 0 (spin-zero), in the system. This is a plausible assumption to describe this alignment behavior because the parallel and perpendicular directions of the crystal c-axis with respect to the field direction give the maximum and the minimum magnetizations, respectively. In other words, rotating a micro-crystal 180° will give the same magnetization as for an original angle of the crystal. The microscopic origin for this is because the degenerate states disappear by applying field for any measurements. The two extreme orientations are simplified by the μ (spin-aligned) and 0 (spin-zero) states. These two levels have an energy of $-\mu \cdot H$ and 0, respectively. To calculate the probability of the system in the spin-up state, a partition function was calculated as $Z = \exp(\mu \cdot H/k_B \cdot T) + \exp(0/k_B \cdot T)$, where $\exp(\mu \cdot H/k_B \cdot T)$ is the Boltzmann factor for the “spin-aligned” state, i.e. the magnetic moment (μ) of the system is parallel to an applied magnetic field (H). The probability that the system is in the “spin-aligned” state is $P_+ =$

$\exp(\mu \cdot H/k_B \cdot T)/Z$, which is the same as the average magnetic moment of this system divided by μ, $<\mu>/\mu$, where $<\mu> = \{\mu \cdot \exp(\mu \cdot H/k_B \cdot T) + 0 \cdot \exp(0/k_B \cdot T)\}/Z$ is the average magnetic moment for this two energy level system. The experimental data is best fitted, if this function is potted as a function of the field, H = 0 Oe – 5000 Oe with $\mu/k_B \cdot T$ = 15 emu·erg^{-1}, as seen in Fig. 3.11.

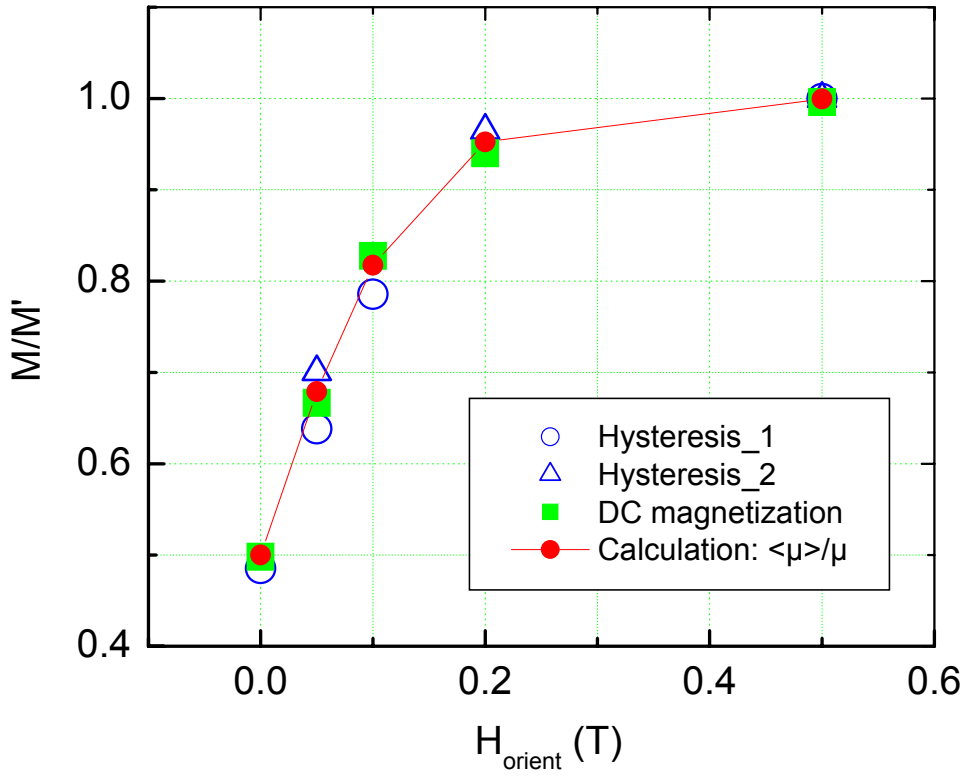

Fig. 3.11. The normalized magnetization (M/M') as a function of the orientation magnetic field (H_{orient}). A best fit of the data was made by an average magnetic moment in the "two energy level model" and using the value of $\mu/k_B \cdot T$ = 15 emu·erg^{-1} in the calculation.

It should be noted that $\mu/k_B \cdot T = 15$ was chosen and used for the best fit. In a calculation based on experimental assumptions as shown in Appendix A, however, $\mu/k_B \cdot T = \chi \cdot V/k_B \cdot T = 6 \times 10^{-3}$ emu·erg^{-1} was obtained, which produces a nearly straight line in the figure between two end fields (0 Oe and 5000 Oe) and this does not fit the data. {$\chi = 2.7 \times 10^{-3}$ emu·mol^{-1}·Oe^{-1}, V = Mole for one micro-crystal of typical size, $3 \times 3 \times 15$ μm^3 = $4 \times 10^{10} \times (6 \times 10^{23})^{-1}$ mol, and $k_B \cdot T = (10^{-16}$ erg·K$^{-1}) \cdot (300$ K) = 3×10^{-14} erg [Appendix A]}. This model is somewhat unphysical, e.g. in assuming S = 10 at the temperature where alignment occurs. A better model is thus necessary.

The other approach to explain the alignment behavior is the "energy competition model". In this calculation, magnetic susceptibility for crystal a- and c-axis was considered (χ_a and χ_c, respectively). And, an applied magnetic field, H, divided into two components; $H \cdot \cos\theta$ seen by crystal c-axis and $H \cdot \sin\theta$ crystal a-axis, as shown in Fig. 3. 12 (a). Therefore, magnetic energy can be calculated as, $U = -\mu \cdot H = -V \cdot \chi \cdot H^2 = -V \cdot (\chi_c \cdot H^2 \cdot \cos^2\theta + \chi_a \cdot H^2 \cdot \sin^2\theta) = -V \cdot H^2 \cdot [\chi_c + (\chi_a - \chi_c) \cdot \sin^2\theta]$. Where, μ = magnetic moment = $\chi \cdot V \cdot H$ and $\cos^2\theta = 1 - \sin^2\theta$ were used. This magnetic energy leads to alignment of a magnetic particle parallel to the field direction, because at $\theta = 0°$ magnetic energy is minimized, as seen in the magnetic energy function. Now, it is possible to add a value of $V \cdot H^2 \cdot \chi_c$ in the magnetic energy, because relative energy is involved in the alignment process rather than absolute energy. Therefore, $U = V \cdot H^2 \cdot \Delta\chi \cdot \sin^2\theta$ can be considered for the alignment process, where, $\Delta\chi = \chi_c - \chi_a$ was used. Fig. 3.12 (b) shows this energy curve as a function of the angle, θ, between the field direction and the crystal c-axis.

A magnetic alignment process of any magnetic particle is a result of energy competition between thermal and magnetic energies. It is known that magnetic anisotropy energy should be larger than the thermal disordering effects (~ k_BT) [53]. Fig. 3.12 (c) shows magnetic energy graphs for two magnetic fields of 50 Oe and 500 Oe, respectively, with arbitrary $\Delta\chi$ value, and these are compared with thermal energy. The maximum angle, θ_2, is determined by thermal and magnetic energies competition at specific field, 500 Oe, in this case for example. Crystals could be fluctuated within this angle, θ_2, at this field. Generally, as field is increasing, this angle is decreasing. As a result, the crystals align better to the field direction.

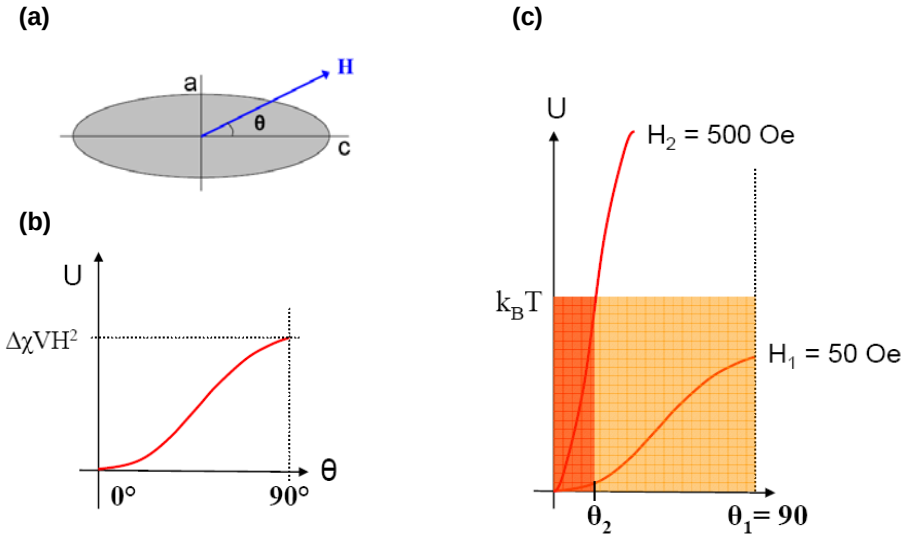

Fig. 3.12. Schematic drawings depict the "energy competition model". (a) An applied magnetic field seen by a- and c-crystal axis. (b) Magnetic energy as a function of an angle (θ) between field direction and crystal c-axis. (c) Thermal and magnetic energy comparison as a function of the angle, θ. Magnetic susceptibility difference ($\Delta\chi = \chi_c - \chi_a$) was chosen in this case in order to the thermal energy is slightly higher than the magnetic energy at H = 50 Oe.

However, applying this model to find alignment behavior as a function of fields is difficult because the value of $\Delta\chi$ is unknown and couldn't be measured on our system. Therefore, two trial values of $\Delta\chi$ were used to see if this model gives a similar graph to the experimental data. First trial value of $\Delta\chi$ was obtained as following. It was found from the experimental data that the relative magnetization (M/M') is 0.5 when H_{orient} = 50 Oe, as seen in Fig. 3.13. And, the relative magnetization (M/M') is proportional to cosθ if the angle, θ, is the same as the angle in Fig. 3.12 (a). Therefore, θ = 60° was obtained by putting cosθ = 0.5. Now, the first trial value of Δχ was obtained by letting $V \cdot H^2 \cdot \Delta\chi \cdot \sin^2 60° = k_B T$, where, H = 50 Oe, Mole (for one micro-crystal) = $4 \times 10^{10} \times (6 \times 10^{23})^{-1}$ mol , and $k_B \cdot T = 3 \times 10^{-14}$ (erg) were used. Using this first trial value, $\Delta\chi = 2.4 \times 10^{-4}$ a first fit was made by the equation of $f(H) = \cos[\sin^{-1}(k_B T \cdot (V \cdot H^2 \cdot \Delta\chi)^{-1})^{-0.5}]$ as a function of field, H, as seen in Fig. 3.13 (At 50 Oe). This function shows a sudden jump to near θ = 90° at H > 50 Oe. As a result, this does not fit the experimental data. A second trial value of $\Delta\chi = 1.25 \times 10^{-6}$ was calculated from the experimental value of M/M' = 0.8 by the same process. The graph $f(H)$ using this $\Delta\chi$ fits the experimental value at H > 1000 Oe much better, as seen in Fig. 3. 13 (At 1000 Oe). However, this graph cannot be drawn below 1000 Oe, because the thermal energy is higher than magnetic energy below 1000 Oe, throughout 0° - 90°. At this time, we do not fully understand this alignment behavior, and so it should be studied more to understand it better.

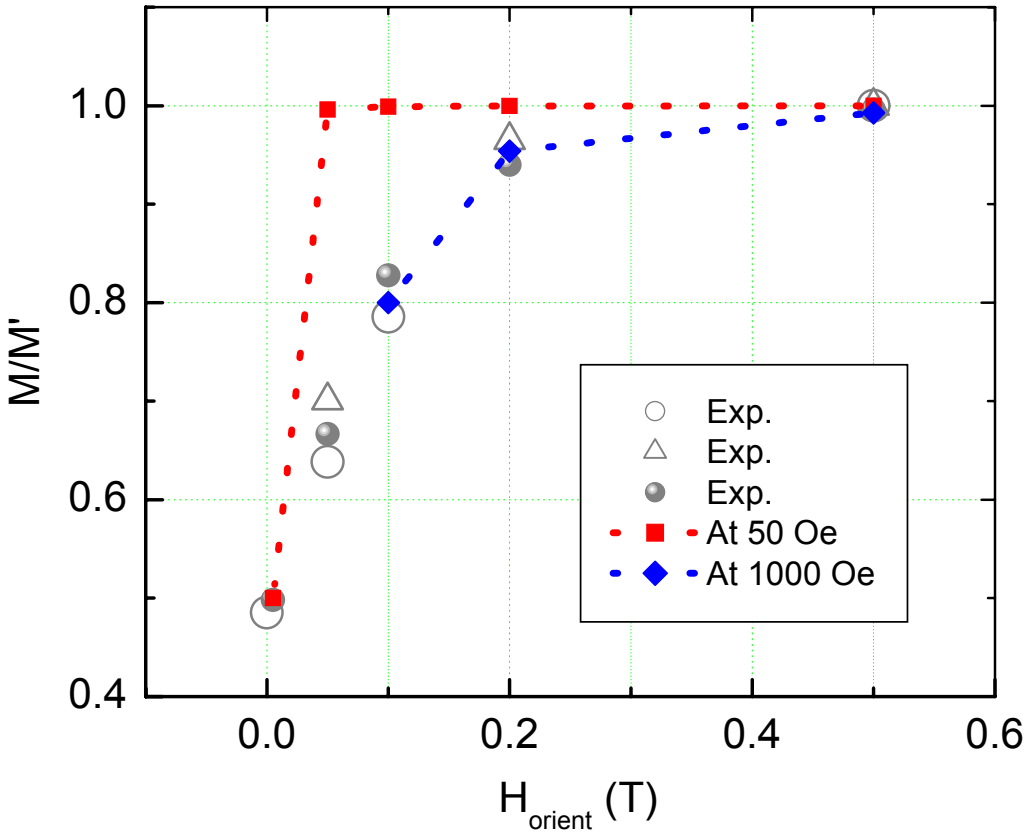

Fig. 3.13. The graph shows both experimental and calculated data. Two calculated graphs, by choosing two different $\Delta\chi$, selected by adjusting these graphs with experimental data at 50 Oe and 1000 Oe, respectively. Both dotted lines are only for eyes.

3.4 Summary

Optical microscopy, SEM, and AFM images support the conclusion that a Mn_{12}-acetate solution in isopropanol beyond the point of saturation is mainly composed of both single molecules and micro-crystals. Magnetic properties of the frozen Mn_{12}-acetate suspension similar to large single crystals, specifically several sharp steps in the low temperature hysteresis loops, indicates significantly enhanced alignment as compared to prior studies of micro-crystals. A magnetic field of ~ 0.5 T above the freezing point of the solvent was sufficient to align the micro-crystals in the organic solvent to a degree previously observed only in much larger single crystals, as studied by both low temperature hysteresis loops and DC magnetization. The greater the external magnetic field during alignment, the sharper the steps became in the low temperature hysteresis loops, indicating that this method can be used for continuous control of alignment. Several orientations of Mn_{12}-acetate micro-crystals in suspension, ranging from random orientation to very good alignment, have been prepared by applying an external magnetic alignment field $0\ T \leq H \leq 1\ T$. DC magnetization has subsequently been measured on warmup for each state in the temperature range $2\ K \leq T \leq 300\ K$.

The relative alignment of the sample as a function of H in DC magnetization data is consistent with the results from magnetization hysteresis loops. Below 50 K, the magnetization for the aligned state is higher than the randomly-oriented state, which is due to the magnetocrystalline anisotropy of the compound. DC magnetization data do not indicate high temperature anisotropy, responsible for the observed magnetic

alignment in the suspension, possibly due to its small size. The observed magnetic alignment in the Mn_{12}-acetate micro-crystals can be explained by the shape anisotropy.

CHAPTER IV

THIN FILM OF MN_{12}-ACETATE

Thin films of Mn_{12}-acetate molecules have been fabricated on both Si/SiO_2 and Highly Ordered Pyrolytic Graphite (HOPG) surfaces by the solution evaporation method, a simple and robust technique. Atomic force microscopy (AFM) and scanning tunneling microscopy (STM) characterizations reveal that homogeneous, thin films with smoothness at the molecular level are deposited. The solution evaporation method is sometimes called the Dip-And-Dry (DAD) method, which, as the name implies, is a simple experimental process.

4.1 Motivation

The interesting magnetic properties in SMMs arise from individual molecules rather than intermolecular interactions [14, 69]. For this reason, single molecules can, in principle, be used to store magnetic information [41]. In order to use these molecules in devices, however, the controlled production of thin films of these materials on a suitable substrate is essential. Only one method of applying Mn_{12} derivatives on surfaces was reported when this project was begun [70], therefore a reliable deposition method for smooth Mn_{12}-acetate thin films was demanded.

After development of thin, homogeneous Mn_{12}-acetate films on Si/SiO_2 by the solution evaporation method [42], STM measurements were considered. It was suggested that magnetic properties of SMMs have an effect on the electronic transport [71]. There are few reports on STM studies of SMMs deposited on either a gold surface [51, 72-76] or a Highly Ordered Pyrolytic Graphite (HOPG) surface [77]. Mn_{12} clusters were deposited on Au surfaces by functionalizing the compound [(a), (c)], using functionalized Au surfaces [(b), (e), and (f)], or utilizing electrostatic interactions (d), as seen in Fig. 4.1. These are early studies as all the images were acquired at room temperature. Moreover, to our knowledge, no 2-D lattice structure of SMMs on a surface was observed in the Mn_{12} family so far. Therefore, STM measurements have been attempted on Mn_{12}-acetate thin films deposited onto HOPG. A self-organized triangular lattice structure of Mn_{12}-acetate molecules was observed in our STM images.

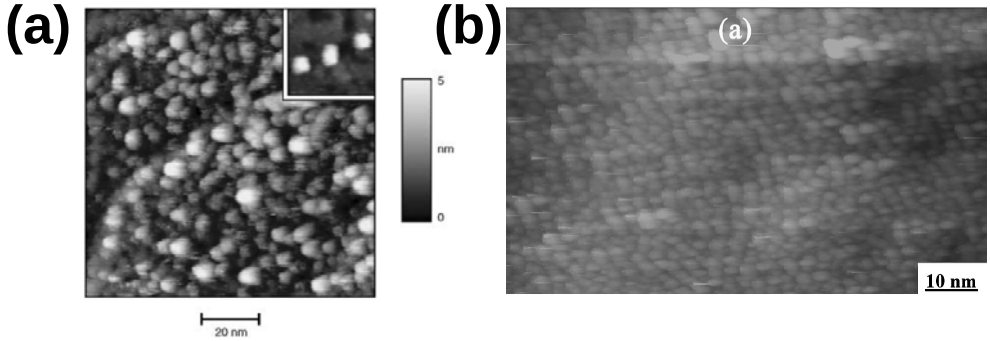

Angew. Chem. Int. Ed. **42,** 1645 (2003)

J. Appl. Phys. **95,** 7345 (2004)

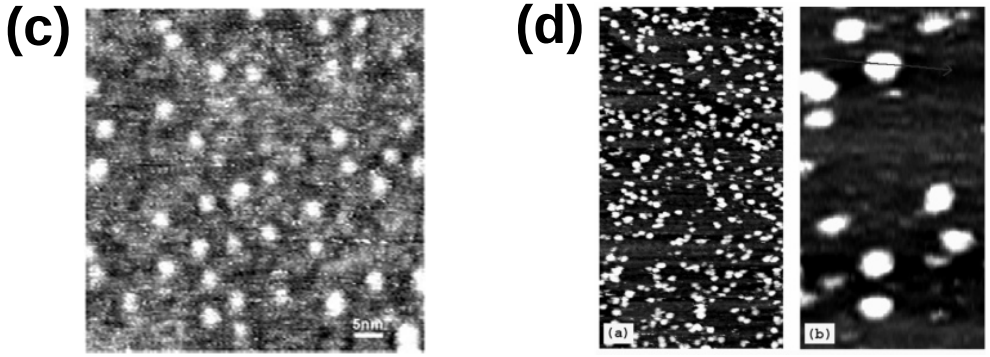

Chem. Commun. 1640 (2005)

Inorg. Chem. **44,** 7693 (2005)

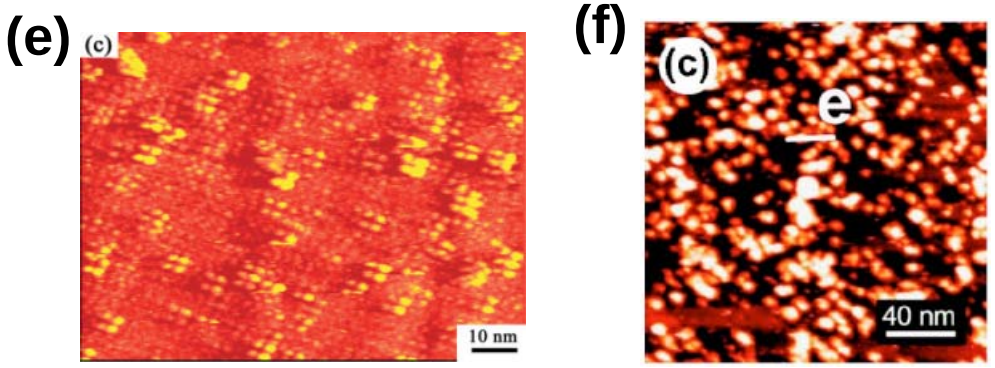

Adv. Mater. **17**, 1612 (2005)

Phys. Rev. B **75,** 045102 (2007)

Fig. 4.1. STM images of Mn_{12} family deposited on Au surface for (a) – (f).

4.2 Experimental

Fresh powder of Mn_{12}-acetate was prepared from Dr. Dunbar's group. For a typical preparation of films described below by the solution evaporation method or Dip-And-Dry (DAD) method, 2.2 mg ± 0.1 mg of Mn_{12}-acetate was dissolved in 10 ml of acetonitrile (CH_3CN) to produce a 1.1×10^{-4} M solution [Appendix C]. Various concentrations ($0.2 - 1.46 \times 10^{-4}$ M) were also used to study the solution concentration dependence on the surface roughness and the formation of films. Prior to the DAD step, the Si/SiO_2 substrate was rinsed with acetone and isopropanol. The clean Si wafer was dipped in the prepared Mn_{12}-acetate solution and immediately removed. Also, the newly cleaved HOPG was attached onto a metal disk using double-sided tape and dipped in the prepared solution. A thin coating of the solution was subsequently observed on the substrates, which dried within several seconds to produce a thin film of Mn_{12}-acetate. All procedures were carried out inside a fume hood under ambient conditions.

After preparation of thin films on both Si and HOPG surfaces, the surface morphology of the films was studied by AFM and STM, with a Digital Instruments Nanoscope IIIa. The AFM images were acquired in the tapping mode with a silicon cantilever and tip under ambient conditions. The STM images were acquired using mechanically sharpened Pt/Ir tips at room temperature under ambient conditions. STM images were acquired only on Mn_{12}-acetate thin films deposited on the HOPG surface. Room temperature core level XPS measurements were performed using a Kratos AXIS ULTRA spectrometer equipped with a concentric hemispherical analyzer using the Al

Kα radiation (hν=1486.6 eV) and a base pressure of ~ 2×10^{-8} Torr. The binding energies were calibrated with respect to the C 1s peak (284.8 eV) [46].

4.3 Results and Discussions

This section is divided into two subsections: (1) Mn_{12}-acetate thin films deposited on Si/SiO_2 characterized by AFM and X-ray photoelectron spectroscopy (XPS), and (2) Mn_{12}-acetate thin films deposited on HOPG characterized by STM, AFM and XPS.

4.3.1 Mn_{12}-acetate Thin Films on Si/SiO_2

Fig. 4.2 shows the AFM images of the Mn_{12}-acetate thin film formed by the solution evaporation method using a concentration of 1.08×10^{-4} M. A topographical top-view, the corresponding 3D image, and height profile are shown, respectively from (a) to (c), for a 1×1 μm^2 scan size. This figure shows a Mn_{12}-acetate thin film, which considering the simplicity of the Dip-and-Dry (DAD) method, is surprisingly homogeneous and smooth. In a control experiment, the DAD method was used with pure acetonitrile without Mn_{12}-acetate. The AFM images did not show any substantial surface corrugations and were identical to those acquired on the bare Si-substrate (Fig. 2.7). This provides evidence that the film is formed by Mn_{12}-acetate instead of any other materials. Clusters up to a micron in size were occasionally observed in the AFM investigation of some samples. Reproducibility of the films formed by the DAD method was checked for more than 30 independent samples all of which exhibited similar AFM images. Moreover, similar AFM images for different scan positions on several samples provide strong evidence of the homogeneity of the films.

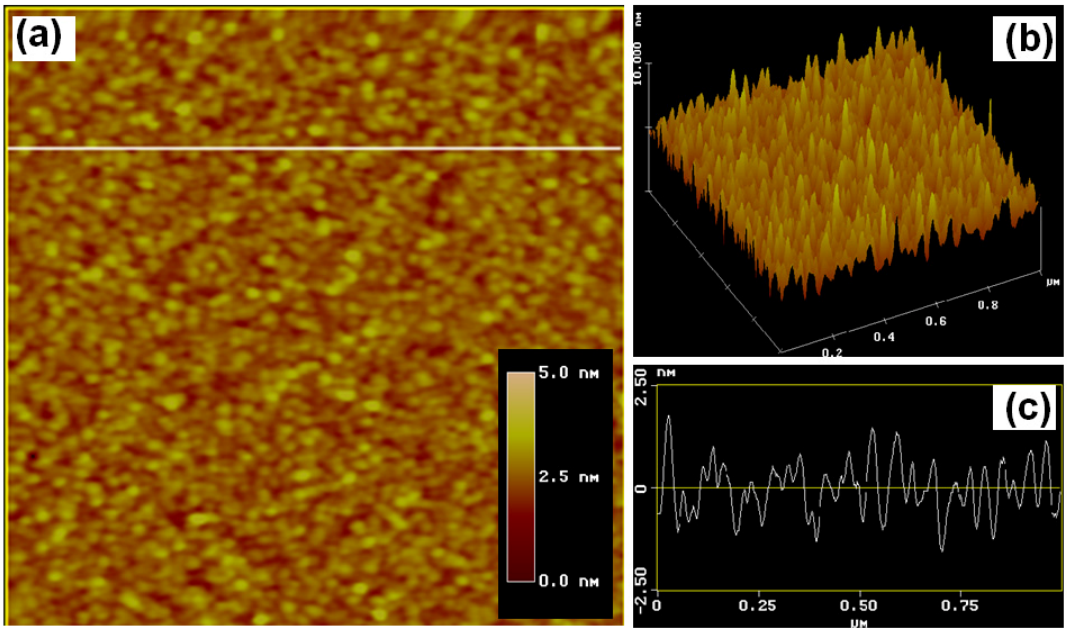

Fig. 4.2. AFM images of a Mn_{12}-acetate thin film formed by the solution evaporation method. (a) Topographical top-view with 1 × 1 μm^2 scan size. (b) The corresponding 3D image of the same area. (c) Height profile, which is taken at the location indicated by the white line in (a). The height scale bar is shown in the topographical top-view.

Fig. 4.3 shows AFM images of the Mn_{12}-acetate thin film with different scan sizes: 2×2 μm^2 and 0.5×0.5 μm^2. A relatively large scan area can be used to check the homogeneity of the film, as seen in Fig. 4.3 (a), and a smaller area to analyze the image, as seen in Fig. 4.3 (b). Fig. 4.3(c) and (d) are height profiles, which are taken at the locations indicated by the white lines in (a) and (b), respectively. Detailed examination of the AFM images reveal that the typical horizontal size of pictured clusters, which is measured at the baseline, is about 40 nm and the average vertical height is about 2 nm. The typical horizontal size of a cluster appears larger than a single molecule, while the height is on the order of single molecular diameter. The apparent horizontal size could be a convolution effect due to the radius of curvature of the AFM tip [78]. However, this effect can be quantitatively applied in a consistent way only when imaging an individual dot or line on an atomically flat surface. Therefore, a different explanation is needed for the apparent lateral size of 40 nm in the film where particles continuously cover a surface. Fig. 4.3 (e) depicts a possible scenario of the difference between the horizontal and vertical sizes of the clusters. An AFM tip with a radius larger than the surface corrugation cannot scan the actual surface [79]. AFM tips with about a 10 nm radius of curvature cannot be used to laterally distinguish single molecules about 2 nm in diameter [7], though the film is formed by monodispersed molecules. Therefore, it is not clear if each spot in the AFM images is a single molecule or a cluster made of more than one molecule. The root mean square (RMS)-roughness of the surface, which can be acquired automatically in the system, is 0.73 nm, considerably smaller than the size of a single molecular diameter.

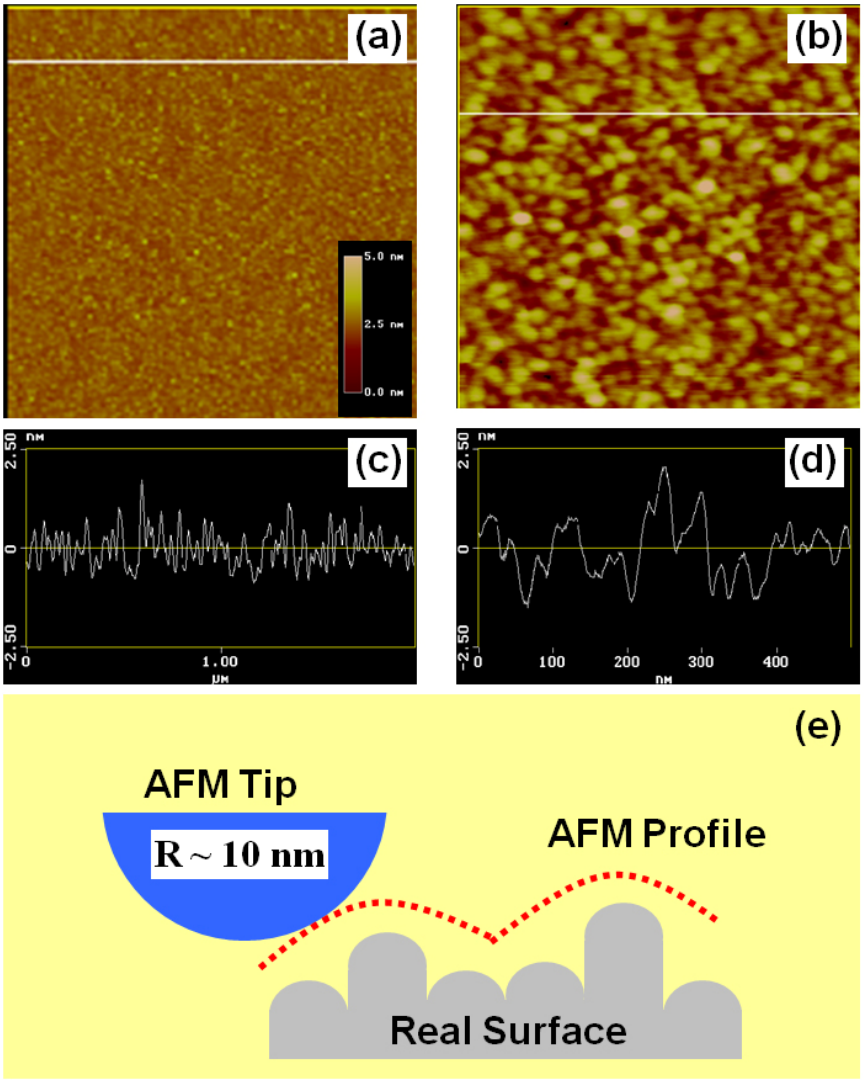

Fig. 4.3. AFM images of the Mn_{12}-acetate thin film with 2 × 2 μm^2 and 0.5 × 0.5 μm^2 scan sizes for (a) and (b), respectively. The corresponding height profiles, which are taken at the locations on (a) and (b) indicated by the white lines for (c) and (d), respectively. (e) Shows a possible situation in the AFM measurement on an Mn_{12}-acetate thin film.

Next, the influence of solution concentration on the surface morphology was investigated. Fig. 4.4 shows 3-dimensional 1 × 1 μm^2 scan size AFM images for four Mn_{12}-acetate films from different solution concentrations (1.46, 0.88, 0.49 and 0.2 × 10^{-4} M). The average surface roughness decreases with decreasing solution concentration. The RMS-roughness varied as 0.86nm, 0.61nm and 0.29nm for 1.46, 0.88 and 0.49 × 10^{-4} M solution concentrations, respectively, as illustrated in Fig. 4.4 (a) - (c). However, a uniform film does not form below ~ 0.4 × 10^{-4} M concentration. Instead, sparse clusters are formed, as illustrated in Fig 4.4 (d).

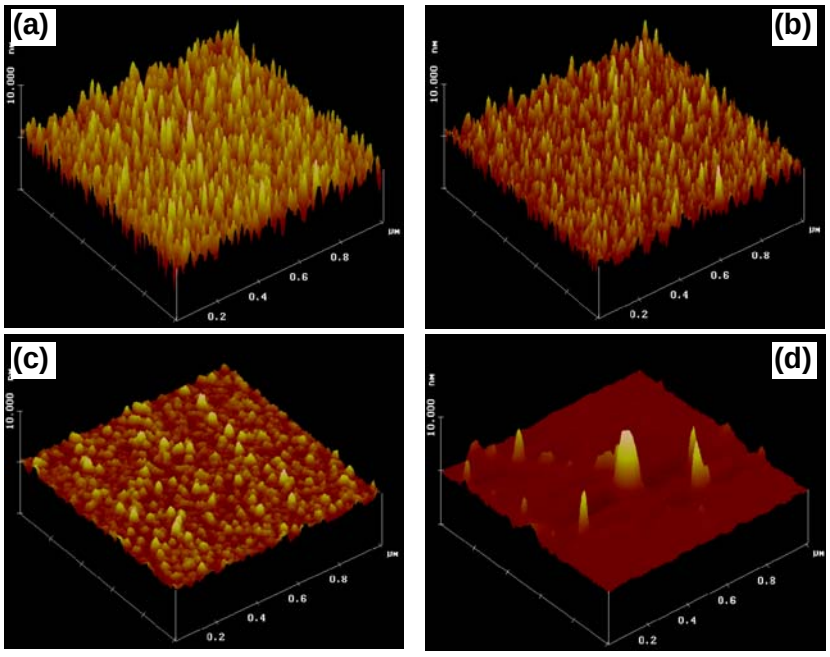

Fig. 4.4. AFM images of four Mn_{12}-acetate films formed using different solution concentrations. (a)1.46, (b) 0.88, (c) 0.49, and (d) 0.2 × 10^{-4} M. The scan size is 1 × 1 μm^2 and a maximum height is 5 nm.

The RMS-roughness dependence on the solution concentration is plotted in Fig. 4.5. All roughness values are an average of at least three scan positions. While the RMS-roughness is in the range 0.55 nm - 0.86 nm for films that were grown from 0.58 - 1.46 × 10^{-4} M solution concentrations, the lowest roughness (0.29 nm) was observed at the 0.49 × 10^{-4} M concentration. While a much more detailed investigation would be necessary to completely delineate the dependence of RMS-roughness on the solution concentration, several conclusions can be made from Fig. 4.5: (1) solution concentrations from 0.49 to 1.46 × 10^{-4} M can be used for the DAD method to make homogeneous thin films; (2) films produced from a ~ 0.5 × 10^{-4} M solution concentration exhibit the lowest surface roughness; (3) solution concentrations below 0.4 × 10^{-4} M form sparse clusters, instead of thin films.

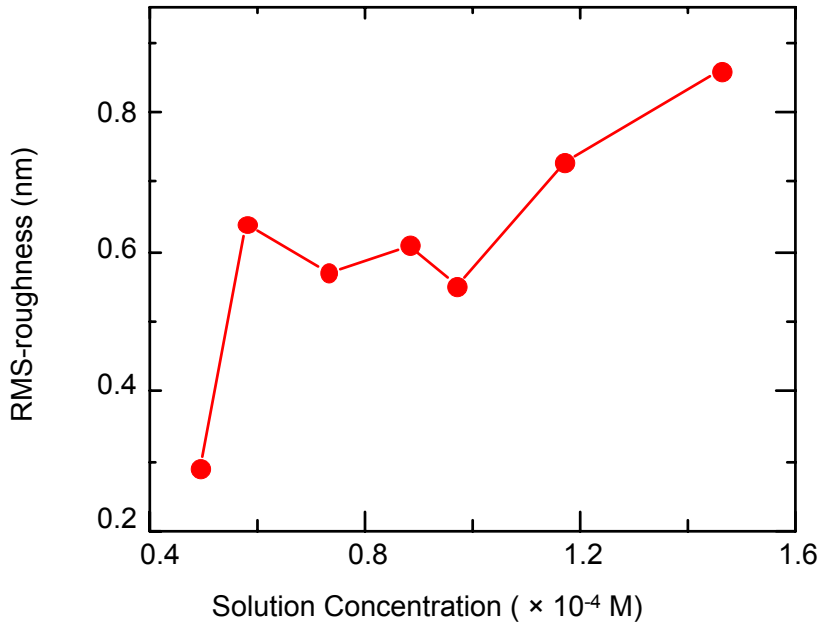

Fig. 4.5. RMS-roughness dependence on the solution concentration.

The surface roughness dependence on the number of DAD cycles was also investigated. Fig. 4.6 shows 500 × 500 nm^2 scan size AFM images of three different samples. These samples were prepared from the 1.02×10^{-4} M concentration but with 1, 2 or 3 DAD cycles, for Fig. 4.6. (a), (b), and (c), respectively. In this case, the RMS-roughness of the samples increases with an increase in the number of DAD cycles. The average RMS-roughness, which is the average of a minimum of five different scans, is 0.65 nm, 0.9 nm, and 1.0 nm, respectively. Although the surface roughness can be determined from these scans, the film thickness cannot. Therefore, a few different thickness measurement techniques were attempted, as described below.

First, an attempt was made to pattern the Mn_{12}-acetate thin film by combining the solution evaporation method with an E-beam lithography technique. However, the PMMA pattern was removed while trying to deposit Mn_{12}-acetate molecules on it by the

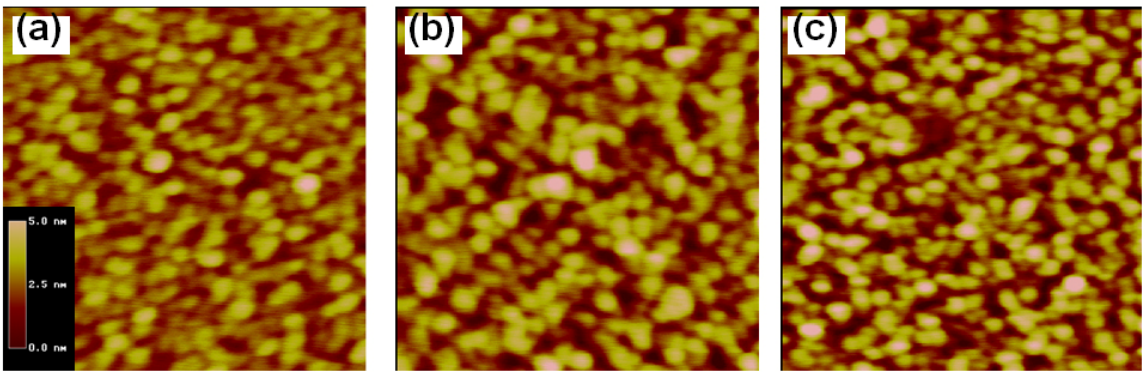

Fig. 4.6. AFM images for different DAD cycles. (a) 1-cycle, (b) 2-cycles, and (c) 3-cycles. The scan size is 500 × 500 nm^2. The height scale bar of 5 nm for all images is shown in (a).

solution evaporation method. This may be from the acetonitrile, which was used as a solvent for the Mn_{12}-acetate solution. The solvent removes the PMMA pattern on Si/SiO_2 during deposition of Mn_{12}-acetate by the DAD process.

Secondly, deposition of Mn_{12}-acetate thin film on a part of the substrate was tried by covering half of the substrate with tape or by partially submersing the substrate in the solution. However, the boundary between regions with and without the molecules on the surface was not clear. The transition between Mn_{12}-acetate film and pure Si/SiO_2 was broader than a few tens of microns in width and gradually changing so that film thickness could not be measured from these films.

Finally, the film thickness was measured on artificially patterned Mn_{12}-acetate films. This sample was prepared by making a scratch on the Mn_{12}-acetate thin film using a razor blade. It was confirmed that a similar treatment on the bare Si substrate does not make a height difference. The thickness of the film after a single DAD step was measured and found to be ~ 2 nm in AFM measurements of patterned Mn_{12}-acetate thin films as seen in Fig. 4.7. Topographical top-view with $20 \times 20\ \mu m^2$ scan size and 10 nm height scale (a), the corresponding height profile image (b) are shown, respectively. The height profile image shows that the film thickness is ~ 2 nm, which is on the order of the molecular diameter [7]. Film regions of Mn_{12}-acetate in this figure show the homogeneity of the film on a larger scale. The Mn_{12}-acetate films were surprisingly homogeneous as indicated by the fact that all the AFM images acquired in different regions of the film show similarly smooth images. While AFM studies for surface

morphology and thickness on the thin films showed promising results, important questions about the actual composition of the films remain.

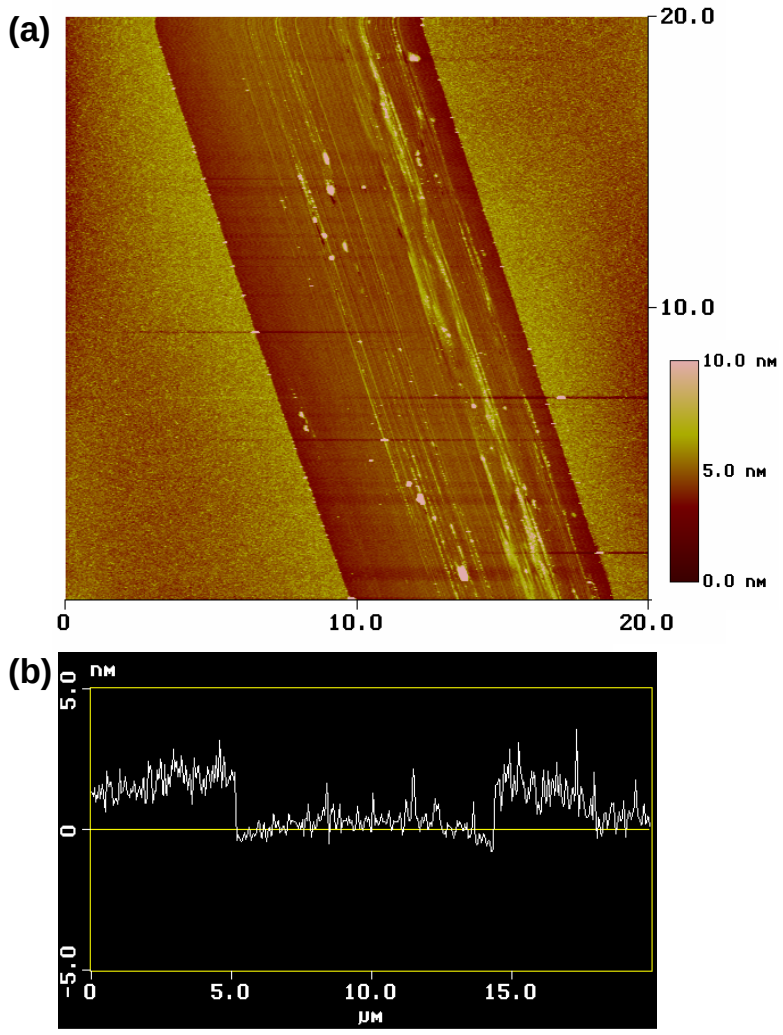

Fig. 4.7. AFM image of artificially patterned Mn_{12}-acetate thin film. (a) Topographical top-view with 20 × 20 μm^2 scan size. (b) Height profile, which is taken across the top-view in (a). The height scale bar of 10 nm is shown.

In order to confirm the presence of intact Mn_{12}-acetate molecules on the substrate after the DAD process, X-ray photoelectron spectroscopy (XPS) measurements have been carried out. XPS analysis measures important information such as composition, chemical state, compositional distribution and thickness [46]. Core-level spectra of Mn 2p for a crystalline Mn_{12}-acetate pellet and the Mn_{12}-acetate thin films, which were used for AFM images [Fig. 4.2, Fig. 4.4 (c), and Fig. 4.6 (c)], are shown in Fig. 4.8. The two peaks for the Mn 2p core-level of Mn_{12}-acetate thin films, at 642 eV and 653.5 eV, correspond to $2p_{3/2}$ and $2p_{1/2}$, respectively [80].

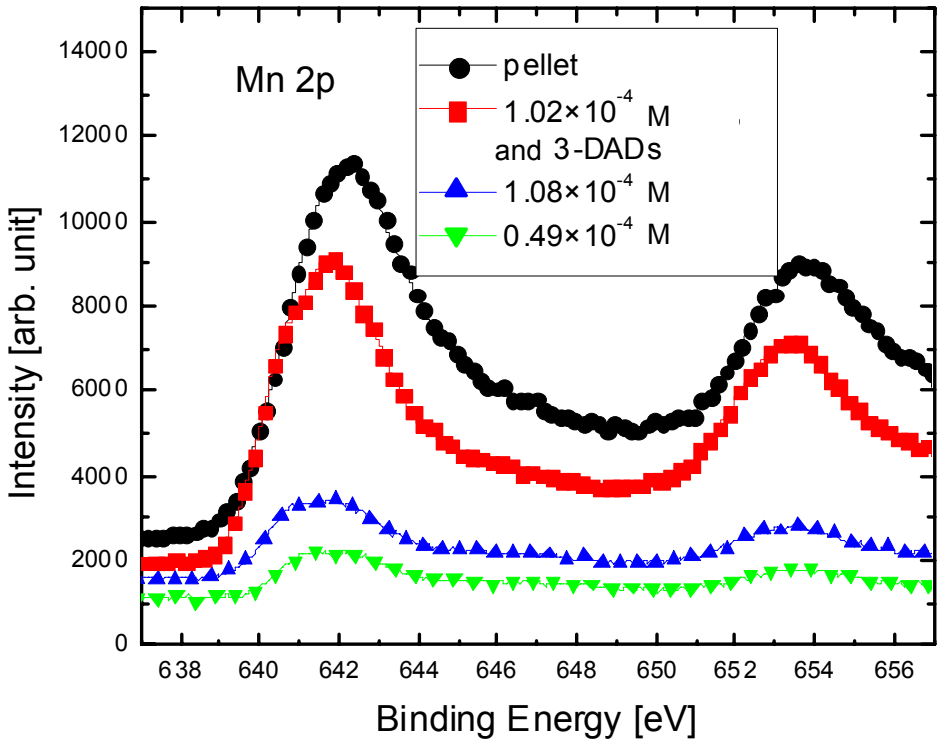

Fig. 4.8. XPS Spectra of the Mn 2p core level for the crystalline Mn_{12}-acetate pellet and the Mn_{12}-acetate thin films.

The Mn 2p peaks provide further evidence that the films are formed by Mn_{12}-acetate rather than other materials. A small shift observed in the binding energy for different samples was within the XPS resolution (0.5 eV). The films are thin enough to observe the Si 2p peak from the substrate, as shown in Fig. 4.9. Two peaks, at 99.5 eV and 103.1 eV, correspond to a pure silicon phase and a silicon oxide phase, respectively [81]. A relative Mn 2p intensity of the film from 3-DADs using 1.02×10^{-4} M is higher than those of the films from 1-DAD using both 1.08×10^{-4} M and 0.49×10^{-4} M, while the Si 2p peaks are reversed.

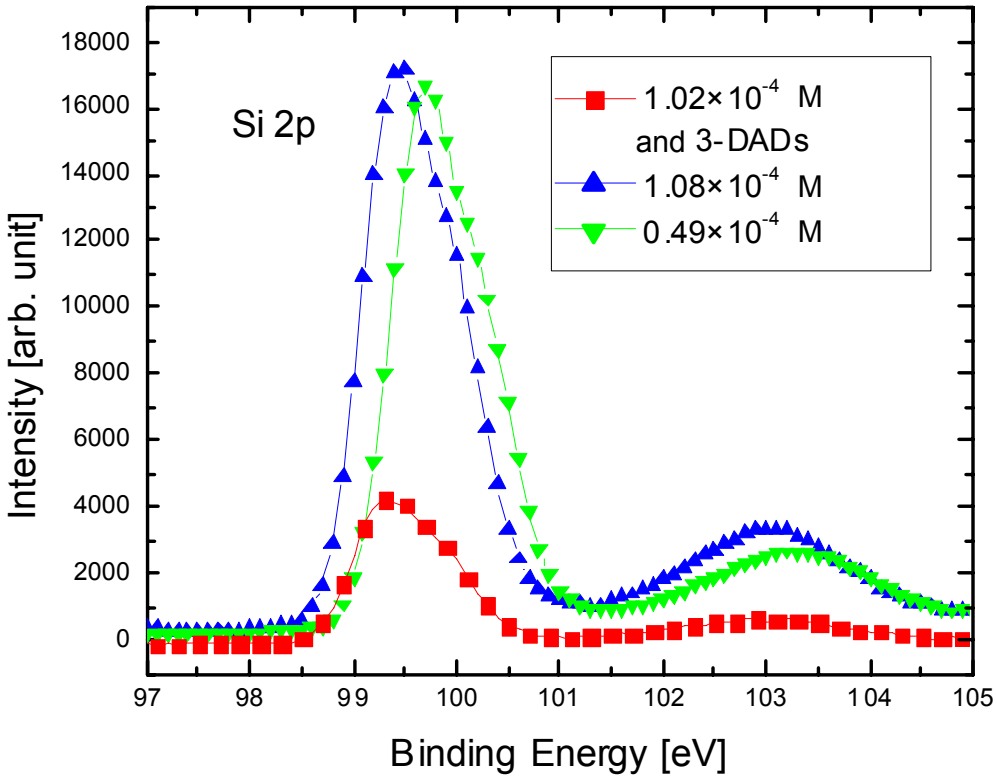

Fig. 4.9. Si 2p narrow scan spectra of the Mn_{12}-acetate thin films which were used for AFM investigations.

The relative intensities of Mn 2p and Si 2p peaks seems to show that additional DAD cycles lead to a thicker Mn_{12}-acetate film. However, thickness measurements on an artificially patterned film, described above, revealed that thickness does not linearly increase with the number of DAD cycles. The first DAD leaves a smooth surface, which may be from the oxide layer. For two or more DAD cycles, however, roughness of the films and a number of speckles that are composed of more than one molecule are increasing, while the thickness of the continuous film is always ~ 2 nm.

The films were stable against certain chemicals and time as verified by AFM and XPS studies. Attempts were made to dissolve the films by spraying them with acetone or isopropanol for a few seconds. The AFM images obtained afterwards are similar to the images from the original films. Additionally, similar AFM images were obtained for the films after one or two months of exposure to ambient conditions. This provides strong evidence for the film stability with respect to chemical decomposition and time. The high stability of the films suggested the possibility of making patterned Mn_{12}-acetate films by combining the DAD-method with a lithographic technique [60].

4.3.2 Mn_{12}-acetate Thin Films on HOPG

Mn_{12}-acetate thin films allow Scanning Tunneling Microscopy (STM) measurements, which give transport properties of the compound. Because the STM is basically operated by applying a bias voltage through a sample and measuring a tunneling current, a conducting substrate should be used. Therefore, Highly Ordered Pyrolytic Graphite (HOPG) surfaces were used for the STM studies instead of Si wafers. As will be clear below, the HOPG based smooth thin films are very difficult to prepare,

which may be due to the absence of an oxidation layer on the HOPG in contrast to the native oxide on silicon wafers.

Fig. 4.10 shows STM images of the Mn_{12}-acetate thin film on HOPG for different scan areas. Evidence that the 2-D lattice in the images arises from Mn_{12}-acetate molecules rather than other substances will be discussed below. A bias voltage of 1200 mV and setpoint current of 15 pA have been used for the 80 × 80 nm^2 scan. A bias voltage of 900 mV and setpoint current of 10 pA have been used for the 50 × 50 nm^2 scan. A triangular lattice structure is seen from both images. To our knowledge, 2-D lattice have never been reported from the Mn_{12} family so far. Intermolecular separation

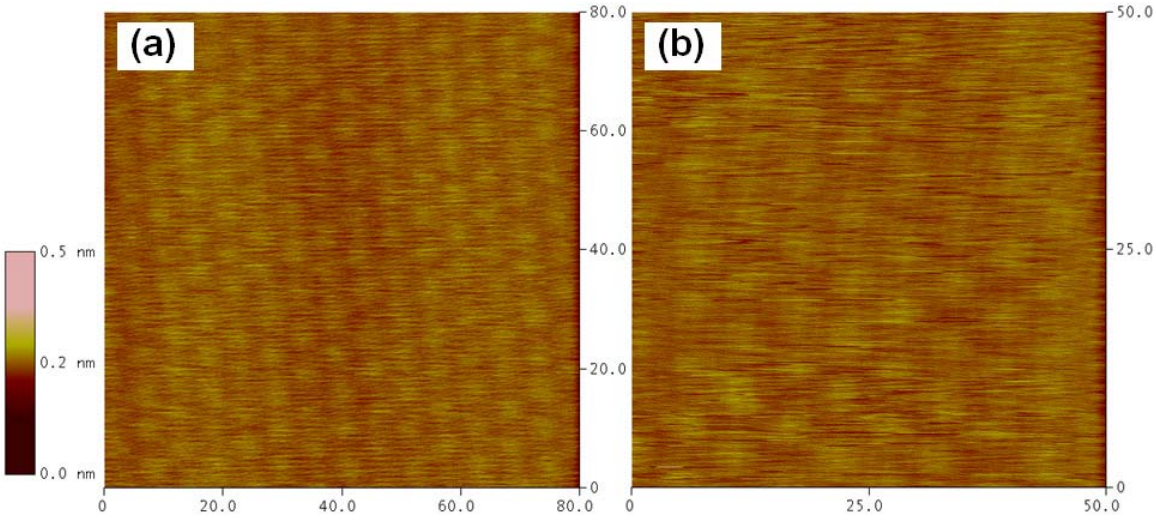

Fig. 4.10. Constant-current STM images of the Mn_{12}-acetate thin film deposited on HOPG. Scan areas are 80 × 80 nm^2 (a) and 50 × 50 nm^2 (b), respectively. Z scale of 0.5 nm is shown left. Setpoint current = 15 pA, bias voltage = 1200 mV, and scan rate = 5 Hz have been used for (a) and 10 pA, 900 mV, and 10 Hz have been used for (b).

in the pictured Mn_{12}-acetate molecules is about 6.3 nm, which is larger than the diameter of a single molecule (1.7 nm) [7]. Reduced vertical height corrugation (less than 0.5 nm in the picture) as compared to the molecular height could be due to either rounding effects of the STM tip [82] or local density of states variation in the film. While semiconductive behavior was previously reported in Mn_{12}-acetate single crystal [83], we do not know details about the electronic properties of our thin film at this time. It should be noted that acquiring STM images that show a 2-D lattice pattern of Mn_{12}-acetate molecules over larger scan areas was quite involved since only ~ 5 % of the regions of the sample clearly indicated such a lattice. The success rate of acquiring STM images with self-assembled Mn_{12}-acetate molecules was somewhat enhanced by performing survey studies on Atomic Force Microscopy (AFM) images, which allows selection of low corrugation surface regions.

Fig. 4.11 shows AFM images of the Mn_{12}-acetate thin film. In the 3×3 μm^2 image (a), the whole surface looks covered with single Mn_{12}-acetate molecules based on the fact that the surface roughness is on the order of the molecular dimension. Maximum height of 5 nm is shown in the scale bar in the left. HOPG steps are seen underneath the Mn_{12}-acetate molecules as indicated by arrows in Fig. 4. 11 (a), which supports that Mn_{12}-acetate films are thin enough to show HOPG steps. By analyzing image (b), however, one can see that single spots in image (a) cannot be single Mn_{12}-acetate molecules. A higher resolution scan of 0.2×0.2 μm^2, image (b), was acquired from scanning the middle region in image (a). Based on the diameter of the single spots in image (b), which are on the order of 50 nm, the spots in (a) and (b) are clusters made

from more than one Mn_{12}-acetate molecule. We think that the triangular lattice structure in STM images like Fig. 4.10 come from relatively smooth regions in the AFM images as marked, for example, by a dashed circle in Fig. 4.11 (b). Therefore, the low probability of seeing the ordered STM images could be explained by observing that most of the surface is covered with clusters rather than single Mn_{12}-acetate molecules, as seen in Fig. 4.11. Now, evidences for the triangular lattice structure in the STM images coming from Mn_{12}-acetate molecules rather than other substances will be discussed.

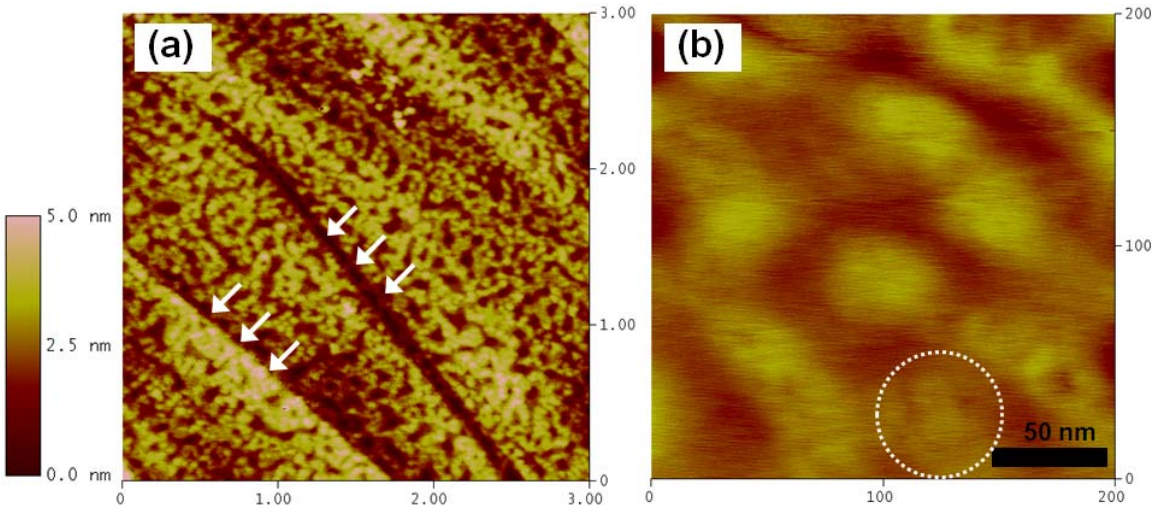

Fig. 4.11. (a) AFM images with 3 × 3 μm^2 scan size, and (b) 0.2 × 0.2 μm^2 scan size on the Mn_{12}-acetate thin film. The Z scale of 5 nm is shown in the height scale bar.

In an important control experiment, the solution evaporation method was used with pure acetonitrile instead of the Mn_{12}-acetate solution. An identical substrate of freshly cleaved HOPG on a metal disk was dipped into pure acetonitrile without Mn_{12}-acetate and pulled out immediately, thus perfectly mirroring the deposition conditions from the film described before. Again, a thin film of the solvent was seen which evaporated within several seconds. However, the resulting STM images did not show any surface corrugations on the lateral lengths of the Mn_{12}-acetate lattice seen earlier. As a matter of fact, as seen in Fig. 4.12 (a) this image is identical to one observed from freshly cleaved, un-dipped HOPG. An STM image of the Mn_{12}-acetate thin film scanned over the same field of view is shown in Fig. 4. 12 (b) for comparison.

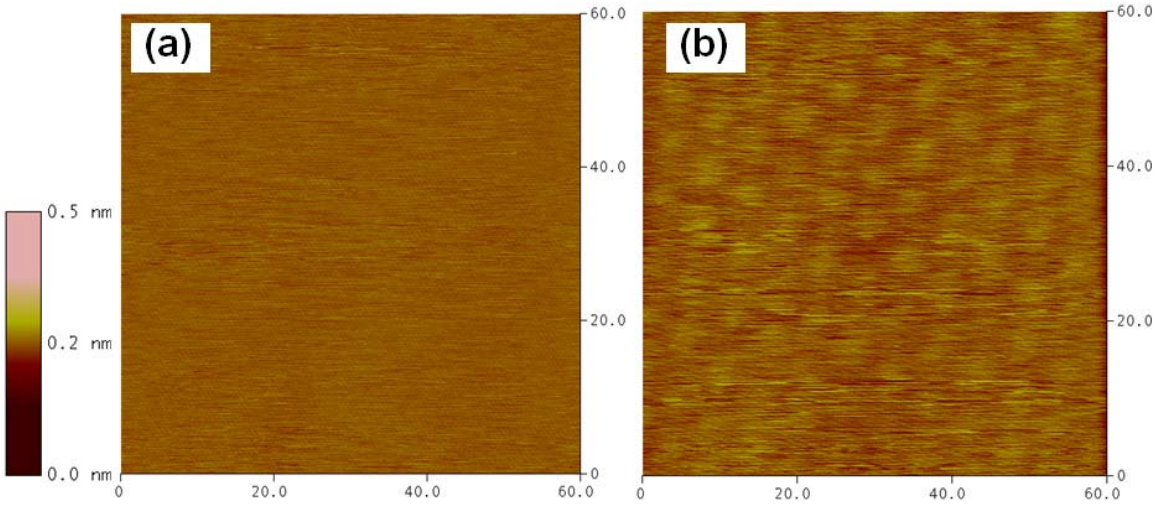

Fig. 4.12. STM images of (a) the solvent exposed HOPG, and (b) the Mn_{12}-acetate thin film on HOPG with same conditions. The scan size of 60 nm and height scale of 0.5 nm are the same for both images. A current setpoint = 10 pA, bias voltage = 900 mV, and scan rate = 4 Hz have been used for both images.

These two images were acquired with exactly the same conditions of bias voltage = 900 mV, setpoint current = 10 pA, and scan rate = 4 Hz. The scan size is 60 nm and the height scale is 0.5 nm for both images. This control experiment demonstrates that the triangular lattices in Fig. 4.10 and Fig. 4. 12 (b) arise from the presence of Mn_{12}-acetate molecules on the HOPG surface. All three STM images of the Mn_{12}-acetate thin film with different scan sizes (50 × 50 nm^2, 60 × 60 nm^2, and 80 × 80 nm^2) show similar intermolecular separation (6.3 ± 0.2 nm). This assures that the triangular lattice structure in the STM images are due to a physical effect rather than electrical noise.

As was mentioned in Fig. 2.8, parameters were changed during other measurements to observe carbon atoms from the HOPG surface. By reducing the bias voltage to typically 50 mV, and increasing the setpoint current to 500 pA, the STM tip may "dig into" the Mn_{12}-acetate molecules in order to allow electrons to tunnel between the HOPG and STM tip directly. The relatively low bias voltage may not allow a high tunneling current while the STM tip scans over the Mn_{12}-aceate molecules (~ 2 nm in diameter) [7]. It was not possible to observe the triangular structure from the Mn_{12}-aceate molecules again after seeing the HOPG surface by this method.

X-ray photoelectron spectroscopy (XPS) measurements on the Mn_{12}-acetate thin film provide a further argument that the triangular lattices in the STM images of Fig. 4.10 and Fig. 4.12 (b) originate from Mn_{12}-acetate molecules. Core-level spectra of Mn 2p for a crystalline Mn_{12}-acetate (pellet) and the Mn_{12}-acetate thin film, which was used for the STM images, are shown in Fig. 4.13. The two peaks at 642 eV and 653.5 eV correspond to $2p_{3/2}$ and $2p_{1/2}$, respectively [80]. Once again, the Mn 2p peaks, which are

normally observed from as-produced Mn_{12}-acetate, show that the molecular compound present on the HOPG surface is Mn_{12}-acetate. The relatively low signal-to-noise ratio in the XPS spectrum of the Mn_{12}-acetate thin film is due to the fact that the amount of Mn_{12}-acetate in the film is very small as compared to the bulk pellet. XPS measurements of HOPG surfaces dipped in pure acetnitrile did not show any Mn 2p peaks.

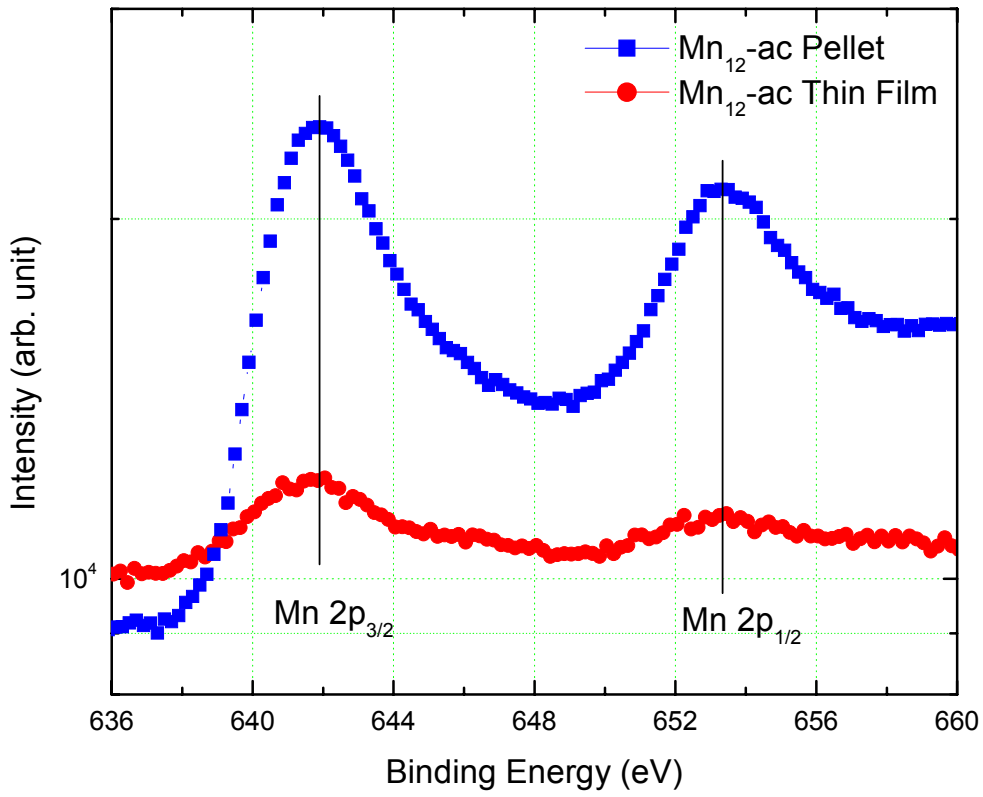

Fig. 4.13. Core level XPS spectra of the Mn 2p peaks for a crystalline Mn_{12}-acetate (pellet) and the Mn_{12}-acetate thin film on HOPG surface. Intensity (y-axis) is shown on a log scale.

4.4 Summary

The deposition of Mn_{12}-acetate directly on a Si/SiO_2 substrate using the Dip-and-Dry (DAD) method yields very smooth, homogeneous thin films. AFM and XPS characterizations were performed on Si/SiO_2 based films to investigate the surface and the elemental composition of the films. A roughness less than the molecular dimension and the thickness of a single layer in the films were confirmed by AFM characterizations. The solution concentration and the number of DAD cycles were varied to change the surface roughness of the films. The films were found to be stable with respect to certain solvents and ambient conditions. Relative intensities were varied in the XPS data for both Mn 2p and Si 2p peaks.

Mn_{12}-acetate thin films were also fabricated on Highly Ordered Pyrolytic Graphite (HOPG) using the same DAD method. Self-organized Mn_{12}-acetate molecules on the HOPG surface were observed to have a triangular lattice structure. AFM images of the Mn_{12}-acetate thin film show the difficulty of getting STM images of the triangular lattice structure. A control experiment for the solution evaporation method without Mn_{12}-acetate and XPS measurements on the Mn_{12}-acetate thin film confirm that the interesting self-assembled triangular lattice structure in the STM images arises from Mn_{12}-acetate molecules rather than other effects.

CHAPTER V

MAGNETIZATION OF THE FILM MATERIAL

5.1 Background

Achieving an increase of the blocking temperature (T_B), as well as addressing of SMMs on surfaces, is an important goal in the field of single molecule magnets [14]. At the time of this study, there were few reports on controlled alterations of magnetic properties from that of the as-produced compound. Two studies regarding the magnetic properties of Mn_{12} derivatives formed by thermal transformation and gas inclusion, as well as incorporation into mesoporous silica, have reported significant changes of magnetic properties from the as-produced compound [84, 85]. An increase of T_B was expected in the thin film of Mn_{12}-acetate due to the interaction with the substrate when the fabrication method for Mn_{12}-acetate thin films was first tried.

Initial magnetization measurements on Mn_{12}-acetate thin films on Si/SiO_2 were not successful due to the small amount of material on the surface and the large background signal from the substrate. Therefore, relatively thick films were prepared by multiple Dip-and-Dry cycles on both Si/SiO_2 and a piece of plastic straw, which was used for the SQUID sample holder. However, these films did not show a detectable signal above the noisy background. Therefore, so called "film material" (acetonitrile exposed Mn_{12}-acetate molecules) was prepared for the magnetization measurements.

Significant changes in magnetic properties of the film material were observed in the relaxation measurements, AC-susceptibility, Field Cooled (FC) & Zero Field Cooled

(ZFC) magnetizations, and M vs. H measurements. The different magnetic properties of the film material from the as-produced Mn_{12}-acetate may be an effect of the solvent. This led us to perform mass spectroscopy measurements on the Mn_{12}-acetate solution to study the solvent's effect on the molecules.

5.2 Experimental

A sample for the magnetization measurements was made by a similar method to the thin films, but on a larger scale to accumulate sufficient sample material. A solution of ~ 1×10^{-3} M (21 mg of Mn_{12}-acetate in 10 mg acetonitrile) concentration was prepared in a beaker. The top ~ 90 % portion of this solution was used to assure that no sediment was present. Subsequently, this solution was evaporated over the course of 1 hour in a glass Petri dish in a fume hood. The magnetization sample was obtained by scraping the powder from the dish. Magnetic measurements were acquired on a Quantum Design MPMS-XL SQUID magnetometer.

Electrospray ionization mass spectrometry (ESI-MS) data on Mn_{12}-acetate solution were used to investigate the solvent's effects on the molecules. ESI-MS data were obtained on a PE SCIEX QSTAR instrument in the TAMU chemistry department. In this case, a relatively low concentration of the compound in acetonitrile (~ 1.3×10^{-5} M) was used to make sure that the signal comes from monodispersed Mn_{12}-acetate molecules in the solvent.

5.3 Results and Discussions

This section has two subsections: (1) magnetization of the Mn_{12}-acetate film material, and (2) mass spectrometry data on the Mn_{12}-acetate solution.

5.3.1 Magnetic Properties of the Film Material

Novel effects were observed in the AC-susceptibility measurements. The temperature dependence of the in-phase (χ') and out-of-phase (χ'') AC-susceptibility for the sample were investigated in an AC field of 3 Oe at different frequencies ranging from 1 Hz to 1000 Hz, as seen in Fig. 5.1. A magnetic transition was observed at ~ 11 K in the χ' data. As the frequency was increased from 1 Hz to 1000 Hz, an increase in this transition temperature was observed. The inset shows a blow up around the transition temperature. Maxima, at 10.5 K (1 Hz) and 10.8 K (10 Hz), were observed in the χ'' data. Moreover, a frequency dependence of the peaks for 100 Hz and 1000 Hz is evident at ~ 11.0 K and ~ 11.6 K, respectively, although the data are noisier. A shift of the maxima in the χ'' data from those of as-produced Mn_{12}-acetate (e.g. 5.0 K at 10 Hz) [28] shows an increase of the blocking temperature (T_B) in our film material.

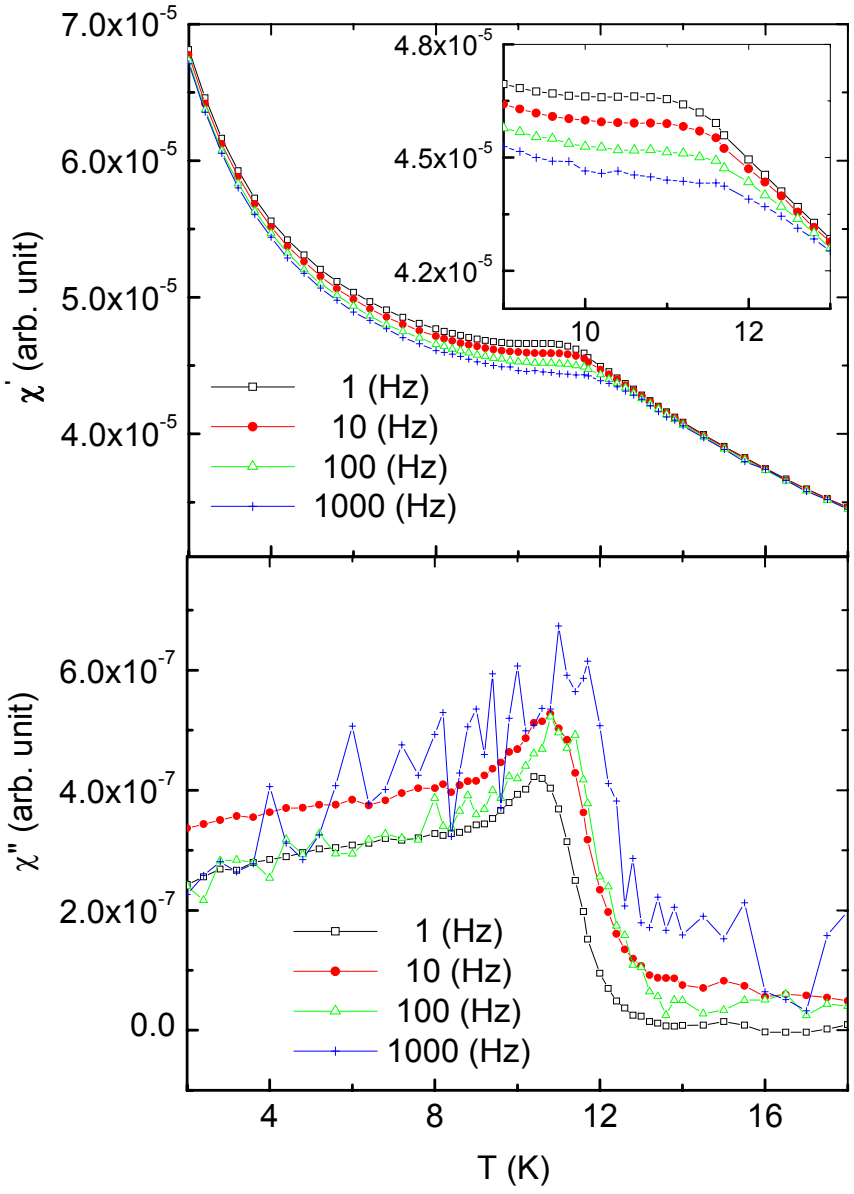

Fig. 5.1. Temperature dependence of real (χ') and imaginary (χ") parts of AC-susceptibility at different frequencies. The inset shows the frequency dependence of the χ' data around the transition temperature.

Fig. 5.2 shows both ZFC and FC magnetization curves, which are split below T ~ 9.6 K in H_{app} = 0.05 T. This diverging point (not a maximum of the ZFC curve) was selected as a T_B. The FC and ZFC magnetization curves are split below T_B, whereas they coincide as the remanence and coercivity have vanished above T_B [17]. T_B is shown in the inset of Fig. 5.2 as a function of applied magnetic fields (H_{app} = 0.001, 0.005, 0.05, 0.3, and 0.5 T). An increased T_B around 10 K is consistent with the AC-susceptibility data.

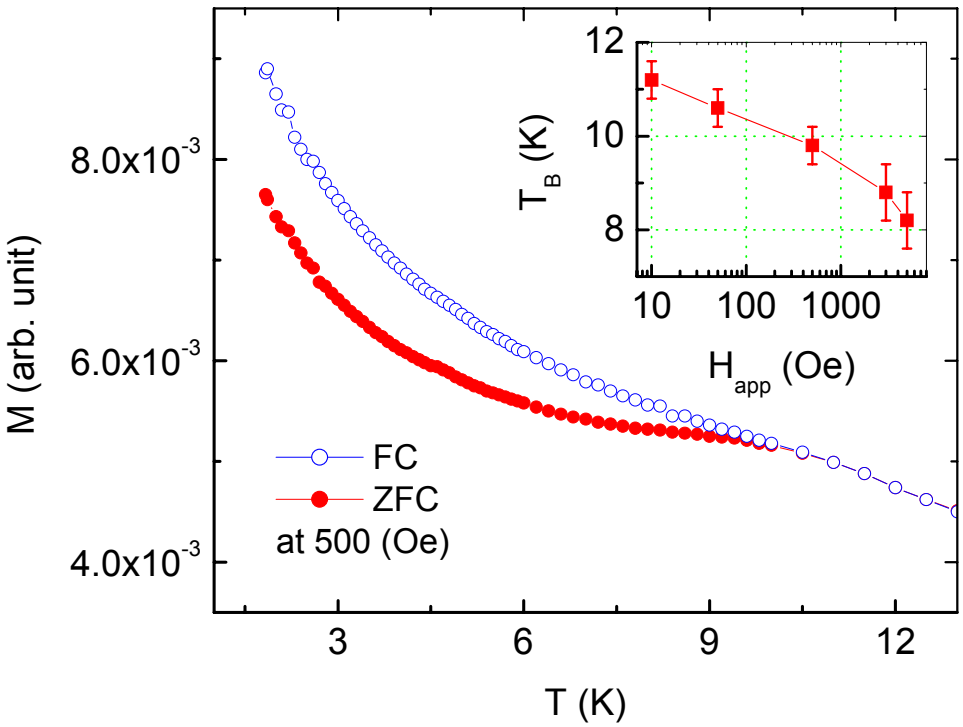

Fig. 5.2. Zero-field-cooled (ZFC) and field-cooled (FC) magnetization vs temperature curves at H_{app}= 500 Oe. The inset shows the blocking temperature (T_B) as a function of different applied magnetic fields (H_{app} = 10, 50, 500, 3000, 5000 Oe),. The connected line is a guide for the eye.

An increased T_B can also be checked by a magnetization relaxation measurement on the film material. A slow relaxation process is normally observed below T_B for the SMM, while this cannot be observed above T_B by the fast relaxation as is described in Chapter I. Fig. 5.3 shows the typical magnetization relaxation of the film material at 5.5 K. Before measuring the magnetization, the magnetization of the sample was saturated by applying a field of 5 T at the base temperature. The field was then decreased to the desired measuring field (- 0.5 T), and magnetization was measured as a function of time [86]. The magnetic relaxation behavior was shown at a higher temperature in the film material (up to 5.5 K) than the as-produced Mn_{12}-acetate. We note that a similarly slow relaxation process at this elevated temperature is not observed in as-produced Mn_{12}-acetate. This temperature enhanced relaxation process confirms an increased blocking temperature (T_B) of the film material as was verified by ZFC and FC magnetizations, as well as AC-susceptibility measurements.

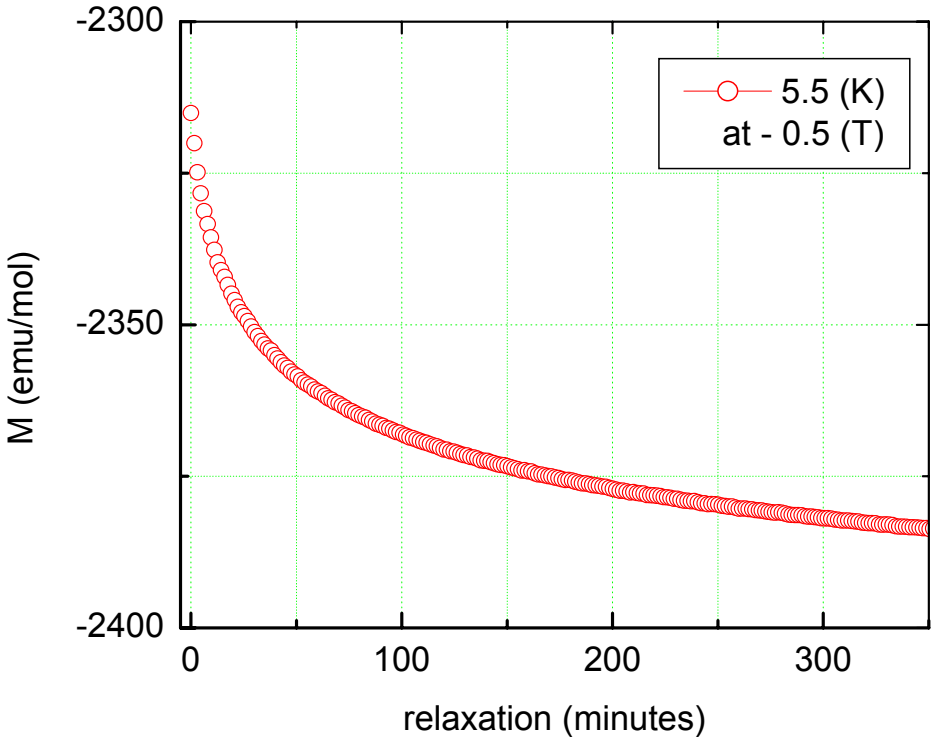

Fig. 5.3. Magnetization relaxation of Mn_{12}-acetate film material at 5.5 K with an applied field of - 0.5 T.

At this point, it should be mentioned that a majority of the film material seems to show paramagnetic behavior based on the above data. This means that there is a non-zero magnetization of both the χ'' (in Fig. 5.1) and the ZFC curve (in Fig. 5.2) below the transition temperature and shows that most of the film material has lost its original magnetization. Also, relaxation of the magnetization starts from a negative value rather than around zero, which implies a fast relaxation of a part of the film material. As a result, reduced coercivity in the hysteresis loops was observed.

The magnetization of the sample was measured as a function of the applied magnetic field at 1.8 K as seen in Fig. 5.4. The hysteresis loop with the coercive field of ~ 0.075 T is shown in the inset, the zoom in of the loop. The low coercive field may be due to the suggested paramagnetic behavior in the majority of the film material as well as a random orientation of the sample. As the magnetization of the film material has changed from the as-produced Mn_{12}-acetate, other measurements, such as a mass spectroscopy, were used to study the solvent's effect on the molecules.

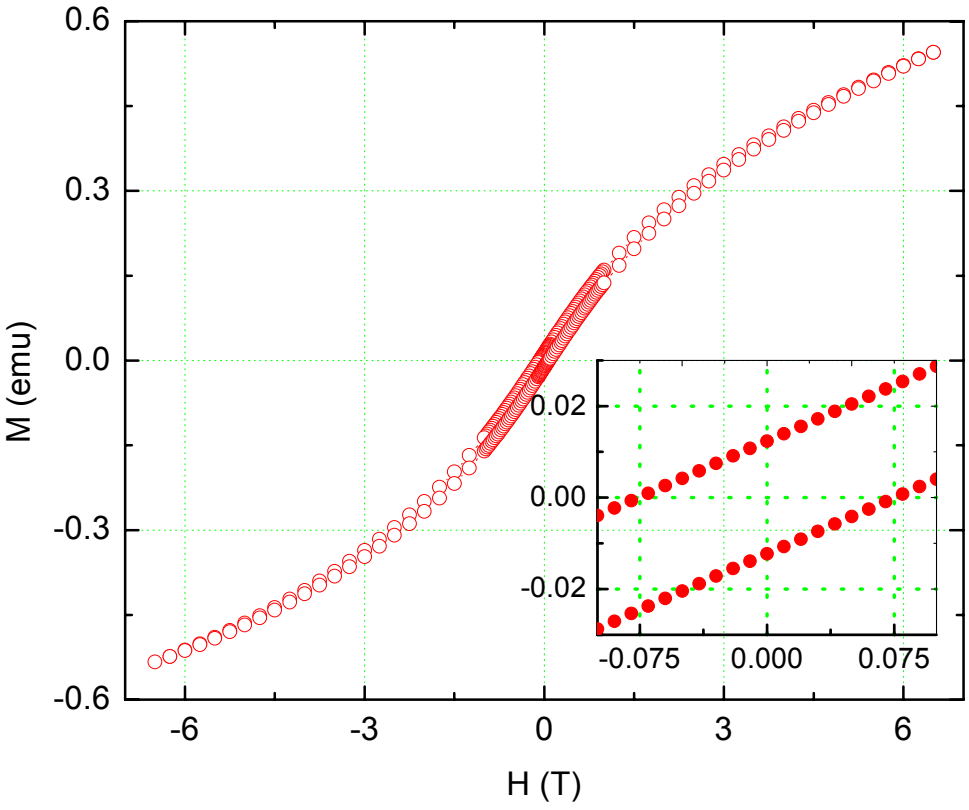

Fig. 5.4 Magnetization versus magnetic field hysteresis loop of Mn_{12}-acetate film material at 1.8 K. The inset, zoom in of the figure, shows a coercivity of 0.075 T.

5.3.2 Mass Spectroscopy Data

To understand the effect of acetonitrile on Mn_{12}-acetate molecules, ESI-MS data were obtained on a PE SCIEX QSTAR instrument in the chemistry department. A diluted solution of the compound in acetonitrile (~ 1.3×10^{-5} M) was used to study how each molecule is affected by the acetonitrile. After immediate dissolution, the data obtained in the negative mode was the same as that previously reported [87]. The ESI-MS data obtained on Mn_{12}-acetate solution that had been in acetonitrile for ~ 30 minutes revealed mass clusters at 1737 Da and 839 Da, as commonly observed in positive mode. These correspond to singly and doubly charged Mn_{12}-acetate molecules, respectively, as shown in Fig. 5.5. In addition, less intense peaks appear at ~ 809 Da, ~780 Da, ~ 750 Da, and ~ 721 Da, which are assigned to clusters with successive loss of acetate ligands. The fact that the Mn_{12}-acetate molecules lose acetate ligands in acetonitrile is expected to affect the magnetic properties of the molecules, in particular the increased T_B that we observed in the magnetization data. Mn_{12}-acetate clusters that are coordinatively unsaturated would exhibit a much lower symmetry than the original cluster. As a result, the magnetic anisotropy should be enhanced, leading to a possible explanation of the observed magnetic data.

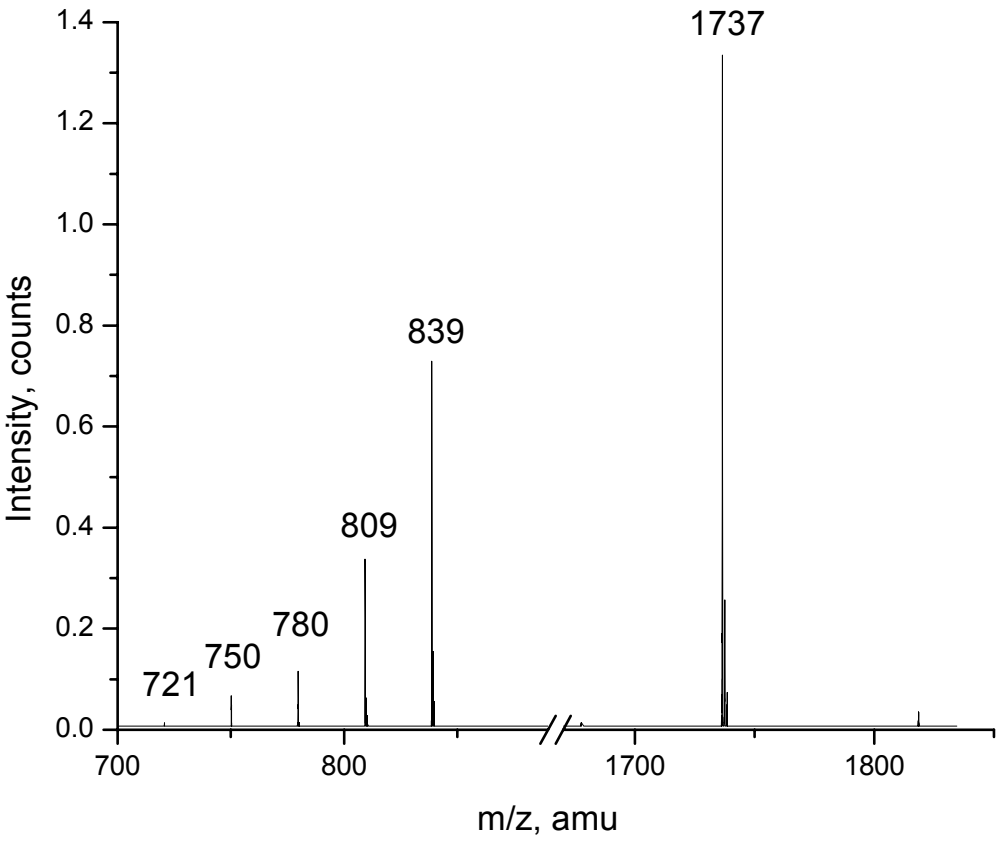

Fig. 5.5. ESI-MS spectrum (positive mode) of a solution of Mn_{12}-acetate in acetonitrile ~ 30 minutes after making the solution.

5.4 Summary

Altered magnetic properties were observed by AC-susceptibility, ZFC and FC magnetizations, and the relaxation measurements. An increase of T_B to > 10 K in the film material was observed, indicating that the magnetic anisotropy of the part of the Mn_{12}-acetate film may have significantly changed during the exposure to the solvent, acetonitrile. A majority of the film material has changed its original magnetization to show paramagnetic behavior. Up to several missing acetate ligands peaks of the $Mn_{12}O_{12}(CH_3COO)_{16}$ molecule in acetonitrile were observed in the positive mode of the ESI-MS data after significant solvent exposure. Based on both magnetization and ESI-MS data, the following possible reasons for the shifted T_B compared to that of the as-produced Mn_{12}-acetate can be suggested: (1) the change in magnetic properties may be the result of structural changes to the Mn_{12}-acetate complex, e.g. missing ligands from the Mn_{12}-acetate molecules or missing water of crystallization, (2) the total spin of the Mn_{12}-acetate molecules may have changed in this process, and (3) intermolecular interaction between the Mn_{12}-acetate molecules may be enhanced due to missing ligands. It is not clear which of the effects or a combination thereof is present in the film material.

CHAPTER VI

CONCLUSIONS

Several sharp steps in the low temperature hysteresis loop indicate alignment of the magnetization easy axis to the applied field. The microscopic Mn_{12}-acetate single crystals were well aligned in the organic solvent by applying ~ 0.5 T above the freezing point of the solvent. The greater the external magnetic field during alignment, the sharper the steps became in the low temperature hysteresis loops, indicating that this method can be used for continuous control of alignment. It may be possible to orient Mn_{12}-acetate micro-crystals on a surface by combining the alignment method with techniques of patterning or depositing SMMs on surfaces, which would be very useful for device applications. This alignment method also serves as a sample for important measurements when big enough single crystals are unavailable. The shape anisotropy could be a major source of the high temperature anisotropy, and thus responsible for the alignment. DC magnetization data, however, do not indicate high temperature anisotropy, possibly due to the small size of the anisotropy.

Deposition of Mn_{12}-acetate directly on Si/SiO_2 and HOPG surfaces using the solution evaporation method has been demonstrated. AFM and XPS characterizations were performed on Si/SiO_2 based films to investigate the surface and the elemental composition of the films. Due to the finite AFM tip radius of curvature, AFM scans do not reveal whether the films were formed by monolayered Mn_{12}-acetate molecules or not. AFM studies, however, showed that homogeneous, molecularly smooth, and

monolayer thick (2 nm) films of Mn_{12}-acetate are being formed. In the STM scans, self-organized Mn_{12}-acetate molecules were observed with a hexagonal lattice structure in the HOPG based films. Based on the studies of both Si/SiO_2 and HOPG based films, the oxidation layer in the Si wafer is probably the source of Mn_{12}-acetate thin film formation. Therefore, the difficulty of getting STM images of Mn_{12}-acetate thin films with a hexagonal lattice structure can be understood by the fact that the oxidation layer does not exist on the HOPG surface. STM measurements on Single Molecule Magnets (SMMs) deposited on metallic surfaces may be important when studying the interplay between the interesting magnetic and transport properties of SMMs.

Altered magnetic properties were observed in the film material that is formed from acetonitrile-exposed Mn_{12}-acetate molecules. The blocking temperature of part of the film material increased to ~ 10 K as verified by magnetization relaxation, AC-susceptibility, and ZFC and FC magnetization measurements. On the basis of this magnetization data and the ESI-MS data, which show that the $Mn_{12}O_{12}(CH_3COO)_{16}$ molecule lost up to several acetate ligands in acetonitrile, it was demonstrated that the magnetization of the Mn_{12}-acetate molecules was easily affected by missing acetate ligands and/or small changes of the surroundings or structure of the Mn_{12}-acetate molecules.

A few important goals in the field of SMMs could be summarized as following; (1) new SMMs with increased T_B should be prepared to realize the suggested applications, (2) techniques of addressing SMMs on various surfaces should be also developed and, (3) understanding the fast quantum dynamics of SMMs is also important in this area.

Two core studies in this dissertation (1) the alignment of micro-crystals and (2) the observation of single molecules of Mn_{12}-acetate are contrubuting a long term goal in this area. Alignment of the magnetization of a single molecule to a specific direction and observation of this molecule on a surface, relevant to the second general goal in the field of SMMs, would be a great challenge in this field. Although this ultimate goal turns out to be very difficult to realize, it would lead to a better understanding of nanomagnetism, magnetism in nanostructures.

REFERENCES

[1] D. Gatteschi, A. Caneschi, L. Pardi, R. Sessoli, Science 265 (1994) 1054.

[2] A.J. Tasiopoulos, A. Vinslava, W. Wernsdorfer, K.A. Abboud, G. Christou, Angewandte Chemie-International Edition 43 (2004) 2117.

[3] L. Neel, Comptes Rendus Hebdomadaires Des Seances De L Academie Des Sciences 224 (1947) 1488.

[4] L. Neel, Comptes Rendus Hebdomadaires Des Seances De L Academie Des Sciences 228 (1949) 664.

[5] R. Sessoli, D. Gatteschi, A. Caneschi, M.A. Novak, Nature 365 (1993) 141.

[6] S.K. Ritter, Chemical & Engineering News 82 (2004) 29.

[7] T. Lis, Acta Crystallographica Section B-Structural Science 36 (1980) 2042.

[8] W. Wernsdorfer, R. Sessoli, Science 284 (1999) 133.

[9] W. Wernsdorfer, N. Aliaga-Alcalde, D.N. Hendrickson, G. Christou, Nature 416 (2002) 406.

[10] I. Chiorescu, W. Wernsdorfer, A. Muller, H. Bogge, B. Barbara, Physical Review Letters 84 (2000) 3454.

[11] M.F. Crommie, Science 309 (2005) 1501.

[12] B. Barbara, W. Wernsdorfer, L.C. Sampaio, J.G. Park, C. Paulsen, M.A. Novak, R. Ferre, D. Mailly, R. Sessoli, A. Caneschi, K. Hasselbach, A. Benoit, L. Thomas, Journal of Magnetism and Magnetic Materials 140 (1995) 1825.

[13] A. Caneschi, T. Ohm, C. Paulsen, D. Rovai, C. Sangregorio, R. Sessoli, Journal of Magnetism and Magnetic Materials 177 (1998) 1330.

[14] G. Christou, D. Gatteschi, D.N. Hendrickson, R. Sessoli, MRS Bulletin 25 (2000) 66.

[15] L. Thomas, A. Caneschi, B. Barbara, Physical Review Letters 83 (1999) 2398.

[16] J.R. Friedman, M.P. Sarachik, J. Tejada, R. Ziolo, Physical Review Letters 76 (1996) 3830.

[17] V. Skumryev, S. Stoyanov, Y. Zhang, G. Hadjipanayis, D. Givord, J. Nogues, Nature 423 (2003) 850.

[18] J. Tejada, X.X. Zhang, E. delBarco, J.M. Hernandez, E.M. Chudnovsky, Physical Review Letters 79 (1997) 1754.

[19] X.X. Zhang, J.M. Hernandez, J. Tejada, R.F. Ziolo, Physical Review B 54 (1996) 4101.

[20] M. Marin-Almazo, D. Garcia-Gutierrez, X. Gao, J.L. Elechiguerra, V.A. Kusuma, W.M. Sampson, M. Miki-Yoshida, A.B. Dalton, R. Escudero, M. Jose-Yacaman, Nano Letters 4 (2004) 1365.

[21] R.M. Achey, P.L. Kuhns, A.P. Reyes, W.G. Moulton, N.S. Dalal, Solid State Communications 121 (2002) 107.

[22] A.L. Barra, D. Gatteschi, R. Sessoli, Physical Review B 56 (1997) 8192.

[23] O. Waldmann, G. Carver, C. Dobe, D. Biner, A. Sieber, H.U. Gudel, H. Mutka, J. Ollivier, N.E. Chakov, Applied Physics Letters 88 (2006) 042507.

[24] J.M. North, L.J. van de Burgt, N.S. Dalal, Solid State Communications 123 (2002) 75.

[25] A.M. Gomes, M.A. Novak, R. Sessoli, A. Caneschi, D. Gatteschi, Physical Review B 57 (1998) 5021.

[26] F. Fominaya, T. Fournier, P. Gandit, J. Chaussy, Review of Scientific Instruments 68 (1997) 4191.

[27] A. Caneschi, D. Gatteschi, R. Sessoli, A.L. Barra, L.C. Brunel, M. Guillot, Journal of the American Chemical Society 113 (1991) 5873.

[28] M.A. Novak, R. Sessoli, A. Caneschi, D. Gatteschi, Journal of Magnetism and Magnetic Materials 146 (1995) 211.

[29] C. Paulsen, J.-G. Park, Evidence for quantum tunneling of the magnetization in Mn_{12}-ac, Academic Publishers, Kluwer, Dordrecht, 1995, p. 189.

[30] A. Caneschi, D. Gatteschi, C. Sangregorio, R. Sessoli, L. Sorace, A. Cornia, M.A. Novak, C. Paulsen, W. Wernsdorfer, Journal of Magnetism and Magnetic Materials 200 (1999) 182.

[31] R. Sessoli, Molecular Crystals and Liquid Crystals 274 (1995) 145.

[32] L. Thomas, F. Lionti, R. Ballou, D. Gatteschi, R. Sessoli, B. Barbara, Nature 383 (1996) 145.

[33] J.M. Hernandez, X.X. Zhang, F. Luis, J. Tejada, J.R. Friedman, M.P. Sarachik, R. Ziolo, Physical Review B 55 (1997) 5858.

[34] L. Bokacheva, A.D. Kent, M.A. Walters, Physical Review Letters 85 (2000) 4803.

[35] A.D. Kent, Y.C. Zhong, L. Bokacheva, D. Ruiz, D.N. Hendrickson, M.P. Sarachik, Europhysics Letters 49 (2000) 521.

[36] A. Cornia, R. Sessoli, L. Sorace, D. Gatteschi, A. L. Barra, C. Daiguebonne, Physical Review Letters 89 (2002) 257201.

[37] K. M. Mertes, Y. Suzuki, M.P. Sarachik, Y. Paltiel, H. Shtrikman, E. Zeldov, E. Rumberger, D.N. Hendrickson, G. Christou, Physical Review Letters 87 (2001) 227205.

[38] I. Chiorescu, R. Giraud, A.G.M. Jansen, A. Caneschi, B. Barbara, Physical Review Letters 85 (2000) 4807.

[39] E. M. Chudnovsky, D. A. Garanin, Physical Review Letters 87 (2001) 187203.

[40] M. N. Leuenberger, D. Loss, Nature 410 (2001) 789.

[41] L. Krusin-Elbaum, T. Shibauchi, B. Argyle, L. Gignac, D. Weller, Nature 410 (2001) 444.

[42] D.M. Seo, V. Meenakshi, W. Teizer, H. Zhao, K.R. Dunbar, Journal of Magnetism and Magnetic Materials 301 (2006) 31.

[43] G. Binnig, C.F. Quate, C. Gerber, Physical Review Letters 56 (1986) 930.

[44] http://en.wikipedia.org/wiki/Van_der_Waals_force, Van der Waals force, From Wikipedia, the free encyclopedia, October 2007.

[45] L.B. R. Howland, A practical guide to scanning probe microscopy, Park Scientific Instruments, sunnyvale, CA, 1996.

[46] J. F. Moulder, W.F. Stickle, P. E. Sobol, K. D. Bomben, Handbook of X-ray photoelectron spectroscopy, Physical Electronics, Eden Prairie, Minnesota, 1995.

[47] A. Kumar, S. Fahler, H. Schlorb, K. Leistner, L. Schultz, Physical Review B 73 (2006) 064421.

[48] H. Zeng, R. Skomski, L. Menon, Y. Liu, S. Bandyopadhyay, D.J. Sellmyer, Physical Review B 65 (2002) 134426.

[49] E.C. Stoner, E.P. Wohlfarth, Philosophical Transactions of the Royal Society of London Series A-Mathematical and Physical Sciences 240 (1948) 599.

[50] B. D. Cullity, Introduction to magnetic materials, Addison-Wesley, Reading, Massachusetts, 1972.

[51] A.N. Abdi, J.P. Bucher, P. Rabu, O. Toulemonde, M. Drillon, P. Gerbier, Journal of Applied Physics 95 (2004) 7345.

[52] J.M. Hernandez, X.X. Zhang, F. Luis, J. Bartolome, J. Tejada, R. Ziolo, Europhysics Letters 35 (1996) 301.

[53] P. Derango, M. Lees, P. Lejay, A. Sulpice, R. Tournier, M. Ingold, P. Germi, M. Pernet, Nature 349 (1991) 770.

[54] S. Liu, Journal of Applied Physics 76 (1994) 6757.

[55] M.J. Matthews, M.S. Dresselhaus, G. Dresselhaus, M. Endo, Y. Nishimura, T. Hiraoka, N. Tamaki, Applied Physics Letters 69 (1996) 430.

[56] T. Okamoto, S. Horii, T. Uchikoshi, T.S. Suzuki, Y. Sakka, R. Funahashi, N. Ando, M. Sakurai, J.I. Shimoyama, K. Kishio, Applied Physics Letters 89 (2006) 081912.

[57] K.M. Mertes, Y. Suzuki, M.P. Sarachik, Y. Myasoedov, H. Shtrikman, E. Zeldov, E.M. Rumberger, D.N. Hendrickson, G. Christou, Solid State Communications 127 (2003) 131.

[58] S. Takahashi, R. S. Edwards, J. M. North, S. Hill, N. S. Dalal, Physical Review B 70 (2004) 094429.

[59] M. Mannini, D. Bonacchi, L. Zobbi, F.M. Piras, E.A. Speets, A. Caneschi, A. Cornia, A. Magnani, B.J. Ravoo, D.N. Reinhoudt, R. Sessoli, D. Gatteschi, Nano Letters 5 (2005) 1435.

[60] K. Kim, D.M. Seo, J. Means, V. Meenakshi, W. Teizer, H. Zhao, K.R. Dunbar, Applied Physics Letters 85 (2004) 3872.

[61] E. Coronado, A. Forment-Aliaga, F.M. Romero, V. Corradini, R. Biagi, V. De Renzi, A. Gambardella, U. del Pennino, Inorganic Chemistry 44 (2005) 7693.

[62] M. Cavallini, J. Gomez-Segura, D. Ruiz-Molina, M. Massi, C. Albonetti, C. Rovira, J. Veciana, F. Biscarini, Angewandte Chemie-International Edition 44 (2005) 888.

[63] D. Seo, W. Teizer, H. Zhao, K.R. Dunbar, Journal of Magnetism and Magnetic Materials 312 (2007) 205.

[64] J.R. Friedman, Physics Department, The City University of New York, New York, 1996.

[65] M.A. Novak and R. Sessoli, Quantum tunneling of magnetization, Academic Publishers, Kluwer, Dordrecht, 1995, p. 171.

[66] D. Gatteschi, R. Sessoli, J. Villain, Molecular Nanomagnets, Oxford University, New York, 2007.

[67] S.J. Park, S. Kim, S. Lee, Z.G. Khim, K. Char, T. Hyeon, Journal of the American Chemical Society 122 (2000) 8581.

[68] V.F. Puntes, K.M. Krishnan, A.P. Alivisatos, Science 291 (2001) 2115.

[69] D. Gatteschi, R. Sessoli, Angewandte Chemie-International Edition 42 (2003) 268.

[70] M. Clemente-Leon, H. Soyer, E. Coronado, C. Mingotaud, C.J. Gomez-Garcia, P. Delhaes, Angewandte Chemie-International Edition 37 (1998) 2842.

[71] G. H. Kim, T. S. Kim, Physical Review Letters 92 (2004) 137203.

[72] A. Cornia, A.C. Fabretti, M. Pacchioni, L. Zobbi, D. Bonacchi, A. Caneschi, D. Gatteschi, R. Biagi, U. Del Pennino, V. De Renzi, L. Gurevich, H.S.J. Van der Zant, Angewandte Chemie-International Edition 42 (2003) 1645.

[73] S. Voss, M. Fonin, U. Rudiger, M. Burgert, U. Groth, Y.S. Dedkov, Physical Review B 75 (2007) 045102.

[74] L. Zobbi, M. Mannini, M. Pacchioni, G. Chastanet, D. Bonacchi, C. Zanardi, R. Biagi, U. Del Pennino, D. Gatteschi, A. Cornia, R. Sessoli, Chemical Communications (2005) 1640.

[75] A. Naitabdi, J.P. Bucher, P. Gerbier, P. Rabu, M. Drillon, Advanced Materials 17

(2005) 1612.

[76] S. Voss, M. Fonin, U. Rudiger, M. Burgert, U. Groth, Applied Physics Letters 90 (2007) 133104.

[77] J. Gomez-Segura, I. Diez-Perez, N. Ishikawa, M. Nakano, J. Veciana, D. Ruiz-Molina, Chemical Communications (2006) 2866.

[78] S. Phark, Z.G. Khim, B.J. Kim, B.J. Suh, S. Yoon, J. Kim, J.M. Lim, Y. Do, Japanese Journal of Applied Physics Part 1-Regular Papers Short Notes & Review Papers 43 (2004) 8273.

[79] K.L. Westra, D.J. Thomson, Journal of Vacuum Science & Technology B 13(1995) 344.

[80] J.S. Kang, J.H. Kim, Y.J. Kim, W.S. Jeon, D.Y. Jung, S.W. Han, K.H. Kim, K.J. Kim, B.S. Kim, Journal of the Korean Physical Society 40 (2002) L402.

[81] M. Molinari, H. Rinnert, M. Vergnat, Applied Physics Letters 82 (2003) 3877.

[82] G. Reiss, J. Vancea, H. Wittmann, J. Zweck, H. Hoffmann, Journal of Applied Physics 67 (1990) 1156.

[83] J. M. North, D. Zipse, N. S. Dalal, E. S. Choi, E. Jobiliong, J. S. Brooks, D. L. Eaton, Physical Review B 67 (2003) 174407.

[84] M. Clemente-Leon, E. Coronado, A. Forment-Aliaga, P. Amoros, J. Ramirez-Castellanos, J.M. Gonzalez-Calbet, Journal of Materials Chemistry 13 (2003) 3089.

[85] J. Larionova, R. Clerac, B. Boury, J. Le Bideau, L. Lecren, S. Willemin, Journal of Materials Chemistry 13 (2003) 795.

[86] C. Paulsen, J.-G. Park, Evidence for quantum tunneling of the magnetization in Mn_{12}-ac, Academic Publishers, Kluwer, Dordrecht, 1995, p. 189.

[87] E. Coronado, M. Feliz, A. Forment-Aliaga, C.J. Gomez-Garcia, R. Llusar, F.M. Romero, Inorganic Chemistry 40 (2001) 6084.

[88] C. Kittel, Introduction to Solid State Physics 7^{th} edition, Wiley, New York, 1995 p. 422.

APPENDIX A

MAGNETIC ENERGY CALCULATION FOR THE ALIGNMENT

When magnetic alignment was discussed in Chapter III, it was suggested that the Mn_{12}-acetate micro-crystals, not single molecules, were aligned to give interesting magnetization data. A simple energy calculation, comparing both magnetic and thermal energies for a Mn_{12}-acetate molecule, shows that a single Mn_{12}-acetate molecule cannot be aligned magnetically. To prove this, the maximum magnetic energy for the single molecule was calculated by assuming an unrealistic upper bound limit, net spin of 10 for the single molecule, and no spin tunneling at H = 1 T up to 300 K. The absence of spin tunneling at H = 1 T, which is impossible even at the base temperature (1.8 K) of our SQUID magnetometer is illustrated in Fig. A.1. The spin is parallel to the molecular c-axis, which is initially perpendicular to the applied magnetic field. After the molecule aligns, the spin is still parallel to the molecular c-axis, which is now parallel to the field, as shown in Fig. A.1.

Paramagnetic susceptibility (χ) was calculated with an effective magnetic moment of 20 μ_B at 300 K to give $\chi = 2.7 \times 10^{-3}$ (emu·mol^{-1}·Oe^{-1}) for the single molecule as below.

$\chi = M/B = (Np^2\mu_B^2) \cdot (3k_BT)^{-1} = (6 \times 10^{23}\ \text{mol}^{-1}) \cdot (20\ \mu_B)^2 \cdot (3\ k_B \cdot 300\ \text{K})^{-1} = 2.7 \times 10^{-3}$ (emu·mol^{-1}·Oe^{-1}) [88].

Where, M = magnetization, H = magnetic field intensity, N = number of molecules per mole, and p = effective number of Bohr magnetons. Both constants $\mu_B = 10^{-21}$ (erg·Oe^{-1}) and $k_B = 10^{-16}$ (erg·K^{-1}) are also use.

The maximum magnetic energy difference, U_M, between initial and final states of a single molecule when applying 1 T at 300 was calculated as

$U_M = \mu \cdot H = \chi \cdot \text{Mole} \cdot H^2 = (2.7 \times 10^{-3}\ \text{emu·mol}^{-1}\text{·Oe}^{-1}) \cdot (<6 \times 10^{23}>^{-1}\ \text{mol}) \cdot (10^4\ \text{Oe})^2 = 4.5 \times 10^{-19}$ (erg).

Where, μ (magnetic moment) = $\chi \cdot \text{Mole} \cdot H$ and [erg] = [emu] · [Oe] were used.

U_M is compared to a thermal energy of the single molecule, $U_T = k_B \cdot T = (10^{-16}\ \text{erg·K}^{-1}) \cdot (300\ \text{K}) = 3 \times 10^{-14}$ (erg).

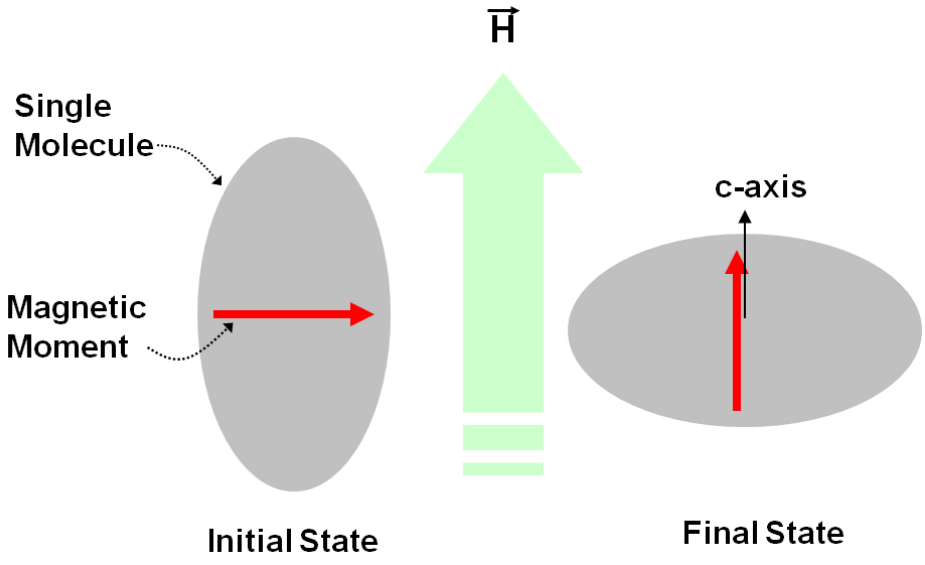

Fig. A.1. Schematic diagram illustrating the absence of spin tunneling at H = 1 T up to 300 K.

By observing that U_T is 10^5 times higher than U_M, we see that a single molecule cannot be aligned magnetically by applying 1 T. Therefore, the observed magnetic alignment is probably happening in micro-crystals.

A single crystal that is made of more than 10^5 molecules can be aligned if the conditions are the same throughout and the maximum magnetic energy is proportional to the number of single molecules. In this regard, micro-crystals with a typical size of 3 × 3 × 15 μm^3, which are made up of ~ 10^{10} molecules as seen in Fig. A.2, can be aligned by applying 1 T at room temperature. However, these calculations are based on an unrealistic upper bound limit.

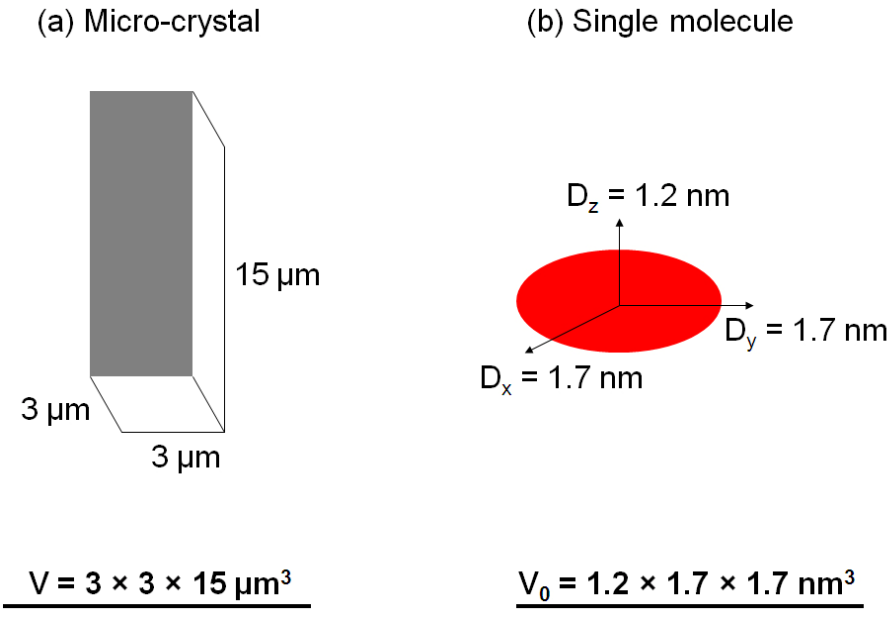

Fig. A.2. A diagram for volume comparison of the Mn_{12}-acetate micro-crystal and the single molecule with typical sizes given. About 10^{10} single molecules exist in the single micro-crystal in this rough size comparison.

APPENDIX B

EXPERIMENTAL EFFORTS TO MEASURE THE HIGH TEMPERATURE ANISOTROPY OF THE MN_{12}-ACETATE

The small adjustment of the magnetization in the DC magnetization data in Chapter III (Fig. 3.11) was carried out for the reason that will be given now. A change of the magnetization up to ~ 5×10^{-5} emu was observed in the DC magnetization at 0.5 T after re-loading the sample. Fig. A.3 shows the DC magnetization at 0.5 T as a function of temperature for differently aligned states of the suspension, which were prepared by applying 0.5 T (open circle) and 0 T (open triangle) at room temperature. After completing measurements for the 0.5 T case, the sample was taken out of the SQUID to homogenize the suspension, re-inserted into the sample space, and subsequently cooled down without field. Then, the DC magnetization was measured during warm up at 0.5 T. DC magnetizations for both cases are different above the melting point of the solvent (185 K). In particular, the randomly-oriented state shows higher magnetization than the well-aligned state, contradicting the minimum energy principle. Micro-crystals were aligned by applying magnetic field to minimize their magnetic energy. As a result, the aligned state must show higher magnetization than the randomly-oriented state. The higher magnetization of the randomly-oriented state over the well-oriented state above 100 K in the measurements may result from the data acquisition process in the SQUID. Since the magnetization of the randomly-oriented state is relatively small, the zero magnetization point is shifted down in order to make a slightly higher magnetization. In

reality, however, both magnetizations should be the same at room temperature as long as there is no alignment memory in the micro-crystals, because both data were acquired in the same field of 0.5 T and the same liquid phase of the solution. Therefore, the graph of the final data (filled triangle) was obtained by subtracting a constant value, X, to make the two graphs overlap at 300 K. The inset emphasizes that this adjustment of the magnetization is small compared to the difference of the two magnetizations at low temperature. The best way to eliminate this effect is to leave the sample in the sample space during the series of measurements. For earlier studies, however, the sample was taken out from the sample space to homogenize the suspension after one measurement (Fig. 3.7, Fig. 3.8, and Fig. 3.9), because it was not clear how the suspension settlement affected the alignment. Recently, an enhanced experiment to find out the high temperature anisotropy was carried out.

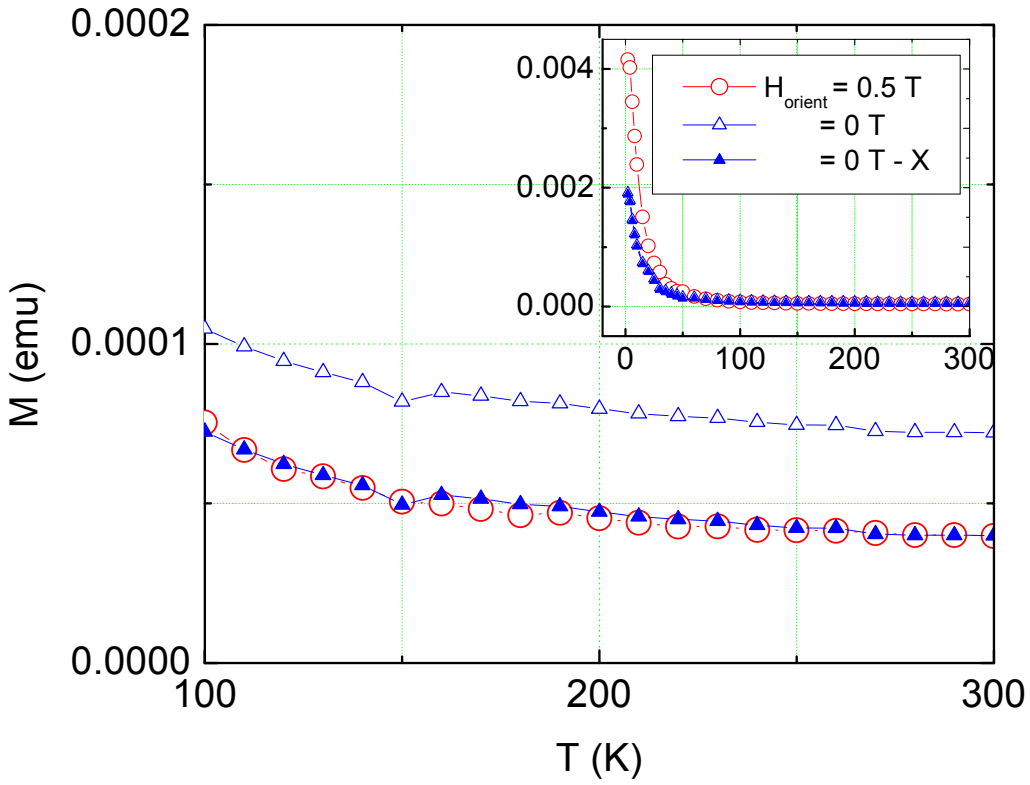

Fig. A.3. DC magnetization at H = 0.5 T as a function of temperature for differently aligned states of the suspension. These states were prepared by applying 0.5 T (open circle) and 0 T (open triangle) at room temperature. The graph with the filled triangle was obtained by subtracting a constant value X from the open triangle to overlay the two graphs. The inset emphasizes that this adjustment is small compared to the difference of the two magnetizations at low temperature.

Achieving a good alignment with sharp steps in the low temperature hysteresis loop is also possible in the settled suspension, which was prepared by putting the solution in the SQUID sample space without magnetic field for more than 1 hour. Fig. A.4 shows hysteresis loop data at 1.8 K for the aligned suspension obtained by applying 1 T at room temperature. The data showed sharp steps, which are only seen in single crystals [38, 57, 58]or aligned samples [16, 52, 64], verifying that the alignment was achieved in the setteled suspension. The schematic diagram in the inset shows the settlement of the Mn_{12}-acetate micro-crystals after remaining stationary for 1 hour and the alignment of these by applying an orientation field (H_{orient}) of 1 T. It is unclear at this time whether the extent of the alignment as a function of the orientation field is the same for the unsettled and settled suspensions. The settled suspension has an advantage over the unsettled suspension in the study of magnetizations between randomly-oriented and well-oriented states. In the settled suspension case, the sample does not need to be taken out from the SQUID sample space to homogenize the suspension. Therefore, the magnetization adjustment is not necessary to compare the small magnetization difference for differently aligned states of the suspension. In the unsettled suspension case, the sample should be taken out from the sample space to homogenize the suspension. This is useful to study the degree of the alignment as a function of applied magnetic field. Both thermal and magnetic energies need to be included for energetic considerations of the alignment. Gravitational force can be neglected.

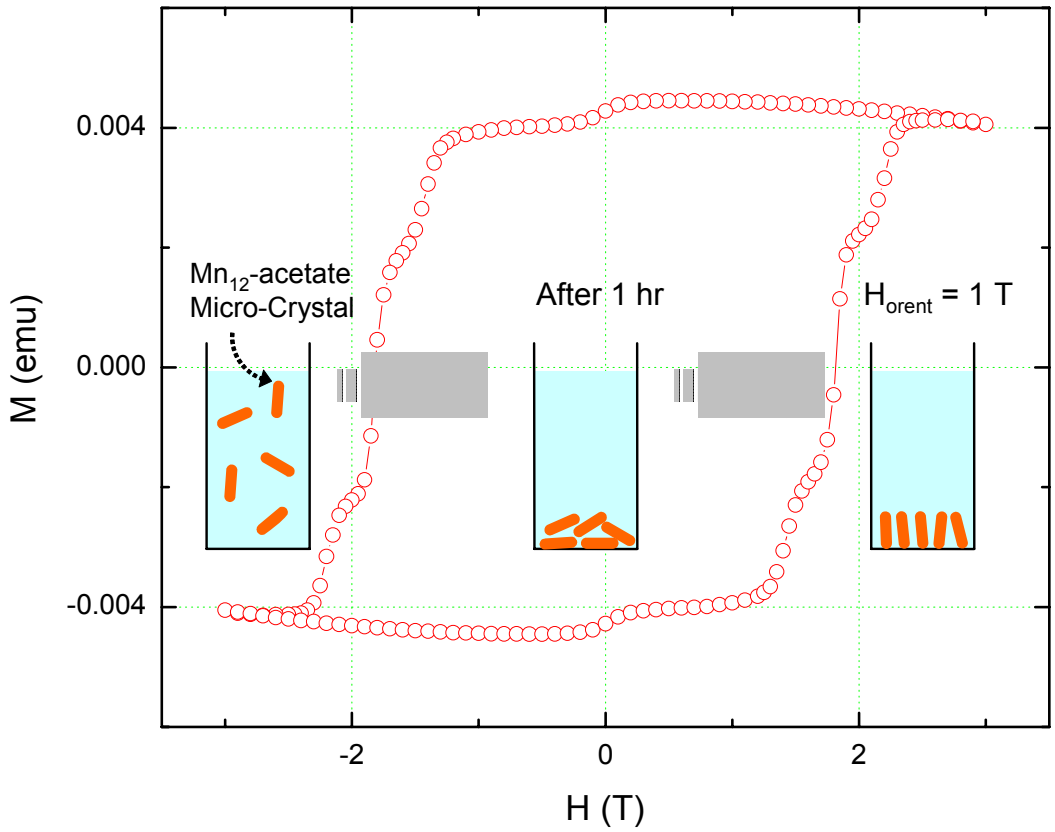

Fig. A.4. M vs. H hysteresis loop data of the aligned suspension at 1.8 K. A diamagnetic background signal did not subtracted, and as a result the decrease of the magnetization is observed at higher magnetic field. Most of the suspension was allowed to settle down by putting the solution in the SQUID sample space for more than 1 hour without magnetic field, as seen in the simplified schematic drawing of the solution. Drawings show only micro-crystals of Mn_{12}-acetate for simplicity. Settled micro-crystals are aligned by applying a magnetic field of 1 T.

Fig. A.5 shows the magnetization difference between the well-aligned and randomly-oriented states. The suspension allowed settling by putting the sample in the SQUID magnetometer without magnetic field for more than 1 hour. The sample was cooled down without magnetic field to 100 K, and DC magnetization (M_{0T}) was measured during warm-up at 0.5 T. Next, it was cooled down again to 100 K, but with an orientation field of 1 T. The magnetization of this state (M_{1T}) was measured at 0.5 T during warm-up. The different magnetization between the two states ($\Delta M = M_{1T} - M_{0T}$) was calculated by subtracting M_{0T} from M_{1T} as shown in Fig. A.5. The magnetization difference between the two states is decreasing with increasing temperature. Only quantitative explanations on this date may be useful as the data is small ($\Delta M/H \sim 2 \times 10^{-10}$ emu·Oe^{-1}), which is on the level of the noise. The decrease of the magnetization difference as increasing temperature can be understood from the fact that the thermal energy increases with increasing temperature while the shape anisotropy energy is constant. It may be also possible that the memory of the alignment is lost as time goes on. Importantly, the reproducibility of this data should be checked.

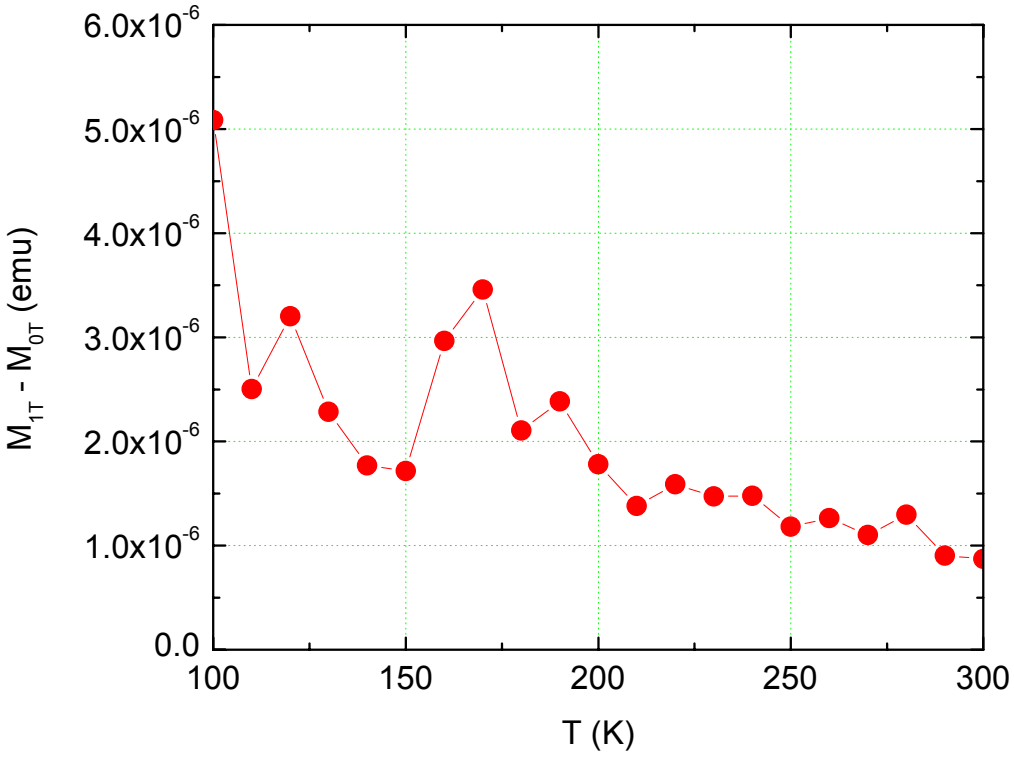

Fig. A.5. Magnetization difference between two extreme states. Well-aligned and randomly-oriented states were prepared by applying 1 T and 0 T at room temperature, respectively. Magnetizations for two extreme states were subsequently measured during warm-up at 0.5 T.

APPENDIX C

MOLAR CONCENTRATION OF MN_{12}-ACETATE SOLUTION

$[Mn_{12}O_{12}(CH_3COO)_{16}(H_2O)_4]\cdot 2CH_3COOH\cdot 4H_2O$ is the full chemical formula for the single Mn_{12}-acetate molecule. Based on the atomic weight and the molecule's weight, a molar concentration of the Mn_{12}-acetate solution can be calculated. For example, 2.06 mg of Mn_{12}-acetate in 10 mL of solvent makes 1×10^{-4} M as below.

$(2.06 \times 10^{-3}$ g/ 2060 g·mol$^{-1})$/ 0.001 L = 1×10^{-4} M

	(Number of atoms)		(Atomic weight)		
Hydrogen (H)	72	×	1	=	72
Carbon (C)	36	×	12	=	432
Oxygen (O)	54	×	16	=	896
Manganese (Mn)	12	×	55	=	660
			(Total)	=	2060 (g)

APPENDIX D

ACETONITRILE VERSUS ISOPROPANOL

One of the advantages of single molecule magnets compared to conventional magnets is the solubility in organic solvents as was mentioned in section 1.2. Mn_{12}-acetate thin films have been deposited on surfaces by the solution evaporation method utilizing the solubility of the compound as discussed in Chapter IV. Two solvents, acetonitrile (CH_3CN) and isopropanol ($CH_3CHOHCH_3$), have been used for the solution evaporation method. The acetonitrile based solution makes smoother Mn_{12}-acetate films than the isopropanol based solution on both Si/SiO_2 and HOPG surfaces. This may be due to the fact that acetonitrile better isolates powder sample into single molecules in solution than the isopropanol. Also, the faster evaporation time of acetonitrile over isopropanol may affect smooth film formation on surfaces. Therefore, thin films have been fabricated by using the acetonitrile based solution as mentioned in Chapter IV. However, the interesting magnetic properties of the as-produced Mn_{12}-acetate do change when the molecules are exposed to acetonitrile for significant times, as was discussed in Chapter V.

Some properties of the two solvent based solutions are summarized in Table 1. A few remarks on the Table are necessary. It is difficult to study the magnetization of the compound in both solvents. In particulars, magnetizations from relatively low concentrations, which are composed of single molecules, are unknown. The extreme concentrations, 1×10^{-4} and 1×10^{-3} M, are only shown in the Table for simplicity,

though in between concentrations exist and are sometimes used. Both extreme compositions, single molecules and micro-crystals, are only shown for simplicity. Intermediate sized clusters made of more than 1 molecule exist. Composition studies are based on the AFM studies.

Table 1. Comparison between acetonitrile and isotropanol based Mn_{12}-acetate solutions

Solvents	**Magnetization**	**Concentration (M)**	**Compositions**	**Usage**
Acetonitrile (CH_3CN)		1×10^{-4}	Single Molecules	Thin Film
	Changing in ~ hrs	1×10^{-3}	Single Molecules & Some Micro-crystals	Film Material
Isopropanol ($CH_3CHOHCH_3$)		1×10^{-4}	Single Molecules & Some Micro-crystals	Thin Film & Pattern
	Stable for ~ 3 days	1×10^{-3}	Single Molecules & Micro-crystals	Alignment

APPENDIX E

MAGNETIZATION FROM MN_{12}-ACETATE FILMS

As discussed in Chapter V, magnetization measurements on Mn_{12}-acetate thin films were not successful due to the small amount of compound on the surface and the large background signal from the substrate. Therefore, so called "film material" (acetonitrile exposed Mn_{12}-acetate molecules) was prepared for the magnetization measurements.

On the other hand, magnetization measurements on Mn_{12}-acetate films were possible when enough Mn_{12}-acetate compound was deposited on a piece of plastic straw used for the SQUID sample holder. The straw piece was used rather than Si/SiO_2 as the former shows much less diamagnetic signal than the latter. Relatively high concentration (typically $\sim 1 \times 10^{-3}$ M) was used for the deposition to be certain of a measurable magnetization from the film. Additionally, isopropanol was used instead of acetonitrile because the hysteresis data show a small coercive field when acetonitrile was used as a solvent, as was discussed in Chapter V. Therefore, the film may be composed of microscopic single crystals as well as single molecules of Mn_{12}-acetate.

Hysteresis loops were then acquired on this Mn_{12}-acetate film deposited on the plastic piece as shown in Fig. A.6. Magnetization as a function of applied field was first measured on the plastic piece before deposition of Mn_{12}-acetate, as seen in Fig. A.6 (a). The same measurement was done after Mn_{12}-acetate was deposited by two Dip-and-Dry (DAD) cycles, as seen in Fig. A.6 (b). Hysteresis loop data from pure Mn_{12}-acetate film was acquired by subtracting magnetization (a) from (b) as seen in Fig. A.6 (c).

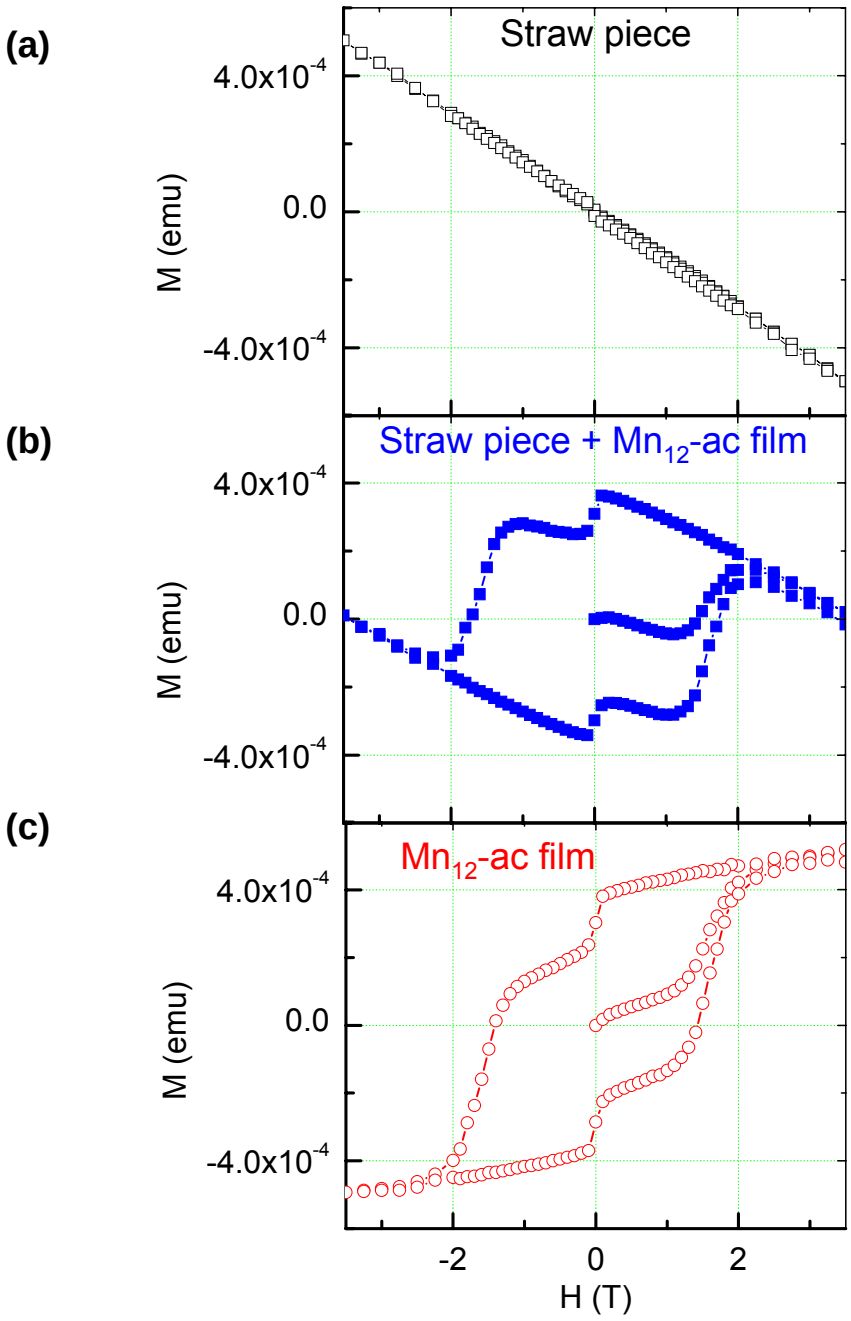

Fig. A.6 (a) M vs. H graph on the straw piece at 1.8 K, (b) hysteresis loop of the Mn_{12}-acetate film deposited on the straw piece at 1.8 K, (c) pure Mn_{12}-acetate film data found by subtracting (a) from (b).

The resulting hysteresis loop of Mn_{12}-acetate film is identical to that of the as-produced Mn_{12}-acetate. To our knowledge, this is the first hysteresis loop data from Mn_{12}-acetate film itself. Also, this data confirms that the isopropanol does not change the magnetization of as-produced Mn_{12}-acetate, as discussed in Appendix D.

It should be mentioned, however, that these data were not easy to acquire. Fig. A.7 shows two sets of magnetization data, commonly observed in this subtracting method, which were acquired by the same process as Fig. A.6. These two series of data were acquired on Mn_{12}-acetate films formed by two DAD-cycles and twenty DAD-cycles using similarly concentrated solution (~ 1×10^{-3} M). By comparing both (c) and (f), one can see that the thicker Mn_{12}-acetate film shows higher magnetization. However, relative magnetization was not linearly proportional to the number of DAD-cycles. This shows that multiple DAD-cycles do not lead to linearly proportional thicker films, as was discussed in Chapter IV. Importantly, these two hysteresis loops, (c) and (f), are different from Fig. A.6 (c), the hysteresis loop of as-produced Mn_{12}-acetate. This discrepancy may be from the subtraction process, but it is not clear at this point. Acquiring a magnetization from Mn_{12}-acetate thin films which is similar to that for the as-produced Mn_{12}-acetate is the first step towards studying the interaction between Mn_{12}-acetate and other magnetic materials.

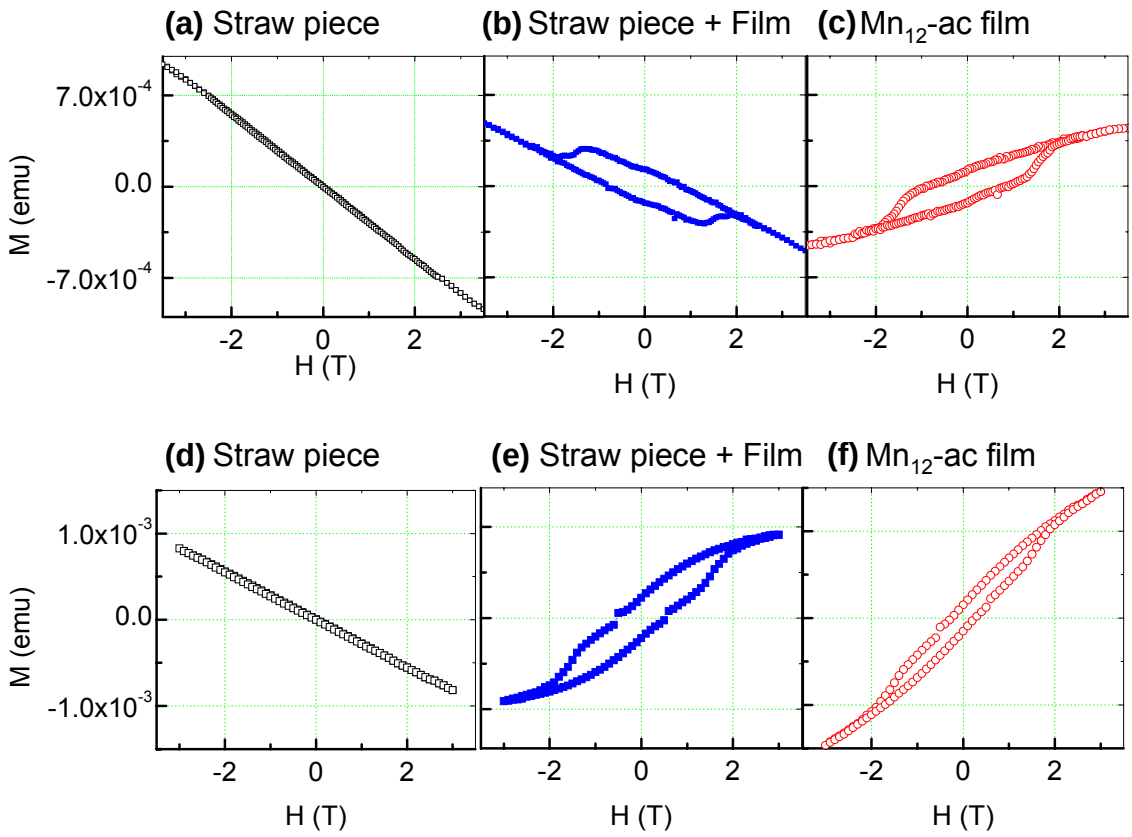

Fig. A.7 (a) M vs. H graph on the straw piece at 1.8 K, (b) magnetization of the Mn_{12}-acetate film by 2 DAD-cycles with the straw piece at 1.8 K, (c) pure Mn_{12}-acetate film data by subtracting (a) from (b), (d) magnetization of the other straw piece at 1.8 K, (e) hysteresis loop of the relatively thick Mn_{12}-acetate film by 20 DAD-cycles with the straw piece, (f) magnetization of the pure Mn_{12}-acetate thick film by subtracting (d) from (e).

VITA

Name:	Dongmin Seo
Address:	Corresponding author: Dr. W. Teizer, Department of Physics Texas A&M University, College Station, TX 77843- 4242, USA
Email Address:	sdm1861@hanmail.net
Education:	B.S., Physics, Dankook University in Korea, 1998 M.S., Physics, Seoul National University in Korea, 2001 M.S., Physics, Texas A&M University, 2005 Ph.D., Physics, Texas A&M University, 2007